ISSN: 2153-1196 Vol.1, No.2, June 2010

Scientific Research

Journal of Modern Physics

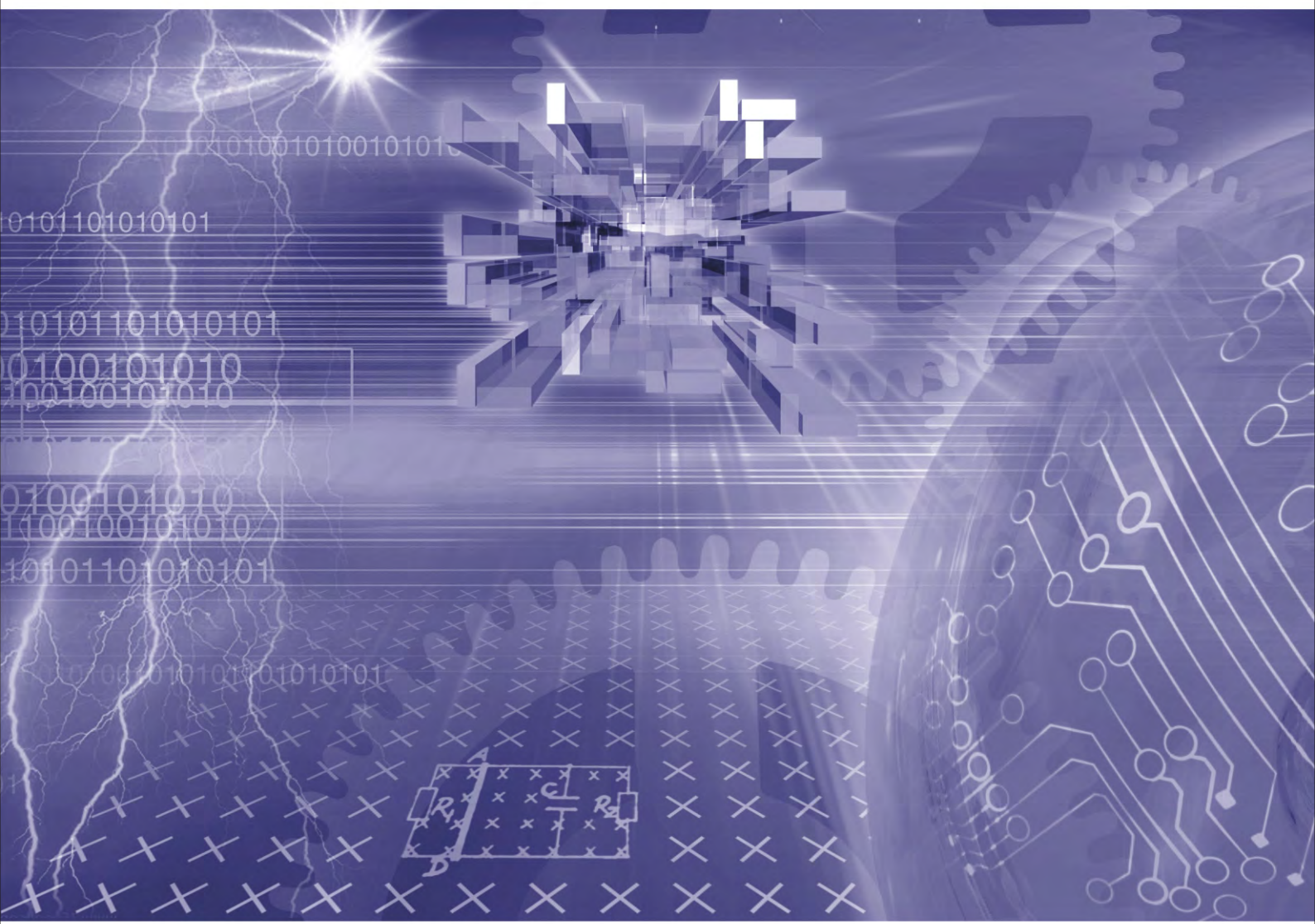

ISSN: 2153-1196

www.scirp.org/journal/jmp

Journal Editorial Board

ISSN: 2153-1196 (Print) ISSN: 2153-120X (Online)

http://www.scirp.org/journal/jmp

J. Modern Physics, **2010, 1, 93-149**
Published Online June 2010 in SciRes (http://www.SciRP.org/journal/jmp)

TABLE OF CONTENTS

Volume 1 Number 2 June 2010

Journal of Modern Physics (JMP)

Journal Information

SUBSCRIPTIONS

The *Journal of Modern Physics* (Online at Scientific Research Publishing, www.SciRP.org) is published bimonthly by Scientific Research Publishing, Inc., USA.

Subscription rates:

Print: $50 per issue.
To subscribe, please contact Journals Subscriptions Department, E-mail: sub@scirp.org

SERVICES

Advertisements
Advertisement Sales Department, E-mail: service@scirp.org

Reprints (minimum quantity 100 copies)
Reprints Co-ordinator, Scientific Research Publishing, Inc., USA.
E-mail: sub@scirp.org

COPYRIGHT

PRODUCTION INFORMATION

For manuscripts that have been accepted for publication, please contact:
E-mail: jmp@scirp.org

J. Modern Physics, **2010, 1, 93-99**
doi:10.4236/jmp.2010.12014 Published Online June 2010 (http://www.SciRP.org/journal/jmp)

Structural, Magnetic and Dielectric Studies on Strontium Substituted Nd_2CuO_4 System

Venugopalan Anbarasu, Appasamy Manigandan, Kandasamy Sivakumar*

Department of Physics, Anna University Chennai, Chennai, India.
Email: ksivakumar@annauniv.edu

Received March 7th, 2010; revised April 23rd, 2010; accepted May 15th, 2010.

Abstract

The substitution of Strontium on T'–structured Nd_2CuO_4 system has been carried out through solid state reaction technique. From the Powder XRD patterns, it is found that the compounds are formed in single phase and crystallizes in orthorhombic structure. The variation in lattice parameters with decreasing nature of volume of the prepared compounds confirms the incorporation of lower atomic radii Strontium in Neodymium site. Surface morphology and elemental composition studies are also carried out to know the nature of the compounds and effect of Strontium substitution in Nd_2CuO_4 system. The paramagnetic nature of all the prepared compounds has been identified through magnetization studies and the results are correlated with the electron spin resonance studies by the way of variation in resonance field and broad peak width. Increasing order of dielectric constant on higher doping concentration of Strontium and the least value of dielectric loss at higher frequencies confirms the improved surface transport properties of the prepared compounds.

***Keywords*:** *Ln_2CuO_4, Structural Analysis, Powder XRD, Dielectric Studies, Magnetization, ESR Analysis*

1. Introduction

The Ln_2CuO_4 oxides exhibit two different crystal structures with respect to the size of the Ln^{3+} ion (Ln, Lanthanide element) that differ mainly in the respective coordination number of cations. In the Nd_2CuO_4 system, two types of crystal structures are observed namely T/O and T'. The occurrence of superconductivity in the $Ln_{2-x}Ce_xCuO_{4-y}$ (Ln = Nd, Pr and Sm) family gives a new prospect for understanding the attractive forces as the valence of the Ce dopant suggests that the superconducting carriers are electrons rather than holes. In most high temperature superconducting compounds, CuO_2 layers are the fundamental structural units, in which the charge carriers responsible for superconductivity are localized. It is known that electron correlations play an important role in determining the physical properties of these materials. These correlations manifest themselves as two dimensional magnetic fluctuations, which are due to a strong super exchange interaction within the CuO_2 layers.

The magnetic properties of the Ln_2CuO_4 (Ln = Nd, Pr, Eu & Gd) compounds have attracted considerable interest since the discovery of high-temperature superconductivity in these compounds when doped by Ce [1,2]. These compounds having tetragonal type structure (T'), in which the Ln^{3+} and Cu^{2+} ions are in eightfold and fourfold coordination respectively [3,4]. The structure of compounds in the Ln_2CuO_4 (where Ln = Nd, Pr, Eu, Sm) system is similar to the compounds in the La based copper oxides [5]. The main difference arises due to the positions of the oxygen atoms, giving rise to an O_2 layer instead of the La–O layer. The most important feature of Nd based materials derives the fact that superconductivity in this system is by electron conduction or n–type rather than hole conduction as in La based superconductors. The electron conducting (n–type) compound $Nd_{1.85}Ce_{0.15}CuO_{4-y}$ with T_C = 24 K is the most studied material in this system [6]. The $Nd_{1.85}Ce_{0.15}CuO_{4-y}$ compound has the same crystal structure as of Nd_2CuO_4 [I4/mmm, a = 3.945 Å and c = 12.17 Å] but has slight variation in lattice parameters [a = 3.945 Å and c = 12.076 Å] due to the substitution of tetravalent Ce in the trivalent Nd lattice [7,8]. It is therefore of high interest to study the structural characteristics of a divalent dopant (Sr^{2+}) in Nd_2CuO_4 system and to assess influence on dielectric and magnetic properties of defective structures.

In the Nd/Ce–Cu–O system, trivalent Nd^{3+} is replaced with tetravalent Ce^{4+} element which induces n–type superconductivity and crystallizes in two different crystal structures as mentioned earlier namely T' and T/O. In the

present work, Strontium doped Nd_2CuO_4 system has been prepared by substituting Strontium (Sr^{2+}) in Neodymium (Nd^{3+}) site inducing excess number of holes in the system which leads to p–type superconductivity in the prepared compounds. Structure identification, surface morphology with composition analysis, magnetic properties, electron spin resonance and dielectric studies have been carried out and the results are discussed.

2. Experimental Model

2.1 Sample Preparation

The ceramic compounds $Nd_{2-x}Sr_xCuO_4$ (where x = 0.05 to 0.2) have been prepared by carefully mixing stoichiometric quantities of Nd_2O_3 (99.9% purity), $SrCO_3$ (99.99% purity) and CuO (99.99% purity) in an agate mortar with acetone as a mixing medium. Solid state reaction takes place during successive sintering sessions in alumina crucibles. The samples were precalcined initially at 850˚C for 24 hours and the calcined samples were once again ground thoroughly prior to heating at 900˚C for 24 hours. The final processing of sintering was done thrice at 925˚C for 24 hours to obtain homogeneity and then slow cooled at a rate of 5˚C/hour down to 300˚C. These hard sintered samples after final sintering were well ground and taken for characterization process.

2.2 Powder X – Ray Diffraction

The single phase formation of the compound was confirmed through powder XRD patterns which were recorded using PANalytical X'Pert PRO Diffractormeter with CuKα1 radiation (λ = 1.54056 Å). The diffraction data of the samples were collected with 0.02˚ 2θ steps and 1 sec count time per step for a 2θ range of 10˚ to 80˚.

2.3 SEM and EDAX

Micro structural surface morphology and elemental composition of the prepared compounds were carried out using Scanning Electron Microscope (SEM) added with Energy Dispersive X–ray Analysis (EDX) facility. In the present work, microscopic imaging and energy dispersive X–ray analysis (EDX) were simultaneously carried out using Hitachi S–3400N instrument. The surface of the pelletized compounds were focused with 5 kV accelerating voltage under high vacuum condition.

2.4 Magnetization Studies

The variation in induced magnetic moment with respect to the applied magnetic field would be identified by Vibrating sample magnetometer (VSM) for the analysis of magnetic nature of the materials. In the present work, the magnetization experiment was carried out by employing LAKESHORE Vibrating Sample Magnetometer at room temperature (300 K) to categorize the magnetic property of all the prepared compounds.

2.5 Electron Spin Resonance Studies

Interaction of unpaired electron spins with respect to the external magnetic field yields the electronic nature of the source material utilized. Electron Spin Resonance (ESR) or Electron Paramagnetic Resonance (EPR) is a sophisticated spectroscopic technique that detects free radicals of inorganic complexes by which electronic structure and magnetic nature may be identified.

In the present work, ESR measurements were carried out using Varian E-4 spectrometer having X-band frequencies (9.45 GHz). ESR spectra were recorded at room temperature and all the observations were performed with approximately 10 mW microwave power incident upon the sample cavity. The spectrometer was equipped with an electromagnet capable of producing a stable magnetic field from 0.001 T up to 0.8 T with the accuracy of 0.0001 T. The spectrum is the first derivative microwave absorption with respect to field (dP/dH). For each sample, the Hr resonant magnetic field [9] and the value of peak-to-peak line-width (ΔHpp) was computed as the difference between the extreme values H_1 and H_2 of the magnetic field (the maximum and minimum of the resonance curves, respectively). The resonant magnetic field (Hr) was computed as $(H_1+H_2)/2$. In order to make better comparative analysis the spectra were recorded by keeping the instrument settings same for all the samples.

2.6 Dielectric Studies

The study on dielectric constant with respect to the applied a.c frequency enumerates the nature of the atoms, ions and its bonding in the material. It is a measure of polarization in the medium. In the present work, HIOKI 3532–50 LCR HITESTER has been employed for the analysis of dielectric nature of the prepared compounds in pelletized form at room temperature condition with in the frequency range of 50 Hz to 5 MHz. Silver electrode pasting has been incorporated for to improve the surface conductivity of the prepared samples.

3. Results and Discussion

3.1 Powder X–ray Diffraction Analysis

The observed powder X–ray diffraction patterns of the prepared polycrystalline samples Nd_2CuO_4, $Nd_{1.95}Sr_{0.05}CuO_{4-y}$, $Nd_{1.9}Sr_{0.1}CuO_{4-y}$, $Nd_{1.85}Sr_{0.15}CuO_{4-y}$ and $Nd_{1.8}Sr_{0.2}CuO_{4-y}$ are shown in **Figure 1(a)** which reveals the single phase formation of the prepared compounds. Lattice parameters of the compounds were calculated through AUTOX–93, a program for auto indexing reflections from multiphase polycrystals [10]. The comparison of lattice parameters observed for the prepared compounds with the parent compound is given in **Table 1**. The calculated unit cell parameters shows that the crystal structure of all the pre-

pared compounds vary from the parent tetragonal structure to orthorhombic with least difference in magnitudes. **Figures 1(b)** and **1(c)** show the shift in the higher intensity peaks of the prepared compounds with the formation of newer peaks (marked in * symbol) which reveals variation in the crystal system and lattice parameters of the prepared compounds. Due to the substitution of lower atomic radii element (Sr – 2.45 Å) in the higher atomic radii element site (Nd – 2.64 Å), the volume of the prepared compounds decreases with respect to the parent compound. Hence from the XRD patterns, it may be concluded that the Neodymium site is partly replaced with the Strontium atom.

3.2 Surface Morphology and Elemental Analysis

The surface morphology and crystallization nature of the samples were analyzed by scanning electron microscope images and the observed images for the prepared compounds are shown in **Figure 2**. In the present work, the pelletized samples annealed at 925˚C were used for the surface morphology analysis.

The images of the inner portion of the pellets show that all the compounds have regular crystallites with the size in the micrometer range. The regular arrangement of particles reveals that the compounds were formed in well crystalline nature without clustering. Some amount of agglomeration of particles in the parent compound may be due to low melting point of the same as compared with Strontium substituted compounds. The elemental composition analysis confirms the presence of Strontium in the host matrix of Nd_2CuO_4 system with increasing concentrations in the samples. The decrease in the concentration of Nd reveals the replacement of trivalent Neodymium with divalent Strontium element.

3.3 Magnetization Analysis

The observed magnetization nature of the prepared compounds is shown in **Figure 3**. It is observed that the intensity of magnetization varies linearly with the applied magnetic field for all the prepared compounds which reveals the paramagnetic nature of the resultant

Table 1. Comparative statement of lattice parameters observed for parent and substituted compounds

Compound	a (Å)	b (Å)	c (Å)	Volume ($Å^3$)	System*
Nd_2CuO_4	3.945	3.945	12.17	189.2	T
$Nd_{1.95}Sr_{0.05}CuO_{4-y}$	3.945(3)	3.927(6)	12.16(1)	188.6	O
$Nd_{1.9}Sr_{0.1}CuO_{4-y}$	3.826(5)	3.943(3)	12.19(1)	184.1	O
$Nd_{1.85}Sr_{0.15}CuO_{4-y}$	3.832(3)	3.946(2)	12.18(6)	184.3	O
$Nd_{1.8}Sr_{0.2}CuO_{4-y}$	3.897(6)	3.901(6)	12.09(1)	183.9	O

* T – Tetragonal and O – Orthorhombic

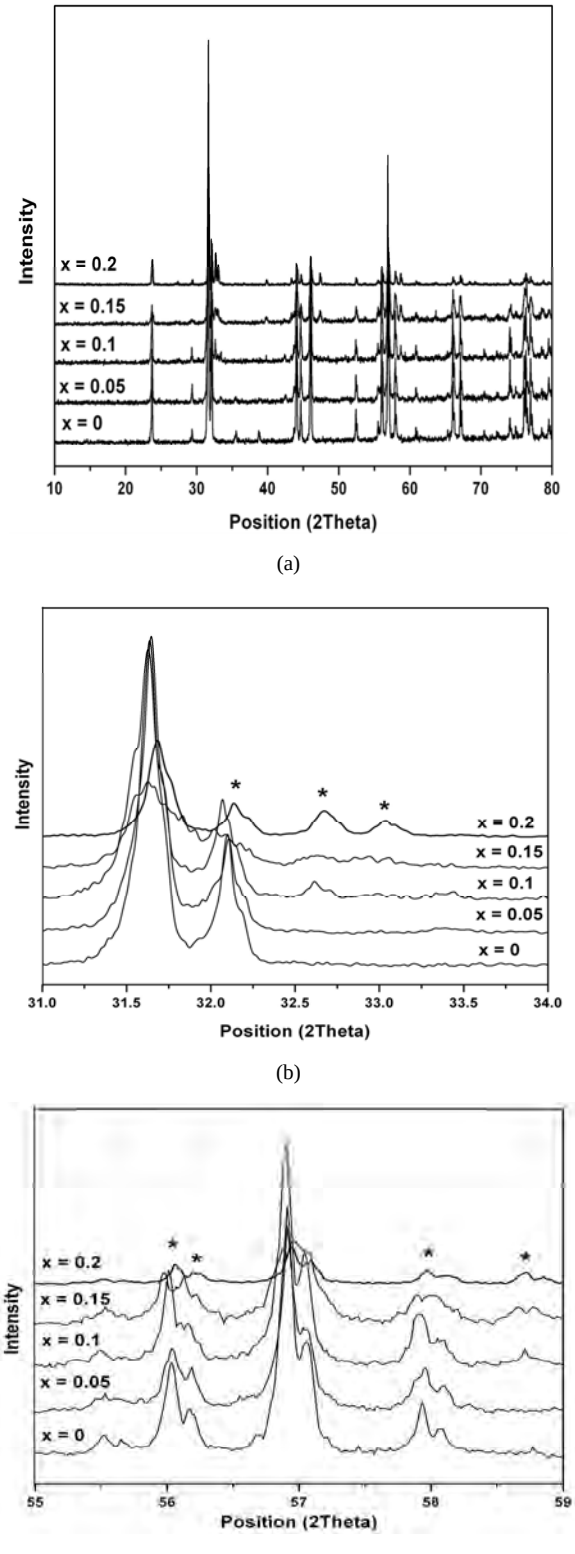

Figure 1. (a) Powder X–Ray Diffraction patterns of the prepared compounds; (b) Comparison of diffraction patterns of the major intensity peak; (c) Comparison of diffraction patterns of the 50% intensity peak

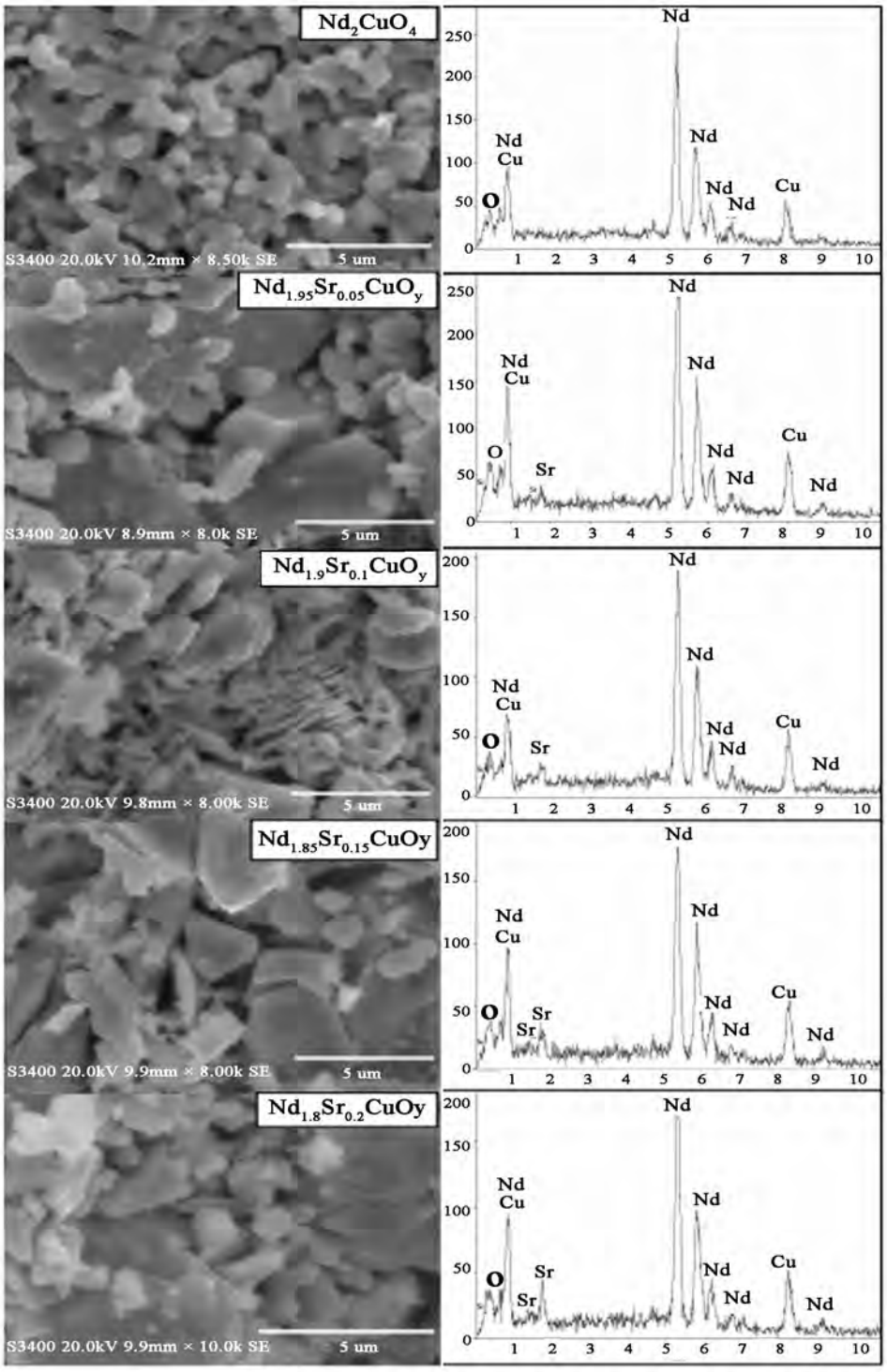

Figure 2. Surface Morphology and EDX spectrum of the prepared compounds

compounds [11,12]. In the earlier reports, it is identified that the parent compound Nd_2CuO_4 exhibits paramagnetic nature [13] and the same is obtained for both parent and prepared compounds now. The net magnetic moment attained by the prepared compounds is in very minimal level (memu/g) which exhibits the least possible magnetization of the prepared compounds and not more significant changes on the magnetization nature are observed on substitution of Strontium in Neodymium site. Hence it is confirmed that all the prepared compounds

are exhibiting paramagnetic nature at room temperature.

3.4 ESR Analysis

Figures 4(a) and **4(b)** show the room-temperature X-band (9.45 GHz) ESR spectra of Nd_2CuO_4 samples with four different concentrations of Strontium. The room temperature ESR spectrum shows an intense resonance signal for the Nd_2CuO_4 and $Nd_{1.95}Sr_{0.05}CuO_{4-y}$ compounds with both peak to peak line width (ΔH_{PP}) and resonance field (H_r) that vary depending on the samples. The line width of the samples was calculated as 0.2852T and 0.2892T for the samples Nd_2CuO_4 and $Nd_{1.95}Sr_{0.05}CuO_{4-y}$ respectively. The Lande factor of the samples with sharp resonance is calculated and the values are 2.37 and 2.33 for Nd_2CuO_4 and $Nd_{1.95}Sr_{0.05}CuO_{4-y}$ respectively. The samples with an effective g value of around 2 shows the paramagnetic behavior which has a good agreement with results obtained from magnetic measurements (M vs H curves). Other three samples with higher Strontium concentration show no resonance absorption bands. But the intensity remains constant up to 3000 Gauss and then decreases exponentially. This condition implies the least magnetization nature of the prepared samples. The variation in ΔH_{PP} with respect to Strontium substitution in the parent system may be due to the presence of inhomogeneities and differences in the chemical composition or in the oxygen stoichiometry [14,15].

3.5 Dielectric Analysis

The dielectric studies have been carried out for the parent and the strontium substituted compounds. This study gives experimental values such as capacitance at parallel and dielectric loss for the frequency range between 50 Hz to 5 MHz at the room temperature for the analysis of

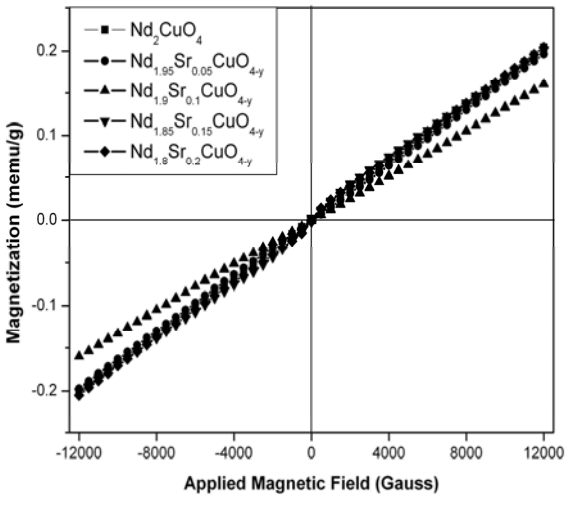

Figure 3. Magnetization nature of the prepared compounds

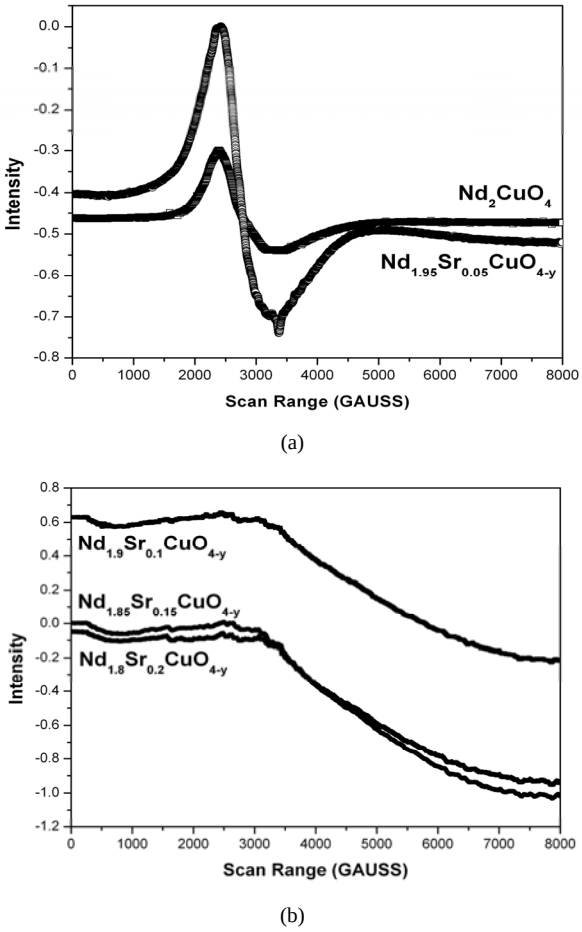

Figure 4. Electron Spin Resonance nature of the prepared compounds

dielectric behaviour of the prepared compounds. The dielectric constant was calculated from the formula; $\varepsilon_r = (C_P\ d)/(\varepsilon_0\ A)$ where C_P is the capacitance in parallel (F), d is the thickness of the pellet (m) and A is the cross sectional area of the pellet (m^2).

The plots of logf versus dielectric constant and dielectric loss have been drawn (**Figures 5(a)** and **5(b)**). It is observed that the parent compound has the highest dielectric constant values than the strontium substituted compounds. It may due to the fact of introduction of holes in the host Nd_2CuO_4 system. At the same time, increasing order of dielectric constant on higher doping concentration of strontium shows the improved surface transport properties. The high value of dielectric constant at low frequencies may be associated with the establishment of polarizations namely; space charge, orientational, electronic and ionic polarization. The low value of dielectric constant at higher frequencies may be due to the loss of significance of these polarizations gradually. The

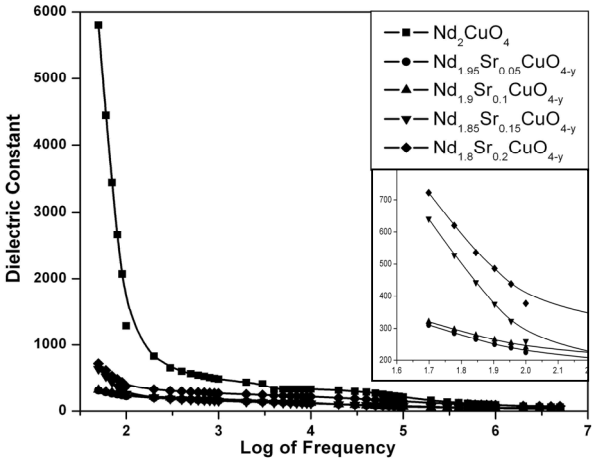

(a)

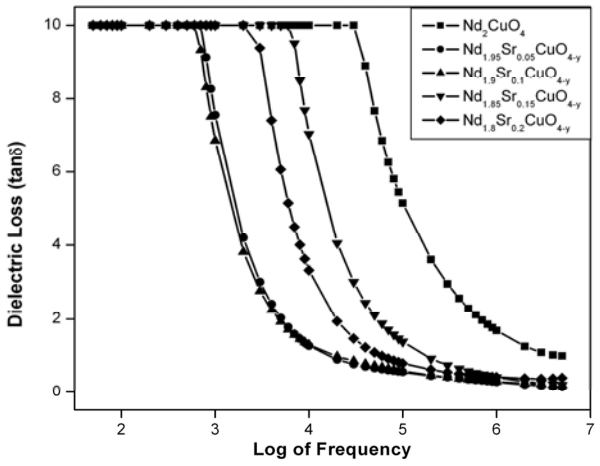

(b)

Figure 5. (a) Plots of dielectric constant of the prepared compounds; (b) Plots of dielectric loss of the prepared compounds

frequency dependence of dielectric loss exhibits interesting results. At the lower frequencies, the dielectric loss reaches the instrumental saturation value (tan δ = 9.9999) but at higher frequencies the value drops down from this saturation drastically. The low value of dielectric loss at higher frequencies implies that all the samples possess superior optical quality and shows the possibility of using the prepared compounds for high frequency applications.

4. Conclusions

In the present work, the effect of partial substitution on Neodymium site in Nd_2CuO_4 system with Strontium was carried out. The ceramic compounds Nd_2CuO_4, $Nd_{1.95}Sr_{0.05}CuO_{4-y}$, $Nd_{1.9}Sr_{0.1}CuO_{4-y}$, $Nd_{1.85}Sr_{0.15}CuO_{4-y}$ and $Nd_{1.8}Sr_{0.2}CuO_{4-y}$ were prepared by solid state reaction technique with high purity chemicals. Structural characterization was carried out by using powder X–ray diffraction technique and it was found that the parent compound crystallized in tetragonal structure and the other newly prepared compounds were crystallized in orthorhombic structure. Surface morphology confirms the high crystalline nature of the prepared compounds whereas increasing order of Strontium in the Nd_2CuO_4 system is confirmed through elemental compositions using energy dispersive analysis. The magnetic nature of the compounds was identified with vibrating sample magnetometer and it was found that both parent and prepared compounds exhibit paramagnetic nature at room temperature. Increasing concentration of Strontium in the Nd_2CuO_4 system results in the decrease in net magnetization of all the prepared compounds. The same results are also identified in the electron paramagnetic resonance studies through the least resonance absorption intensity of the parent and the prepared compounds. Increase in dielectric constant on higher doping concentration confirms the incorporation of Strontium in the Nd_2CuO_4 system and the least value of dielectric loss at higher frequencies confirms the improved surface transport properties of the prepared compounds.

REFERENCES

[1] Y. Tokura, H. Takagi and S. Uchida,"A Superconducting Copper Oxide Compound with Electrons as the Charge Carriers," *Nature*, Vol. 337, 1989, pp. 345-347.

[2] H. Takagi, S. Uchida and Y. Tokura, "Superconductivity Produced by Electron Doping in CuO_2-Layered Com-Pounds," *Physical Review Letters*, Vol. 62, No. 10, 1989, pp. 1197-1200.

[3] H. Muller-Buschbaum and W. Z. Wollschlager, "Über Ternäre Oxocuprate. VII. Zur Kristallstruktur von Nd_2CuO_4," *Zeitschrift für Anorganische und Allgemeine Chemie*, Vol. 414, 1975, pp. 76-80.

[4] H. Muller-Buschbaum and W.Z. Wollschlager, "Über Oxocuprate. XV Zur Kristallstruktur von Seltenerd Metal Oxocupraten: La_2CuO_4, Gd_2CuO_4," *Zeitschrift für Anorganische und Allgemeine Chemie*, Vol. 428, 1975, pp. 120-124.

[5] T. V. Ramakrishnan and C. N. R. Rao, "Superconductivity Today–An Elementary Introduction," 2nd Edition, Universites Press (India), Hyderabad, 1999, pp. 26-54.

[6] G. H. Kwei, S. W. Cheong, Z. Fisk, F. H. Garzon, J. A. Goldstone and J. D. Thompson, "Structure and Oxygen Stoichiometry for the Electron-Doped Cuprate Superconductor $Nd_{1.85}Ce_{0.15}CuO_{4-d}$," *Physical Review B*, Vol. 40, 1989, pp. 9370-9373.

[7] X. Zhang, C. R. A. Catlow, S. C. Parker and A. Wall, "Simulation Study of Pressure-Induced Structural Changes in La_2CuO_4 and in $La_{1.83}Sr_{0.17}CuO_4$," *Journal of Physics*

and Chemistry of Solids, Vol. 53, No. 6, 1992, pp. 761-770.

[8] E. F. Paulus, I. Yehia, H. Fuess, J. Rodriguez, T. Vogt, J. Ströbel, M. Klauda and G. Saemann-Ischenko, "Crystal Structure Refinement of $Nd_{2-x}Ce_xCuO_{rm4}$ (x = 0.05−0.30) by X-Ray (295 K) and Neutron (1.5 K) Powder Diffraction," *Solid State Communications*, Vol. 73, No. 11, 1990, pp. 791-795.

[9] J. F. Raber, "Experimental Methods in Polymer Chemistry–Physical Principal and Applications," John Wiley, New York, 1980, pp. 332-352.

[10] V. B. Zlokazov, "AUTOX–A Program for Autoindexing Reflections from Multiphase Polycrystals," *Computer Physics Communications*, Vol. 85, No. 3, 1995, pp. 415-422.

[11] O. D. Jayakumar, I. K. Gopalakrishnan and S. K. Kulshreshtha, "The Structural and Magnetization Studies of Co-Doped ZnO Co-Doped with Cu: Synthesized by Co-Precipitation Method," *Journal of Materials Chemistry*, Vol. 15, No. 34, 2005, pp. 3514-3518.

[12] O. D. Jayakumar, I. K Gopalakrishnan, and S. K. Kulshreshtha, "On the Room Temperature Ferromagnetism of Mn Doped ZnO," *Physica B*, Vol. 381, No. 1-2, 2006, pp. 194-198.

[13] H. Samata, T. Komiyama, S. Tsuboi, Y. Nagata, T. Uchid, M. Ohtsuk and M. Der Lan, "Electrochemical Crystal Growth of Superconducting Cuprates," *Journal of Physics and Chemistry of Solids*, Vol. 58, No. 10, 1997, pp. 1547-1552.

[14] J. A. Olarte, L. C. Moreno and A. Mariño, "Susceptibility and EPR Studies of $LaMn_{x-1}Co_xO_3$ Synthesized by Citrate Precursor Method," *Microelectronics Journal*, Vol. 39, No. 11, 2008, pp. 1245-1247.

[15] S. Angappane, M. Pattabiraman, G. Rangarajan, K. Sethupathi, B. Varghese and V. S. Sastry, "ESR Study of Spin–Lattice Correlated Clusters in Single Crystalline $Nd_{0.7}Sr_{0.3}MnO_3$," *Journal of Physics*: *Condensed Matter*, Vol. 19, 2007, pp. (036207)1-16.

J. Modern Physics, **2010, 1, 100-107**
doi:10.4236/jmp.2010.12015 Published Online June 2010 (http://www.SciRP.org/journal/jmp)

A Second-Order Eigen Theory for Static Electromagnetic Fields

Shaohua Guo

School of Civil Engineering and Architecture, Zhejiang University of Science and Technology, Hangzhou, China
Email: gsh606@yahoo.com.cn

Received March 28th, 2010; revised May 1st, 2010; accepted May 20th, 2010

Abstract

The static electromagnetic fields are studied here based on the standard spaces of the physical presentation, and the modal equations of static electromagnetic fields for anisotropic media are deduced. By introducing a set of new potential functions of order 2*, several novel theoretical results were obtained: The classical potential functions of order* 1 *can be expressed by the new potential functions of order* 2*, the electric or magnetic potentials are scalar for isotropic media, and vector for anisotropic media. The amplitude and direction of the vector potentials are related to the anisotropic subspaces. Based on these results, we discuss the laws of static electromagnetic fields for anisotropic media.*

***Keywords*:** *Anisotropic Media, Static Electromagnetic Field, Standard Spaces, Modal Equation Formatting*

1. Introduction

By the Maxwell's electromagnetic field equations, we know that the electric and magnetic field are independent each other under the condition of static fields. The classical electromagnetic field theory also believes that the static electric field can be described by a scalar potential function, and the magnetic field by a vector one. Furthermore, for the passive region, the magnetic field can also be described by a scalar potential function [1,2]. But it should be pointed out that these results can only be obtained in the condition of isotropy, and are also only suit for the isotropic media. However, with the development of material science, more and more anisotropic dielectric or magnetic materials are applied to various fields, such as electron devices, communications and sensors, even for the traditional geological structure, we also can see the electrically anisotropic media or magnetically anisotropic media. It is found by recent research works that the limitations of classical static electromagnetic field theory have become obvious for these anisotropic media. For example, the above results for isotropic media don't exist for anisotropic media, even we don't know the definite form of the electric field potential function or magnetic field potential function, which make a great difficulty in solving the problem of anisotropic static electric or magnetic fields [3-5]. Unlike the classical static electromagnetic field theory, which studies the Maxwell's equations under the geometric representation, in this paper, the Maxwell's equations are restudied under the physical representation. As the result of this, the modal equations of static electric or magnetic fields are deduced, which give the novel expressions for the potential functions of static electric or magnetic fields for anisotropic media, and bring to light the intrinsic laws of static electromagnetic field.

2. Standard Spaces of Electromagnetic Media

In anisotropic electromagnetic media, the dielectric permittivity and magnetic permeability are tensors instead of scalars. The constitutive relations are expressed as follows

$$D = \varepsilon \times E \tag{1}$$

$$B = \mu \times H \tag{2}$$

where the dielectric permittivity matrix ε and the magnetic permeability matrix μ are usually symmetric ones, and the elements of the matrixes have a close relationship with the selection of reference coordinate. Suppose that if the reference coordinates is selected along principal axis of electrically or magnetically anisotropic media, the elements at non-diagonal of these matrixes turn to be zero. Therefore, Equations (1) and (2) are called the constitutive equations of electromagnetic media under the geometric presentation. Now we intend to get rid of effects of geometric coordinate on the constitutive

equations, and establish a set of coordinate-independent constitutive equations of electromagnetic media under physical presentation. For this purpose, we solve the following problems of eigen-value of matrixes

$$\left(\varepsilon - \lambda I\right) j = 0 \tag{3}$$

$$\left(\mu - \gamma I\right) \varphi = 0 \tag{4}$$

where $\lambda_i \left(i = 1,2,3\right)$ and $g_i \left(i = 1,2,3\right)$ are respectively eigen dielectric permittivity and eigen magnetic permeability, which are constants of coordinate-independent. $j_i \left(i = 1,2,3\right)$ and $\varphi_i \left(i = 1,2,3\right)$ are respectively eigen electric vector and eigen magnetic vector, which show the electrically principal direction and magnetically principal direction of anisotropic media, and are all coordinate-dependent. We call these vectors as standard spaces. Thus, the matrix of dielectric permittivity and magnetic permeability can be spectrally decomposed as follows

$$\varepsilon = \Phi \Lambda \Phi^{\mathrm{T}} \tag{5}$$

$$\mu = \Psi \Pi \Psi^{\mathrm{T}} \tag{6}$$

where $\Lambda = diag\left[\lambda_1, \lambda_2, \lambda_3\right]$ and $\Pi = diag\left[\gamma_1, \gamma_2, \gamma_3\right]$ are the matrix of eigen dielectric permittivity and eigen magnetic permeability, respectively. $\Phi = \left\{j_1, j_2, j_3\right\}$ and $\Psi = \left\{\varphi_1, \varphi_2, \varphi_3\right\}$ are respectively the modal matrix of electric media and magnetic media, which are both orthogonal and positive definite ones, and satisfy $\Phi^T \Phi = I$, $\Psi^T \Psi = I$.

Projecting the electromagnetic physical qualities of the geometric presentation, such as the electric field intensity vector E, magnetic field intensity vector H, magnetic flux density vector B and electric displacement vector D, into the standard spaces of the physical presentation, we get

$$D_i^* = j_i^{\mathrm{T}} \times D \qquad i = 1,2,3 \tag{7}$$

$$E_i^* = j_i^{\mathrm{T}} \times E \qquad i = 1,2,3 \tag{8}$$

$$B_i^* = \varphi_i^{\mathrm{T}} \times B \qquad i = 1,2,3 \tag{9}$$

$$H_i^* = \varphi_i^{\mathrm{T}} \cdot H \qquad i = 1,2,3 \tag{10}$$

These are the electromagnetic physical qualities under the physical presentation.

Substituting Equations (7)-(10) into Equations (1) and (2) respectively, and using Equations (5) and (6) yield, we have

$$\left\{D^*\right\} = \left[\Lambda\right]\left\{E^*\right\} \tag{11}$$

$$\left\{B^*\right\} = \left[\Pi\right]\left\{H^*\right\} \tag{12}$$

or

$$D_i^* = \lambda_i E_i^* \qquad i = 1,2,3 \tag{13}$$

$$B_i^* = \gamma_i H_i^* \qquad i = 1,2,3 \tag{14}$$

The above equations are just the modal constitutive equations in the form of scalar.

3. Matrix form of Static Electromagnetic Field Equation

The classical static Maxwell's equations in passive region can be written as

$$\nabla \times E = 0,\ \nabla \cdot D = 0 \tag{15}$$

$$\nabla \times H = 0,\ \nabla \cdot B = 0 \tag{16}$$

where ∇ is a Hamilton operator. It is seen from the above equations that the electric field and magnetic field are not only independent, but also the same in the form of equation. So, it is undistinguishable to study the problems of electric field or magnetic field under the static condition. For this purpose, we consider here only the problem of electric field.

From Equation (15), we can see that one is a vector equation, another is scalar one. It is well known that the vector equation can be written as the matrix one, but the scalar equation can not. By the first one of Equation (15), we have

$$\left[\partial\right]\left\{E\right\} = 0 \tag{17}$$

where

$$\left[\partial\right] = \begin{bmatrix} 0 & -\partial_z & \partial_y \\ \partial_z & 0 & -\partial_x \\ -\partial_y & \partial_x & 0 \end{bmatrix} \tag{18}$$

It is an operator matrix of order 1.

In order get the matrix expression of static electromagnetic equations, both of Equation (15) should be reformed in a suitable form.

For dynamic electromagnetic fields, a matrix equation of electromagnetic waves be dedued by author [6]

$$\left[\Delta\right]\left\{E\right\} = -\nabla_t^2 \left[\mu\right]\left[\varepsilon\right]\left\{E\right\} \tag{19}$$

where

$$\left[\Delta\right] = \left[\partial\right]\left[\partial\right] = \begin{bmatrix} -\left(\partial_{zz} + \partial_{yy}\right) & \partial_{xy} & \partial_{xz} \\ \partial_{yx} & -\left(\partial_{xx} + \partial_{zz}\right) & \partial_{yz} \\ \partial_{zx} & \partial_{zy} & -\left(\partial_{xx} + \partial_{yy}\right) \end{bmatrix} \tag{20}$$

It is an operator matrix of order 2. For static electromag-netic fields, we have

$$\left[\Delta\right]\left\{E\right\} = 0 \tag{21}$$

Now, rewriting the second one of Equation (15) in the

index form of tensor

$$D_{i'i} = 0 \tag{22}$$

Differentiating the above equation with index j, it become a vectorial one

$$D_{i'ij} = 0 \tag{23}$$

Rewritting it in the matrix form, we get

$$[\nabla]\{D\} = 0 \tag{24}$$

where

$$[\nabla] = \begin{bmatrix} \partial_{11} & \partial_{21} & \partial_{31} \\ \partial_{12} & \partial_{22} & \partial_{32} \\ \partial_{13} & \partial_{23} & \partial_{33} \end{bmatrix} \tag{25}$$

In this paper, $[\Delta]$ and $[\nabla]$ is defined as the matrix of electic intensity and electic displacement operators respectively

4. Eigen Equations of Static Electric Fields

Now, we transform the matrix equations of static electric field into modal ones.

Substituting Equation (7) into Equation (21), and multiplying it with the transpose of modal matrix in left, we have

$$[\Phi]^T [\Delta][\Phi]\{E^*\} = 0 \tag{26}$$

It be proved [6] that the matrix of electric intensity operator can also be spectrally decomposed, that is

$$[\Phi]^T [\Delta][\Phi] = [\Delta^*] \tag{27}$$

Thus, Equation (26) can be uncoulped and become

$$[\Delta^*]\{E^*\} = 0 \tag{28}$$

or

$$\Delta_i^* E_i^* = 0 \qquad i = 1,2,3 \tag{29}$$

in which

$$\Delta_i^* = \{\partial_i^*\}^T \cdot \{\partial_i^*\} \qquad i = 1,2,3 \tag{30}$$

where

$$\{\partial_i^*\} = \{\phi_i\}^T [\partial]\{\phi_i\} \tag{31}$$

In same way, substituting Equation (7) into Equation (24), and multiplying it with the transpose of modal matrix in left, we have

$$[\Phi]^T [\nabla][\Phi]\{D^*\} = 0 \tag{32}$$

let

$$[\Phi]^T [\nabla][\Phi] = [\nabla^*] \tag{33}$$

and substituting Equation (11) into Equation (32),we have

$$[\nabla^*][\Lambda]\{E^*\} = 0 \tag{34}$$

Comparing Equation.(34) with Eq.(28) ,we get

$$[\nabla^*][\Lambda] = [\Delta^*] \tag{35}$$

It is seen that $[\nabla^*]$ is also a diagonal matrix. We call it as eigen matrix of electric displacement operator. Thus, we have

$$\nabla_i^* D_i^* = 0 \qquad i = 1,2,3 \tag{36}$$

So, Equations (29) and (36) constitute of the eigen equations of static electric field. Different from the classical ones, they show the simplicity and symmetry of static electromagnetic law.

5. General Solution of Eigen Equations of Static Electric Fields

Let

$$E_i^* = \nabla_i^* \chi_i \qquad i = 1,2,3 \tag{37}$$

$$D_i^* = \Delta_i^* \chi_i \qquad i = 1,2,3 \tag{38}$$

where $\{\chi\}$ is an unknown row vector, which is new electric potential function of order 2.

Substituting Equations (37) and (38) into Equations (29) and (36) respectively, a unified equation are obtained as follows

$$\square_i^* \chi_i^* = 0 \qquad i = 1,2,3 \tag{39}$$

where, $\square_i^* = \Delta_i^* \cdot \nabla_i^* (i = 1,2,3)$ is i th modal operator of electric field, and a differential operator of order 4. Deferent from the Laplce's equation for the classical electric potential function of order 1, the new electric potential function of order 2 can be solved by the modal differential equation of higher order, and the classical electric potential function of order 1 can be expressed by the new electric potential function of order 2. Once the modal potential functions are solved from Equation (41), the electric intensity and electric displacement can be obtained by the following conversion

$$\{\boldsymbol{E}\} = \{\phi_1\}\nabla_1^* \chi_1 + \{\phi_2\}\nabla_2^* \chi_2 + \{\phi_3\}\nabla_3^* \chi_3 \tag{40}$$

$$\{\boldsymbol{D}\} = \{\phi_1\}\lambda_1 \nabla_1^* \chi_1 + \{\phi_2\}\lambda_2 \nabla_2^* \chi_2 + \{\phi_3\}\lambda_3 \nabla_3^* \chi_3 \tag{41}$$

In order to get the classical electric potential function of order 1, we rewritting Equation (40) by using Equations (30) and (35)

$$\{\boldsymbol{E}\} = \sum_i \{\phi_i\}\{\partial_i^*\}^T \{\partial_i^*\}\chi_i = \sum_i \{\partial_i^*\}\left(\{\phi_i\}\{\partial_i^*\}^T \chi_i\right) \tag{42}$$

let

$$\psi_i = -\{\phi_i\} \cdot \{\partial_i^*\}^T \chi_i \tag{43}$$

It is just the electric potential function of order 1 for anisotropic media. Thus the electric intensity and electric displacement can be expressed by the electric potential function of order 1 as follows

$$\{\boldsymbol{E}\} = -\{\partial_1^*\}\psi_1 - \{\partial_2^*\}\psi_2 - \{\partial_3^*\}\psi_3 \tag{44}$$

$$\{\boldsymbol{D}\} = -\{\partial_1^*\}\lambda_1\psi_1 - \{\partial_2^*\}\lambda_2\psi_2 - \{\partial_3^*\}\lambda_3\psi_3 \tag{45}$$

6. The Modal Boundary Condition of Static Electric Field

It is seen from above that in order to get the solutions of the electric intensity and electric displacement, we can turn to solving the modal potential functions. So, the modal Equation (39) should have the corresponding modal boundary condition.

An effective boundary case is: Electric displacement functions of two side of interface should be equal

$$\{D^{(1)}\} = \{D^{(2)}\} \tag{46}$$

or

$$D_i^{(1)} = D_i^{(2)} \qquad i = 1,2,3 \tag{47}$$

Rewriting Equation (46) in the modal form, we have

$$[\Delta^{(1)*}]\{\chi^{(1)*}\} = [\Delta^{(2)*}]\{\chi^{(2)*}\} \tag{48}$$

or

$$\Delta_i^{(1)*}\chi_i^{(1)*} = \Delta_i^{(2)*}\chi_i^{(2)*} \qquad i = 1,2,3 \tag{49}$$

and

$$\lambda_i^{(1)}\nabla_i^{(1)*}\chi_i^{(1)*} = \lambda_i^{(2)}\nabla_i^{(2)*}\chi_i^{(2)*} \qquad i = 1,2,3 \tag{50}$$

7. Application

In this section, we discuss the laws of static electric field only in anisotropic dielectrics.

7.1. Isotropic Crystal

The matrix of dielectric permittivity of isotropic dielectrics is following

$$\boldsymbol{\varepsilon} = \begin{bmatrix} \varepsilon_{11} & 0 & 0 \\ 0 & \varepsilon_{11} & 0 \\ 0 & 0 & \varepsilon_{11} \end{bmatrix} \tag{51}$$

The eigen-values and eigen-vectors are respectively shown as below

$$\boldsymbol{\Lambda} = diag[\varepsilon_{11}, \varepsilon_{11}, \varepsilon_{11}] \tag{52}$$

$$\boldsymbol{\Phi} = \begin{bmatrix} 1 & 0 & 0 \\ 0 & 1 & 0 \\ 0 & 0 & 1 \end{bmatrix} \tag{53}$$

We can see from the above equations that there is only one eigen-space in isotropic crystal, which is a triple-degenerate one, and the space structure is following

$$\boldsymbol{W} = W_1^{(3)}[\phi_1, \phi_2, \phi_3] \tag{54}$$

The basic vector of one dimension in a triple-degenerate subspace is

$$\boldsymbol{\phi}_1^* = \frac{\sqrt{3}}{3}\{1,1,1\}^T \tag{55}$$

The eigen electric displacement operator of isotropic crystal are

$$\nabla_1^* = \frac{1}{3}\left(\partial_1^2 + \partial_2^2 + \partial_3^2\right) \tag{56}$$

$$\{\partial_1^*\} = \frac{\sqrt{3}}{3}\{\partial_1, \partial_2, \partial_3\} \tag{57}$$

Therefore, the static electric field equation in isotropic crystal can be written as below

$$\left(\partial_x^2 + \partial_y^2 + \partial_z^2\right)^2 \chi_1 = 0 \tag{58}$$

Thus, the electric strength and electric displacement of isotropic crystal become

$$\{E\} = \{\phi_1\}\nabla_1^*\chi_1 = \left(\partial_1^2 + \partial_2^2 + \partial_3^2\right)\begin{Bmatrix} 1 \\ 1 \\ 1 \end{Bmatrix}\chi_1 \tag{59}$$

$$\{\boldsymbol{D}\} = \{\phi_1\}\lambda_1\nabla_1^*\chi_1 = \varepsilon_{11}\left(\partial_1^2 + \partial_2^2 + \partial_3^2\right)\begin{Bmatrix} 1 \\ 1 \\ 1 \end{Bmatrix}\chi_1 \tag{60}$$

The classical electric potential function of order 1 is

$$\psi_1 = -\left(\partial_1 + \partial_2 + \partial_3\right)\chi_i \tag{61}$$

So, the electric intensity and electric displacement of isotropic crystal can also be expressed by the classical electric potential function of order 1 as follows

$$\{E\} = -\begin{Bmatrix} \partial_x \\ \partial_y \\ \partial_z \end{Bmatrix}\psi_1 \tag{62}$$

or

$$\boldsymbol{E} = -\nabla\psi_1 \tag{63}$$

$$\{D\} = -\varepsilon_{11}\begin{Bmatrix}\partial_x\\ \partial_y\\ \partial_z\end{Bmatrix}\psi_1 \tag{64}$$

or

$$\boldsymbol{D} = -\varepsilon_{11}\boldsymbol{\nabla}\psi_1 \tag{65}$$

It is seen that Equations (62)-(65) are the same as the classical results, in which the electric potential is a scalar. But from the following analysis, we will see that only for isotropy we have same results as classical theory.

7.2. Uniaxial Crystal

The matrix of dielectric permittivity of uniaxial dielectrics is following

$$\boldsymbol{\varepsilon} = \begin{bmatrix}\varepsilon_{11} & 0 & 0\\ 0 & \varepsilon_{11} & 0\\ 0 & 0 & \varepsilon_{33}\end{bmatrix} \tag{66}$$

The eigen-values and eigen-vectors are respectively shown as below

$$\boldsymbol{\Lambda} = diag\left[\varepsilon_{11}, \varepsilon_{11}, \varepsilon_{33}\right] \tag{67}$$

$$\boldsymbol{\Phi} = \begin{bmatrix}1 & 0 & 0\\ 0 & 1 & 0\\ 0 & 0 & 1\end{bmatrix} \tag{68}$$

We can see from the above equations that there are two eigen-spaces in uniaxial crystal, one of which is a double-degenerate space, and the space structure is following

$$\boldsymbol{W} = W_1^{(2)}\left[\phi_1, \phi_2\right] \oplus W_2^1\left[\phi_3\right] \tag{69}$$

The basic vectors in two subspaces are following

$$\boldsymbol{\phi}_1^* = \frac{\sqrt{2}}{2}\{1,1,0\}^T \tag{70}$$

$$\boldsymbol{\phi}_2^* = \{0,0,1\}^T \tag{71}$$

The eigen electric strength qualities of uniaxial crystal are respectively shown as below

$$E_2^* = \boldsymbol{\phi}_2^{\mathrm{T}} \cdot \boldsymbol{E} = E_3 \tag{72}$$

$$\boldsymbol{\phi}_1^{\mathrm{T}} E_1^* = \boldsymbol{E} - \boldsymbol{\phi}_2^{\mathrm{T}} E_2^* \tag{73}$$

Multiplying Equation (57) with $\boldsymbol{\phi}_2$, using $\boldsymbol{\phi}_2^{\mathrm{T}} \cdot \boldsymbol{\phi}_1 = 0$ and $\boldsymbol{\phi}_i^{\mathrm{T}} \cdot \boldsymbol{\phi}_i = 1\ (i = 1,2)$, we get

$$\left|E_1^*\right| = \sqrt{\left(\boldsymbol{E} - \boldsymbol{\phi}_2^{\mathrm{T}} E_2^*\right)^{\mathrm{T}}\left(\boldsymbol{E} - \boldsymbol{\phi}_2^{\mathrm{T}} E_2^*\right)} = \sqrt{E_1^2 + E_2^2} \tag{74}$$

The eigen electric displacement operators of uniaxial crystal are respectively shown as below

$$\nabla_1^* = \frac{1}{2}\left(\partial_{11} + \partial_{22}\right) \tag{75}$$

$$\nabla_2^* = \partial_{33} \tag{76}$$

$$\left\{\partial_1^*\right\} = \frac{\sqrt{2}}{2}\{\partial_1, \partial_2, 0\} \tag{77}$$

$$\left\{\partial_2^*\right\} = \left\{0, 0, \partial_3\right\} \tag{78}$$

Therefore, the static electric field equation in uniaxial crystal can be written as below

$$\left(\partial_x^2 + \partial_y^2\right)^2 \chi_1^* = 0 \tag{79}$$

$$\partial_z^4 \chi_2^* = 0 \tag{80}$$

It is seen from Equations (79) and (80) that there are two static electric fields in uniaxial crystal. Thus, the electric intensity and electric displacement become

$$\begin{aligned}\{E\} &= \{\phi_1\}\nabla_1^*\chi_1 + \{\phi_2\}\nabla_2^*\chi_2\\ &= \begin{Bmatrix}1\\1\\0\end{Bmatrix}\left(\partial_{11} + \partial_{22}\right)\chi_1 + \begin{Bmatrix}0\\0\\1\end{Bmatrix}\partial_{33}\chi_2\\ &= \begin{Bmatrix}\left(\partial_{11} + \partial_{22}\right)\chi_1^*\\ \left(\partial_{11} + \partial_{22}\right)\chi_1^*\\ \partial_{33}\chi_2^*\end{Bmatrix}\end{aligned} \tag{81}$$

$$\begin{aligned}\{D\} &= \{\phi_1\}\lambda_1\nabla_1^*\chi_1 + \{\phi_2\}\lambda_2\nabla_2^*\chi_2\\ &= \begin{Bmatrix}\varepsilon_{11}\left(\partial_{11} + \partial_{22}\right)\chi_1^*\\ \varepsilon_{11}\left(\partial_{11} + \partial_{22}\right)\chi_1^*\\ \varepsilon_{33}\partial_{33}\chi_2^*\end{Bmatrix}\end{aligned} \tag{82}$$

The classical electric potential function of order 1 is

$$\psi_1 = -\frac{1}{2}\left(\partial_1 + \partial_2\right)\chi_1 \tag{83}$$

$$\psi_1 = -\partial_3\chi_2 \tag{84}$$

So, the electric intensity and electric displacement of uniaxial crystal can also be expressed by the classical electric potential function of order 1 as follows

$$\{E\} = -\begin{Bmatrix}\partial_1\psi_1\\ \partial_2\psi_1\\ \partial_3\psi_2\end{Bmatrix} \tag{85}$$

$$\{D\} = -\begin{Bmatrix}\varepsilon_{11}\partial_x\psi_1\\ \varepsilon_{11}\partial_y\psi_1\\ \varepsilon_{33}\partial_z\psi_2\end{Bmatrix} \tag{86}$$

It is seen that the electric intensity and electric displacement of uniaxial crystal are quite different from

those in isotropic crystal, and there exist two kinds of modal electric potential functions in uniaxial crystal, so they become vectorial ones, this is also different from the classical results of static electric field.

7.3. Biaxial Crystal

The matrix of dielectric permittivity of biaxial dielectrics is following

$$\boldsymbol{\varepsilon} = \begin{bmatrix} \varepsilon_{11} & 0 & 0 \\ 0 & \varepsilon_{22} & 0 \\ 0 & 0 & \varepsilon_{33} \end{bmatrix} \tag{87}$$

The eigen-values and eigen-vectors are respectively shown as below

$$\boldsymbol{\Lambda} = diag\left[\varepsilon_{11}, \varepsilon_{22}, \varepsilon_{33}\right] \tag{88}$$

$$\boldsymbol{\Phi} = \begin{bmatrix} 1 & 0 & 0 \\ 0 & 1 & 0 \\ 0 & 0 & 1 \end{bmatrix} \tag{89}$$

We can see from the above equations that there are three eigen-spaces in biaxial crystal, and the space structure is following

$$\boldsymbol{W} = W_1^{(1)}\left[\phi_1\right] \oplus W_2^{(1)}\left[\phi_2\right] \oplus W_3^{(1)}\left[\phi_3\right] \tag{90}$$

The eigen-qualities and eigen electric displacement operators of biaxial crystal are respectively shown as below

$$E_1^* = \boldsymbol{\phi}_1^{\mathrm{T}} \cdot \boldsymbol{E} = E_1 \tag{91}$$

$$E_2^* = \boldsymbol{\phi}_2^{\mathrm{T}} \cdot \boldsymbol{E} = E_2 \tag{92}$$

$$E_3^* = \boldsymbol{\phi}_3^{\mathrm{T}} \cdot \boldsymbol{E} = E_3 \tag{93}$$

$$\nabla_1^* = \partial_{11} \qquad \left\{\partial_1^*\right\} = \left\{\partial_1, 0, 0\right\}^T \tag{94}$$

$$\nabla_2^* = \partial_{22} \qquad \left\{\partial_2^*\right\} = \left\{0, \partial_2, 0\right\}^T \tag{95}$$

$$\nabla_3^* = \partial_{33} \qquad \left\{\partial_3^*\right\} = \left\{0, 0, \partial_3\right\}^T \tag{96}$$

Therefore, the static electric field equation in biaxial crystal can be written as below

$$\partial_x^4 \chi_1^* = 0 \tag{97}$$

$$\partial_y^4 \chi_2^* = 0 \tag{98}$$

$$\partial_z^4 \chi_3^* = 0 \tag{99}$$

It is seen from Equations (97)-(99) that there are three static electric fields in biaxial crystal. Thus, the electric intensity and electric displacement become

$$\begin{aligned} \{E\} &= \{\phi_1\}\nabla_1^*\chi_1 + \{\phi_2\}\nabla_2^*\chi_2 + \{\phi_3\}\nabla_3^*\chi_3 \\ &= \begin{Bmatrix} 1 \\ 0 \\ 0 \end{Bmatrix}\nabla_1^*\chi_1 + \begin{Bmatrix} 0 \\ 1 \\ 0 \end{Bmatrix}\nabla_2^*\chi_2 + \begin{Bmatrix} 0 \\ 0 \\ 1 \end{Bmatrix}\nabla_3^*\chi_3 \\ &= \begin{Bmatrix} \partial_{11}\chi_1 \\ \partial_{22}\chi_2 \\ \partial_{33}\chi_3 \end{Bmatrix} \end{aligned} \tag{100}$$

$$\{D\} = \begin{Bmatrix} \varepsilon_{11}\partial_{11}\chi_1 \\ \varepsilon_{22}\partial_{22}\chi_2 \\ \varepsilon_{33}\partial_{33z}\chi_3 \end{Bmatrix} \tag{101}$$

The classical electric potential function of order 1 is

$$\psi_1 = -\partial_1\chi_1 \tag{102}$$

$$\psi_2 = -\partial_2\chi_2 \tag{103}$$

$$\psi_3 = -\partial_3\chi_2 \tag{104}$$

So, the electric intensity and electric displacement of uniaxial crystal can also be expressed by the classical electric potential function of order 1 as follows

$$\{E\} = -\begin{Bmatrix} \partial_1\psi_1 \\ \partial_2\psi_2 \\ \partial_3\psi_3 \end{Bmatrix} \tag{105}$$

$$\{D\} = -\begin{Bmatrix} \varepsilon_{11}\partial_x\psi_1 \\ \varepsilon_{22}\partial_y\psi_2 \\ \varepsilon_{33}\partial_z\psi_3 \end{Bmatrix} \tag{106}$$

It is seen that the electric intensity and electric displacement of biaxial crystal are quite different from those in isotropic crystal, and there exist three kinds of modal electric potential functions in uniaxial crystal, so they become vectorial ones, this is also different from the classical results of static electric field.

7.4. Monoclinic Crystal

The matrix of dielectric permittivity of monoclinic dielectrics is following

$$\boldsymbol{\varepsilon} = \begin{bmatrix} \varepsilon_{11} & \varepsilon_{12} & 0 \\ \varepsilon_{12} & \varepsilon_{22} & 0 \\ 0 & 0 & \varepsilon_{33} \end{bmatrix} \tag{107}$$

The eigen-values and eigen-vectors are respectively shown as below

$$\boldsymbol{\Lambda} = diag\left[\lambda_1, \lambda_2, \varepsilon_{33}\right] \tag{108}$$

$$\begin{cases} \boldsymbol{\phi}_1 = \dfrac{\varepsilon_{12}}{\sqrt{\left(\lambda_1-\varepsilon_{11}\right)^2+\varepsilon_{12}^2}}\left[\dfrac{\lambda_1-\varepsilon_{11}}{\varepsilon_{12}},\ 1,\ 0\right]^{\mathrm{T}} \\ \boldsymbol{\phi}_2 = \dfrac{\varepsilon_{12}}{\sqrt{\left(\lambda_2-\varepsilon_{11}\right)^2+\varepsilon_{12}^2}}\left[1,\ \dfrac{\lambda_2-\varepsilon_{11}}{\varepsilon_{12}},\ 0\right]^{\mathrm{T}} \\ \boldsymbol{\phi}_3 = \left[0,\ 0,1\right]^{\mathrm{T}} \end{cases} \tag{109}$$

where

$$\lambda_{1,2} = \frac{\left(\varepsilon_{11}+\varepsilon_{22}\right)}{2} \pm \sqrt{\left[\frac{1}{2}\left(\varepsilon_{11}-\varepsilon_{22}\right)\right]^2+\varepsilon_{12}^2} \quad \lambda_3 = \varepsilon_{33} \tag{110}$$

We can see from the above equations that there are also three eigen-spaces in monoclinic crystal, and the space structure is following

$$\boldsymbol{W} = W_1^{(1)}\left[\phi_1\right] \oplus W_2^{(1)}\left[\phi_2\right] \oplus W_3^{(1)}\left[\phi_3\right] \tag{111}$$

The eigen-qualities and eigen electric displacement operators of monoclinic crystal are respectively shown as below

$$E_1^* = \boldsymbol{\phi}_1^{\mathrm{T}} \cdot \boldsymbol{E} = \frac{1}{\sqrt{\left(\lambda_1-\varepsilon_{11}\right)^2+\varepsilon_{12}^2}}\left[\left(\lambda_1-\varepsilon_{11}\right)E_1+\varepsilon_{12}E_2\right] \tag{112}$$

$$E_2^* = \boldsymbol{\phi}_2^{\mathrm{T}} \cdot \boldsymbol{E} = \frac{1}{\sqrt{\left(\lambda_2-\varepsilon_{11}\right)^2+\varepsilon_{12}^2}}\left[\varepsilon_{12}E_1+\left(\lambda_2-\varepsilon_{11}\right)E_2\right] \tag{113}$$

$$E_3^* = \boldsymbol{\phi}_3^{\mathrm{T}} \cdot \boldsymbol{E} = E_3 \tag{114}$$

$$\begin{cases} \nabla_1^* = a_1^2\partial_{11}+b_1^2\partial_{22}+2a_1b_1\partial_1\partial_2 \\ \left\{\partial_1^*\right\} = \left\{a_1\partial_1+b_1\partial_2,\ a_1\partial_1+b_1\partial_2,\ 0\right\}^T \end{cases} \tag{115}$$

$$\begin{cases} \nabla_2^* = a_2^2\partial_{11}+b_2^2\partial_{22}+2a_2b_2\partial_1\partial_2 \\ \left\{\partial_2^*\right\} = \left\{a_2\partial_1+b_2\partial_2,\ a_2\partial_1+b_2\partial_2,\ 0\right\}^T \end{cases} \tag{116}$$

$$\nabla_3^* = \partial_{33} \qquad \left\{\partial_3^*\right\} = \left\{0,0,\partial_3\right\}^T \tag{117}$$

where

$$b_i = \frac{\varepsilon_{12}}{\sqrt{\left(\lambda_i-\varepsilon_{11}\right)^2+\varepsilon_{12}^2}} \qquad a_i = b_i\frac{\lambda_i-\varepsilon_{11}}{\varepsilon_{12}} \qquad i=1,2$$

Therefore, the static electric field equation in monoclinic crystal can be written as below

$$\left(a_1^2\partial_{11}+b_1^2\partial_{22}+2a_1b_1\partial_1\partial_2\right)^2\chi_1^* = 0 \tag{118}$$

$$\left(a_2^2\partial_{11}+b_2^2\partial_{22}+2a_2b_2\partial_1\partial_2\right)^2\chi_2^* = 0 \tag{119}$$

$$\partial_z^4\chi_3^* = 0 \tag{120}$$

It is seen from Equations (118)-(120) that there exist also three static electric fields in monoclinic crystal, which is a little different from the results in biaxial crystal because of the distortion of static electric fields. Thus, the electric intensity and electric displacement become

$$\begin{aligned} \{E\} &= \{\phi_1\}\nabla_1^*\chi_1 + \{\phi_2\}\nabla_2^*\chi_2 + \{\phi_3\}\nabla_3^*\chi_3 = \\ &\begin{Bmatrix} a_1\partial_1+b_1\partial_2 \\ a_1\partial_1+b_1\partial_2 \\ 0 \end{Bmatrix}\left(a_1^2\partial_{11}+b_1^2\partial_{22}+2a_1b_1\partial_1\partial_2\right)\chi_1 \\ &+\begin{Bmatrix} a_2\partial_1+b_2\partial_2 \\ a_2\partial_1+b_2\partial_2 \\ 0 \end{Bmatrix}\left(a_2^2\partial_{11}+b_2^2\partial_{22}+2a_2b_2\partial_1\partial_2\right)\chi_2 \\ &+\begin{Bmatrix} 0 \\ 0 \\ 1 \end{Bmatrix}\partial_{33}\chi_3 \end{aligned} \tag{121}$$

$$\begin{aligned} \{D\} &= \{\phi_1\}\lambda_1\nabla_1^*\chi_1 + \{\phi_2\}\lambda_2\nabla_2^*\chi_2 + \{\phi_3\}\lambda_3\nabla_3^*\chi_3 = \\ &\begin{Bmatrix} a_1\partial_1+b_1\partial_2 \\ a_1\partial_1+b_1\partial_2 \\ 0 \end{Bmatrix}\lambda_1\left(a_1^2\partial_{11}+b_1^2\partial_{22}+2a_1b_1\partial_1\partial_2\right)\chi_1 \\ &+\begin{Bmatrix} a_2\partial_1+b_2\partial_2 \\ a_2\partial_1+b_2\partial_2 \\ 0 \end{Bmatrix}\lambda_2\left(a_2^2\partial_{11}+b_2^2\partial_{22}+2a_2b_2\partial_1\partial_2\right)\chi_2 \\ &+\begin{Bmatrix} 0 \\ 0 \\ 1 \end{Bmatrix}\lambda_3\partial_{33}\chi_3 \end{aligned} \tag{122}$$

The classical electric potential function of order 1 is

$$\psi_1 = -\left[a_1\left(a_1\partial_1+b_1\partial_2\right)+b_1\left(a_1\partial_1+b_1\partial_2\right)\right]\chi_1 \tag{123}$$

$$\psi_2 = -\left[a_2\left(a_2\partial_1+b_2\partial_2\right)+b_2\left(a_2\partial_1+b_2\partial_2\right)\right]\chi_2 \tag{124}$$

$$\psi_3 = -\partial_3\chi_3 \tag{125}$$

So, the electric intensity and electric displacement of monoclinic crystal can also be expressed by the classical electric potential function of order 1 as follows

$$\{E\} = -\begin{Bmatrix} a_1\partial_1+b_1\partial_2 \\ a_1\partial_1+b_1\partial_2 \\ 0 \end{Bmatrix}\psi_1 - \begin{Bmatrix} a_2\partial_1+b_2\partial_2 \\ a_2\partial_1+b_2\partial_2 \\ 0 \end{Bmatrix}\psi_2 - \begin{Bmatrix} 0 \\ 0 \\ \partial_3 \end{Bmatrix}\psi_3 \tag{126}$$

$$\{D\} = -\lambda_1 \begin{Bmatrix} a_1\partial_1 + b_1\partial_2 \\ a_1\partial_1 + b_1\partial_2 \\ 0 \end{Bmatrix} \psi_1 \\ -\lambda_2 \begin{Bmatrix} a_2\partial_1 + b_2\partial_2 \\ a_2\partial_1 + b_2\partial_2 \\ 0 \end{Bmatrix} \psi_2 - \varepsilon_{33} \begin{Bmatrix} 0 \\ 0 \\ \partial_3 \end{Bmatrix} \psi_3 \quad (127)$$

It is seen that the electric intensity and electric displacement of biaxial crystal are aiso quite different from those in isotropic crystal.

8. Conclusions

In this paper, we construct the standard spaces under the physical presentation by solving the eigen-value problem of the matrixes of dielectric permittivity and magnetic permeability, in which we get the eigen dielectric permittivity and eigen magnetic permeability, and the corresponding eigen vectors. The former are coordinate-independent and the latter are coordinate-dependent. Because the eigen vectors show the principal directions of electromagnetic media, they can be used as standard spaces. Based on the spaces, we get the modal equations of static electromagnetic fields by converting the classical Maxwell's vector equation to the eigen Maxwell's scalar equation, each of which shows the existence of an static electromagnetic field. For example, there is only one kind of static electromagnetic field in isotropic crystal, which is identical with the classical result; there are two kinds of static electromagnetic fields in uniaxial crystal; three kinds of static electromagnetic fields in biaxial crystal and three kinds of distorted static electromagnetic fields in monoclinic crystal. All of these new theoretical results need to be proved by experiments in the future.

After the text edit has been completed, the paper is ready for the template. Duplicate the template file by using the Save As command, and use the naming convention prescribed by your conference for the name of your paper. In this newly created file, highlight all of the contents and import your prepared text file. You are now ready to style your paper; use the scroll down window on the left of the MS Word Formatting toolbar.

REFERENCES

[1] J. Kong, "Theory of Electromagnetic Waves," Wiley-Interscience, New York, 1975.

[2] D. Frankl, "Electromagnetic Theory," Prentice-Hill, New Jersey, 1986.

[3] M. Zuniga and J. Kong, "Modified Radiative Transfer Theory for a Twolayer Random Medium," *Journal of Applied Physics*, Vol. 51, August 1987, pp. 5228-5244.

[4] V. Tamoikin, "The Average Field in a Medium Having Strong Anisotropic Inhomogeneities," *Radiophysics and Quantum Electronics*, Vol. 14, No. 2, March 1987, pp. 228-233.

[5] K. Chari and P. Silvester, "Finite Elements in Electric and Magnetic Field Problems," John Wiley and Sons, New York, 1980.

[6] S. Guo, "An Eigen Theory of Electromagnetic Waves Based on the Standard Spaces," *International Journal of Engineering Science*, Vol. 47, No. 3, May 2009, pp. 405-412.

J. Modern Physics, 2010, 1, 108-109
doi:10.4236/jmp.2010.12016 Published Online June 2010 (http://www.SciRP.org/journal/jmp)

The Empirical Rule for Calculating the Electric Charge of Elementary Particles

Aydin G. Kyazym-zade

Semiconductor Physics Department, Baku State University, Baku, Azerbaijan
E-mail: bsu_aydin@yahoo.com

Received March 28th, 2010; revised May 7th, 2010; accepted May 21st, 2010.

Abstract

The empirical rule for calculation of electric charges of the elementary particles is offered. The given rule contains two parameters: full number of colors N_c of which color of the given particle is formed and a color index L - number of colors which the given particle possesses. The offered rule allows calculating electric charges of all elementary particles - leptons, quarks and intermediate vector bosons.

Keywords: *Elementary Particles, Leptons, Quarks, Intermediate Vector Bosons*

1. Introduction

As is well known [1] without antiparticles experimentally opened 12 fermions (6 leptons and 6 quarks) and 4 intermediate vector boson: carrier of strong interactions (gluon-g), carrier of electromagnetic interactions (photon -γ), and carriers of weak interactions (the neutral weak boson Z^0 and charged weak bosons $W^{\pm}$, which are the antiparticles to each other). All these particles are elementary, *i.e.*, at the present level of knowledge they do not consist of more elementary particles. Symbols designations and electric charges Q (in units of elementary charge) of these particles are shown in **Table 1**.

In this paper we propose a generalized empirical rule for calculating the electric charges of all elementary particles - leptons, quarks and intermediate vector bosons.

2. Some Preliminary Remarks

As far as we know, currently there is no generalized rule for calculating the charge of all elementary particles, *i.e.* quarks, leptons and intermediate bosons. There is only a generalized formula of Gell-Mann-Nishidzhimy [2], whereby the electric charge of quark (in units of elementary charge) is expressed through the internal quantum numbers

$$Q = I_z + (B+S+C-b+t) \qquad (1)$$

which define the so-called flavor quark. Here, I_z - the projection of the isotopic spin I, B - baryon number, S - strangeness, C - charm, b - beauty, t - the truth quark. Doubled value of the second term $Y = B + S + C - b + t$ is called hypercharge. The values of quantum numbers and the resulting electric charge of quarks are given in **Table 2**.

In the electroweak theory introduces the concept of "weak hypercharge" Y^w distinguishing leptons left and right helicity. At the same time $Y_L^w = -1$ for the "left" leptons and $Y_R^w = -2$ for the "right" leptons. Such introduction of the weak hypercharge and the assumption

Table 1. Elementary particles

Particles		Symbols designations			Q
Leptons	upper row	ν_e	ν_μ	ν_τ	0
	bottom row	e	μ	τ	–1
Quarks	upper row	u	c	t	+2/3
	bottom row	d	s	b	–1/3
Bosons	upper row		γ, Z^0		0
	bottom row		g		0
			W		±1

Table 2. Characteristics of quarks

Aroma of quark	B	I	I_z	S	C	b	t	Q
u	1/3	1/2	+1/2	0	0	0	0	2/3
d	1/3	1/2	–1/2	0	0	0	0	1/3
c	1/3	0	0	0	1	0	0	2/3
s	1/3	0	0	-1	0	0	0	–1/3
t	1/3	0	0	0	0	0	1	2/3
b	1/3	0	0	0	0	1	0	–1/3

that the isotopic spin $I = 1/2$ for the "left" lepton and $I = 0$ for the "right" lepton can be used to calculate the charge leptons the same formula as for hadrons:

$$Q = I_z^w + \frac{Y^w}{2}, \tag{2}$$

where I_z^w — the third component "of the weak isotopic spin" of the "left" leptons ($I_z = -1/2$ for e_L^- and $I_z = 1/2$ for ν_{eL}).

In [3] proposed a formula whereby the electric charge of quark (in units of elementary charge) is expressed through the number of colors N_c:

$$Q = \frac{1}{2}\left(\frac{1}{N_c} \pm 1\right), \tag{3}$$

where the plus sign corresponds to the upper line of quarks (u, c, t) and the minus sign corresponds to the bottom line of quarks (d, s, b). Given $N_c = 3$ we obtain $Q = +2/3$ for quarks of upper line and $Q = -1/3$ for quarks of bottom line.

3. Proposal Rule

The Formula (3) allows calculating of electric charges only for quarks. We propose a generalized rule that the electric charge of quarks, leptons and intermediate bosons is expressed in terms of the number of colors N_c (which make up the color of a given particle), the color index L (number of colors which the given particle possesses) and is given (in units of elementary charge) by the formula:

$$Q = \frac{N_c - 3}{6} + \frac{1}{2}\left(\frac{L}{1 - L + N_c} \pm 1\right). \tag{4}$$

Here, L- is a certain color index, which is set $L = 1$ in the presence of one color, $L = 2$ in the presence of two color and $L=0$ in the absence of color of the particles. Plus sign corresponds to quarks and leptons of the upper line (u, c, t, ν_e, ν_μ, ν_τ), and the minus sign corresponds to quarks and leptons of the bottom line (d, s, b, e, μ, τ). If we assume that the leptons are colorless, *i.e.* for them $L = 0$ and $N_c = 0$, then from Formula (4) we obtain $Q = 0$ for leptons the upper line (plus sign) and $Q = -1$ for leptons bottom line (minus sign). For quarks $L = 1$ and $N_c = 3$. In this Formula (4) coincides with Formula (3) and for the charge of quarks we obtain the above values.

Equation (4) also allows us to calculate the electric charges of the intermediate vector bosons γ, Z^0, W^- and g. When $L = 0$ and $N_c = 0$ Formula (4) gives the value of $Q = 0$ and $Q = -1$, respectively for the intermediate bosons γ, Z^0 (plus sign) and W^- (minus sign). A gluon electric charge $Q = 0$ is obtained from (4) with the sign "minus" in parenthesis, if we assume that $L = 2$ and $N_c = 3$, since the gluon is not one, but two color index.

In conclusion, we note that the electrical charges antileptons, quarks and W^+ boson can also be calculated by Formula (4), taken with opposite sign.

REFERENCES

[1] L. B. Okun, "Current Status of Elementary Particle Physics," Physics-Uspekhi, Vol. 41, No. 6, June 1998, pp. 553-558.

[2] L. B. Okun, "Leptons and Quarks," Nauka, Moscow, 1990.

[3] R. N. Rogalev, "The Remark on Use Kiral Anomalies for Definition of Number of Colours," *Nuclear Fizika*, Vol. 66, No. 1, January 2003, pp. 195-198.

J. Modern Physics, **2010, 1, 110-123**
doi:10.4236/jmp.2010.12017 Published Online June 2010 (http://www.SciRP.org/journal/jmp)

Numerical Simulation of Near-Field Seismoacoustic Probing of a Layer Inclusion in a Homogeneous Infinite Medium

Yury Mikhailovich Zaslavsky, Vladislav Yuryevich Zaslavsky

Institute of Applied Physics, Russian Academy of Sciences, Nizhny Novgorod, Russia
Email: zaslav@hydro.appl.sci-nnov.ru

Received February 19th, 2010; revised April 2nd, 2010; accepted May 3rd, 2010.

Abstract

Spatial distribution of acoustic and elastic waves generated by an elementary vibration source at seismic profiling frequencies in an infinite medium close to a layer inclusion, i.e., an extended layer, is numerically simulated. Point dipole radiation in a homogeneous infinite medium separated by a liquid layer of different medium density or acoustic wave velocity is considered. Transverse elastic SH-waves excited by an oscillating power source in a solid medium also located close to the layer of different propagation velocity than the velocity of the vicinity are analyzed. Formulae for the spatial distribution of the wave field amplitude are derived and computer graphics of field distribution images is presented. Wave reflection, penetration deep into the layer inclusion, and transmittance through it are examined. Results of the analysis can be applied to seismoacoustic probing of geologic environment by the near field of a harmonic vibration source.

Keywords*: *Seismoacoustic Probing, Vibration Source, Acoustic, Transverse Waves, Wave Field Amplitudes, Spatial Distribution, Inhomogeneity

1. Introduction

New methods of acoustic remote diagnostics of materials and vibroseismic probing of geologic environment are actively developing now. This research is eventually focused on solving the so-called inverse problems, *i.e.*, problems of inversion or reconstruction of a medium by vibroseismic (acoustic) probing data [1,2]. Although some fundamental results have been achieved in developing the theoretical basis of these methods, the relation between the radiation field configurations at the distances of several tens of wavelengths from a vibration source to the parameters of a layered medium structure is not yet studied thoroughly [3]. The study of this relation is required for optimal solution of this problem; analytical results of the so-called direct problems can be used for this purpose. The existence of this relation was considered in previous papers devoted to the analysis of the near elastic-wave field configuration in a medium with an elementary plane layered structure [4-6]. It is assumed that at the distances of the order of several near-surface layer depths being simultaneously the probing inhomogeneity, the field configuration strongly depends on the geometrical parameters of the layered structure and the acoustic parameters of the medium. This informative relation decays, as the distance between the source and the receivers grows. Thus the problem analyzed in the paper can be formulated as numerical simulation and visualization of the structural features of the near field of a harmonic acoustic (vibration) source located close to a layer inclusion characterized by a jump of wave velocity or density relatively to the analogous parameter of the ambient homogeneous medium. The results of the analysis can be of interest for solving the problem of productive layer probing in entrails of the earth using structural features of near seismoacoustic fields of vibration sources, similarly to "near-field" location of inhomogeneities by pulse signals. If this probing is carried out by means of a vibration source operating in the harmonic vibration mode, precisely field configurations should be considered as characteristic informative features. In this case, the problems solved by probing can be generally formulated as the localization of the nearest boundary of inhomogeneity relatively to the source location, the determination of the characteristic spatial scale of the region occupied by inhomogeneity, the estimation of contrast in densities or wave velocities of media in the region

of inhomogeneity (layer) relatively to internal and external regions.

Analogous problems are set when determining productive layer features in the bottom marine environment, which are probably present in the characteristics of hydroacoustic signals recorded in shelf probing [1,2,7,8].

To extend the application area of the acoustic probing analysis and generalize it to solid media, we also set forth the results of numerical simulation of the amplitude distribution of elastic transverse *SH*-waves excited by an oscillating power source located analogously to that in the previous acoustic case, *i.e.*, at some distance from the plane parallel layer inclusion having the thickness of one or several wavelengths. To describe the field of a scalar medium (liquid or gas), one scalar potential is sufficient, while the oscillation source is a point oscillating dipole. To describe elastic *SH*-waves in a solid medium in the two-dimensional formulation, we use one component of the vector potential; a harmonically oscillating power source uniformly distributed along an infinite line parallel to the layer boundary has the same orientation of the momentum and radiates transverse *SH*-waves perpendicular to this line. It is interesting to compare wave patterns of acoustic and elastic-wave fields. First we consider a scalar acoustic field and then results of transverse elastic wave analysis.

2. Near Acoustic Field of a Point Dipole Located Close to a Layer Inclusion in a Homogeneous Infinite Medium

The geometry of the problem is shown in **Figure 1**. Three-dimensional infinite space filled with a liquid or gaseous medium and characterized by the parameters ρ and C, *i.e.*, the density and the acoustic wave velocity, is separated by a layer infinite in the x and y directions and enclosed in the limits $h < z < h + H$ in the vertical z direction; it has the same density ρ as the vicinity and differs only by the sound velocity c ($c \neq C$). The source $F_0 \vec{z}^0 \delta(r)\delta(z)e^{-i\omega t}$ is a point dipole having the power (momentum) F_0 and the oscillation frequency ω; it is a perturbation in the form of δ-functions of the radial r and axial z coordinates, oriented along the vertical axis ($\vec{z}^0$ is the corresponding unitary vector), and located at the distance h twice larger than its thickness H relatively to one of the layer boundaries (this value is taken for definiteness of calculations). In **Figure 1**, the entire space is divided into four artificially isolated zones (numerated by 1, 2, 3, and 4). In these four calculation regions due to axial symmetry,

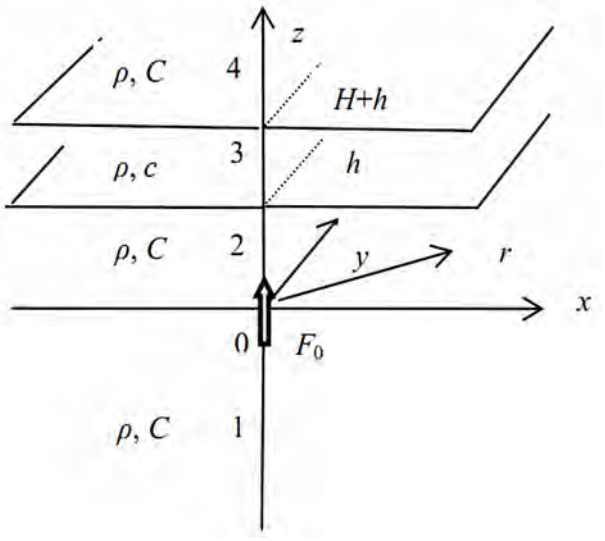

Figure 1. Medium structure and source arrangement for the "scalar" problem

the acoustic shift field can be described by the scalar potential φ represented for each of them as Fourier-Bessel integrals, *i.e.*, by the following expressions (the factor $e^{-i\omega t}$ is omitted):

$$\phi^{(1)} = \int_0^\infty a(k)e^{-iKz} J_0(kr)\,dk\,,\ z < 0\,,$$

$$\phi^{(2)} = \int_0^\infty \left(b(k)e^{iKz} + b'(k)e^{-iKz}\right) J_0(kr)dk\,,\ h > z > 0\,, \quad (1)$$

$$\varphi^{(3)} = \int_0^\infty \left(B(k)e^{i\kappa z} + B'(k)e^{-i\kappa z}\right) J_0(kr)dk\,,$$

$$H + h > z > h\,,$$

$$\varphi^{(4)} = \int_0^\infty d(k)e^{iKz} J_0(kr)dk\,,\ z > H + h\,,$$

where $J_0(kr)$ is the zero-order Bessel function, r is the radial coordinate, k is the radial wave number component, *i.e.*, the integration variable, $K = \sqrt{\omega^2/C^2 - k^2}$, $\kappa = \sqrt{\omega^2/c^2 - k^2}$, and the indefinite coefficients a, b, b', B, B', d are further calculated from the matching conditions of the z-component of the wave displacements u_z and the acoustic pressure p at the boundaries of all the four isolated regions.

The problem is based on the solution of a homogeneous acoustic wave equation:

$$\Delta\varphi^{(1,2,4)} - \frac{1}{C^2}\frac{\partial^2\varphi^{(1,2,4)}}{\partial t^2} = 0\,,$$

$$\Delta\varphi^{(3)} - \frac{1}{c^2}\frac{\partial^2\varphi^{(3)}}{\partial t^2} = 0; \tag{2}$$

the source operation is written under the appropriate boundary condition instead of being written in the right-hand side of the wave equation:

$$p^{(2)}(z=0) - p^{(1)}(z=0) = F_0\delta(r) = \frac{F_0}{2\pi}\int_0^\infty J_0(kr)kdk \tag{3}$$

The relation between the potential φ, the acoustic pressure p, and the *z*-component of the wave displacement u_z is commonly known:

$$p = \rho\omega^2\varphi,\ u_z = \nabla_z\varphi = \partial\varphi/\partial z \tag{4}$$

Since the explicit forms of the unknown coefficients are determined, the expressions for acoustic displacements in all spatial regions are written using standard expansions:

$$u_z^{(1)} = \frac{iF_0}{4\pi\rho\omega^2}$$

$$\cdot\int_0^\infty\left\{1-\left(1+\frac{2\kappa\left((\mathrm{K}-\kappa)e^{i\kappa H}+(\mathrm{K}+\kappa)e^{-i\kappa H}\right)}{(\mathrm{K}-\kappa)^2e^{i\kappa H}-(\mathrm{K}+\kappa)^2e^{-i\kappa H}}\right)e^{i2\mathrm{K}h}\right\},$$

$$\cdot e^{-i\mathrm{K}z}J_0(kr)\mathrm{K}kdk$$

$$u_z^{(2)} = \frac{iF_0}{4\pi\rho\omega^2}$$

$$\int_0^\infty\left\{e^{i\mathrm{K}z}-e^{i\mathrm{K}(2h-z)}\left(1+\frac{2\kappa\left((\mathrm{K}-\kappa)e^{i\kappa H}+(\mathrm{K}+\kappa)e^{-i\kappa H}\right)}{(\mathrm{K}-\kappa)^2e^{i\kappa H}-(\mathrm{K}+\kappa)^2e^{-i\kappa H}}\right)\right\},$$

$$\cdot J_0(kr)\mathrm{K}kdk \tag{5}$$

$$u_z^{(3)} = \frac{-iF_0}{2\pi\rho\omega^2}$$

$$\cdot\int_0^\infty\frac{(\mathrm{K}+\kappa)e^{-i\kappa(H+h-z)}+(\mathrm{K}-\kappa)e^{i\kappa(H+h-z)}}{(\mathrm{K}-\kappa)^2e^{i\kappa H}-(\mathrm{K}+\kappa)^2e^{-i\kappa H}}e^{i\mathrm{K}h}J_0(kr)\mathrm{K}\kappa kdk$$

$$u_z^{(4)} = \frac{-iF_0}{\pi\rho\omega^2}$$

$$\cdot\int_0^\infty\frac{e^{i\mathrm{K}(z-H)}}{(\mathrm{K}-\kappa)^2e^{i\kappa H}-(\mathrm{K}+\kappa)^2e^{-i\kappa H}}$$

$$\cdot J_0(kr)\mathrm{K}^2\kappa kdk$$

Specifically, it follows from the latter formula that field $u_z^{(4)}$ transmitted through the layer does not depend on the distance h from the source to the layer boundary closest to it. The first and the last formulae describe the acoustic wave field traveling for small distances and also lengths much larger than the wavelength from inhomogeneity and the source. In this case, the integrals in Formulae (5) can be asymptotically estimated, while the wave displacements corresponding to regions *1* and *4* can be given by the expressions:

$$u_z^{(1)} = \frac{F_0\cos^2\theta G(\theta)}{4\pi\rho C^2R}e^{i\omega R/C}, \tag{6}$$

In Formula (7), $\Omega = \omega H/c$, $c' = c/C$, $\chi = H/h$, and the angle θ is measured from the vertical axis *z*.

The angular characteristics of wave radiation are obtained by Formulae (6) and (7); they show the amplitude angular dependences for the far backscattered wave fields $u_z^{(1)}$ and for the fields traveling forward $u_z^{(4)}$.

$$G(\theta) = 1 - e^{i\frac{2\Omega c'\cos\theta}{\chi}} -$$

$$\frac{\sqrt{1-c'^2\sin^2\theta}\left[\left(c'\cos\theta-\sqrt{1-c'^2\sin^2\theta}\right)e^{i\Omega\sqrt{1-c'^2\sin^2\theta}}+\left(c'\cos\theta+\sqrt{1-c'^2\sin^2\theta}\right)e^{-i\Omega\sqrt{1-c'^2\sin^2\theta}}\right]}{\left[\left(c'\cos\theta-\sqrt{1-c'^2\sin^2\theta}\right)^2e^{i\Omega\sqrt{1-c'^2\sin^2\theta}}-\left(c'\cos\theta+\sqrt{1-c'^2\sin^2\theta}\right)^2e^{-i\Omega\sqrt{1-c'^2\sin^2\theta}}\right]}$$

$$\cdot e^{i\frac{2\Omega c'\cos\theta}{\chi}}$$

$$u_z^{(4)} = \frac{-iF_0\Phi(\theta)}{\pi\rho C^2c'R}e^{-i\omega H\cos\theta/C+i\omega R/C}, \tag{7}$$

$$\Phi(\theta) = \frac{\cos^3\theta\sqrt{1-c'^2\sin^2\theta}}{\left[\left(c'\cos\theta-\sqrt{1-c'^2\sin^2\theta}\right)^2e^{i\Omega\sqrt{1-c'^2\sin^2\theta}}-\left(c'\cos\theta+\sqrt{1-c'^2\sin^2\theta}\right)^2e^{-i\Omega\sqrt{1-c'^2\sin^2\theta}}\right]},$$

The far field characteristics are displayed in **Figures 2(a)** and **(b)** (in curves 1, 2, and 3, $\Omega = \pi/2,\ \pi,\ 2.5\pi$); these characteristics correspond to waveguide propagation in the layer, *i.e.*, for $c' = 0.9$. It is seen that in the far zone, the angular pattern of backscattered waves changes as the frequency grows, while the directivity of the field transmitted through the layer remains unchanged and close to the directivity of the dipole source oscillating in a homogeneous infinite medium. The calculation results of antiwaveguide propagation for $c' = 1.1$ are shown in **Figures 3(a)** and **(b)**. There is a considerable difference in the angular dependences of the backscattered far field and the field scattered forward. The characteristic of the field traveling forward is the occurrence of sharply directed maxima with simultaneous presence of the central lobe describing the smooth dependence. The backscattered field pattern has only sharply directed maxima analogous to those mentioned above, as applied to the wave field transmitted through the layer, which exist there together with smooth lobes. They, probably, exist due to the so-called nonray waves [3-6].

The spatial distribution of the acoustic field amplitude can be also analyzed by means of numerical calculation of the integrals in Formula (5); in this case, the calculated distances do not exceed the first tens of wavelengths. Since the numerical approach has been employed, the choice of integral signs eliminating ambiguity in the variable k on two-lobe surfaces and the choice of the integration methods essential in the analytical calculations are not discussed.

Now we consider patterns of the spatial amplitude distribution of the *z*-component of wave displacements, which are obtained as a result of numerical simulation using Formula (5) for the same values of acoustic wave velocity jump in the media located inside and outside the layer, *i.e.*, for the waveguide propagation $c' = c/C = 0.9$ and for the antiwaveguide propagation $c' = c/C = 1.1$. Note that the actual pattern of the acoustic shift field is to be axially symmetrical relatively to the axis z and can be a set of interleaved axially symmetrical bodies. However in graphical presentation of the amplitude field distribution, we use the isometric projection, in which the field level is represented as relief rising above the plane $r,\ z$. The calculated structure of the acoustic displacement field $|u_z|$ is shown in **Figures 4(a)**, **4(b)**, **4(c)** and **4(d)** for $c' = c/C = 0.9$ and in **Figures 5(a)**, **5(b)**, **5(c)** and **5(d)** for $c' = c/C = 1.1$.

Figure 4(a) displays the field fragment corresponding to region *1* located behind the source on the opposite side of the layer region, *i.e.*, for $z < 0$; thus it should be considered turned in the opposite direction along the vertical coordinate *z* and the corresponding axis in it is denoted *-z*. The same scale is used in both axes. The level decrease is accompanied by the presence of a fan-shaped structure in the field image over the entire plane, which means the oscillating dependence of $|u_z|$ on r for constant z or the oscillating dependence on z for constant r. It follows from the dependence $|u_z|$ on the coordinates that there is an acoustic radiation maximum directed at a small angle to the axis z, which is indicated by "elevation" in the appropriate relief region inclined to this axis. As distinct from **Figure 4(a)**, in **Figures 4(b)** and **4(c)** the scale of the axis z is 100 times smaller than the scale of the axis r. The analyzed spatial interval along the vertical axis amounts to $0 \le z \le h$ in **Figure 4(b)** and to $h \le z \le h + H$ in **Figure 4(c)**. In **Figure 4(c)** for more detailed consideration of the pattern in the radial $r-$direction in the layer region, we used a 10 times smaller scale. In regions *2* and *3* at larger distances from the source, the field amplitude sharply decreases both in radius and vertical z - direction, which is seen in **Figures 4(b)** and **4(c)**. After deep minimum when the face boundary of the layer is approached, sharp decrease of the level is changed by the amplitude growth accompanied by its oscillations. Oscillation amplitude decreases in region *3* are not strong, which indicates that there is the excitation of several interfering modes in the layer; each of the resonance frequencies of these modes being far from the chosen frequency of the source. In region *4* (**Figure 4(d)**), one can see a comparatively rapid decrease of the field level; it is not so sharp as the level differences in **Figures 4(b)** and **4(c)**, if 100-fold scale difference along z axis in these figures is taken into account. The pattern of the near field in region *4* does not reveal details of the angular concentration of the acoustic field radiated beyond the layer and going to infinity. Therefore, the calculation data obtained from (7) and shown in **Figure 3(a)** supplement the entire field pattern. At the same time it is evident that even at small distances, the field backscattered by the layer has more peculiarities in its spatial configuration than the field transmitted through the layer outward has in its amplitude distribution. If it is assumed that the spatial configuration can be the informativeness parameter representing the characteristics of the layer itself, then it is seen from comparison that the reflected field contains more information than the field transmitted on the opposite side. In conclusion of this brief review of the wave pattern it can be assumed that amplitude oscillations along the radial and axial coordinates in the near backscattered field is the consequence of interference of the waves reflected from the nearest (face) and the second (external relatively to the source) boundaries. This statement is also applicable to

other cases considered below, although wave interference in the field transmitted outward is not always so strong.

It follows from **Figures 5(a)** and **5(b),** and ***c*** that for $c' = c/C = 1.1$, the spatial distributions of the wave amplitudes corresponding to spatial regions 1, 2, and 3 have the forms essentially analogous to those considered above. There is an apparent difference from the previous case only in the amplitude distribution in spatial region 4 corresponding to the field transmitted through the layer (**Figure 5(d)**). In the first case, space-angular oscillations in the transmitted field level were absent; while in considered case, they are present in the three-dimensional image of amplitudes. This is indicated by the fan-shaped angular-periodic structure observed up to some angle to the vertical axis and similar to the structure shown in **Figure 4(a)**; its angular periodic repetition is approximately the same as in region *1*. The primary role here is, probably, played by nonray waves having a rather high level in the spatial region limited by the sector forming the angle $\gamma = \pm \arccos(C/c)$ with normal to the boundary [3-6].

Thus in the considered cases, there is some difference in the entire pattern of the spatial distribution of acoustic fields, which can be used for remote diagnostics of a probed inhomogeneity. It is evident that spatial amplitude distributions of both the backscattered field and the field transmitted through the layer should be recorded, since the near field structure of the acoustic wave transmitted through inhomogeneity also represents the influence of

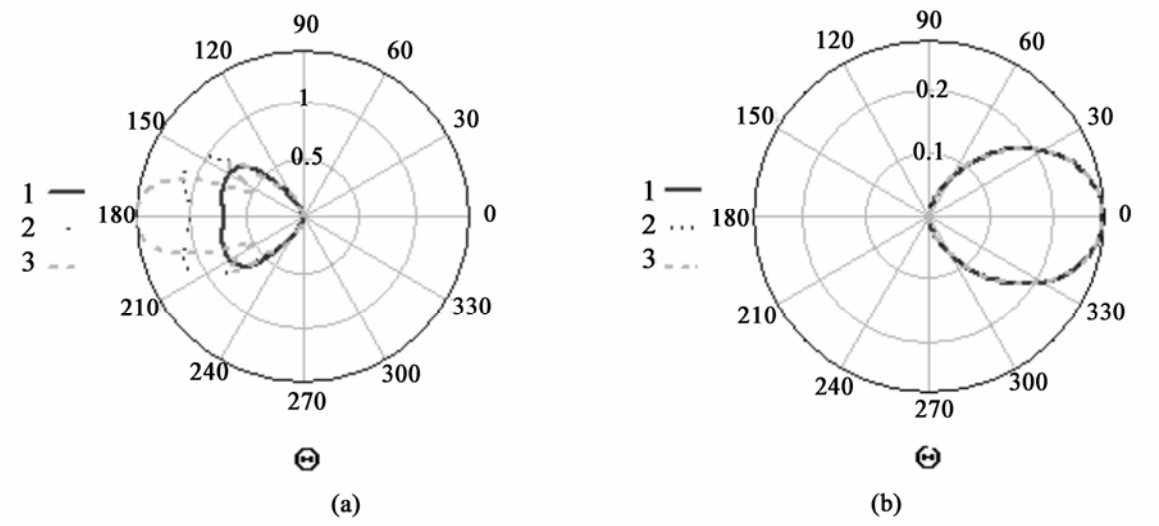

Figure 2. Angular field characteristics (a) – $u_z^{(1)}$, (b) – $u_z^{(4)}$. Curves 1, 2, and 3 – $\Omega = \pi/2,\ \pi,\ 2.5\pi$, $c' = 0.9$

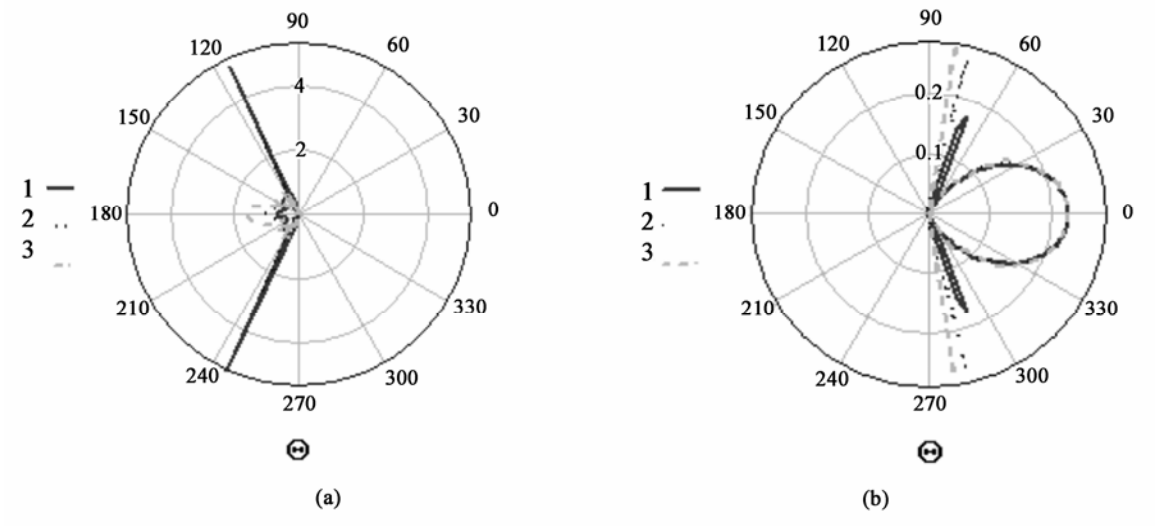

Figure 3. Angular field characteristics: (a) – $u_z^{(1)}$, (b) – $u_z^{(4)}$. Curves 1, 2, and 3 – $\Omega = \pi/2,\ \pi,\ 2.5\pi$, $c' = 1.1$

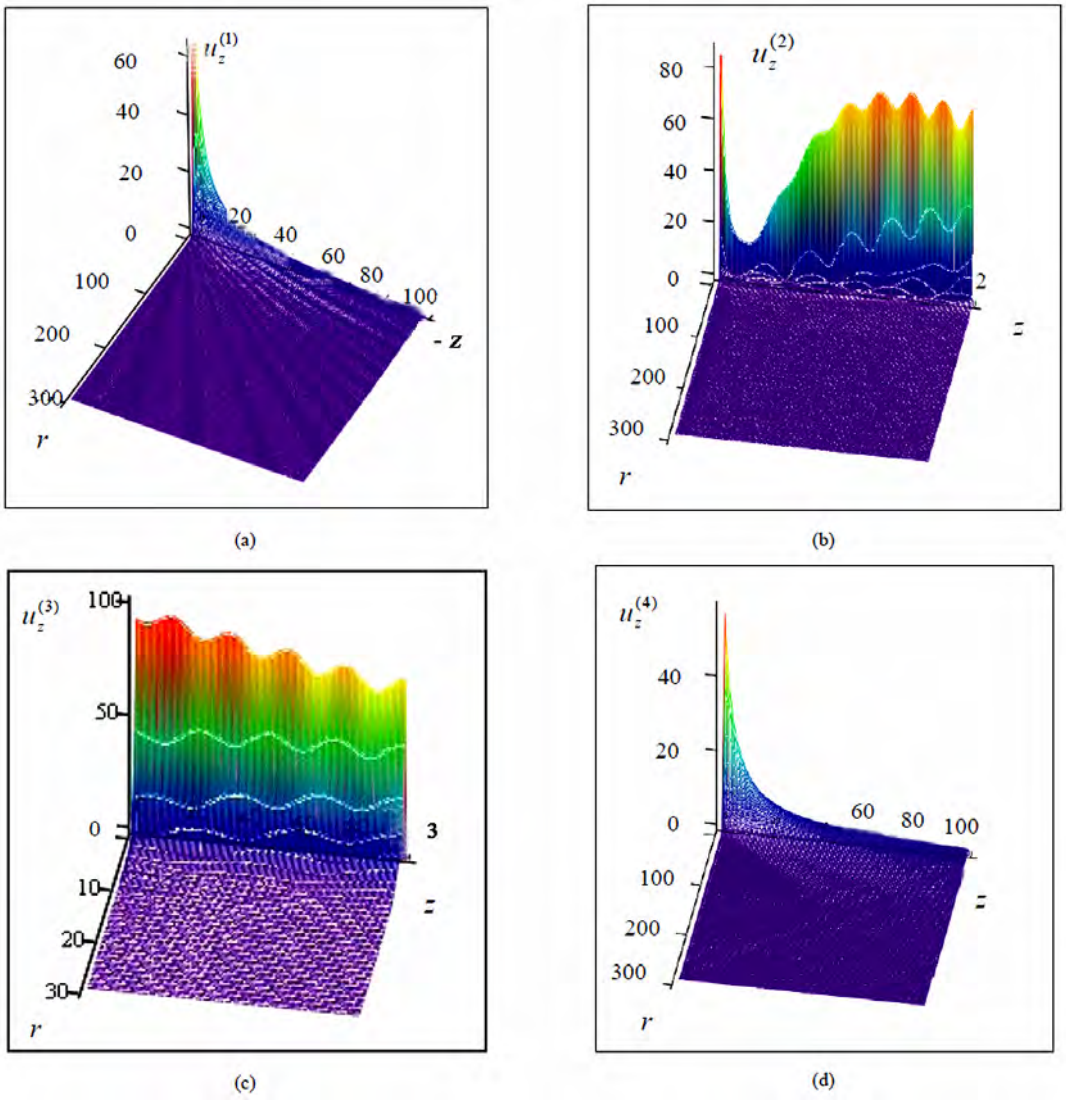

Figure 4. Fragments of the amplitude distribution pattern of the field $|u_z|$; relief over the coordinate plane $r-z$: (a) – Region 1; (b) – Region 2; (c) – Region 3; (d) – Region 4. $c' = 0.9$, $\omega h/C = 11.1\pi$, $\omega H/c = 5\pi$

the inhomogeneity parameters.

The problems of the backscattered acoustic field of a dipole harmonic source and of the field transmitted through a layer inclusion into a homogeneous infinite medium (when the media differ only in density) are solved analogously to the stated above. If we consider the same geometry of the layer-medium structure as in the case of **Figure 1**, use the same arrangement of the source relatively to the boundaries (h is the distance between the source and the face boundary of the layer and H is the layer thickness), and assume that the sound velocity C is equal everywhere, the density of the medium in the vicinity is ρ_1, while in the layer is ρ_2, it is easy to obtain the following expressions for the acoustic displacements in the reflected acoustic field $u_z^{(1)}$ and the acoustic field $u_z^{(4)}$ transmitted through the layer:

$$u_z^{(1)} = \frac{-iF_0}{4\pi\rho_1\omega^2}\int_0^\infty \left(e^{i2\mathrm{K}h} - 1 - \frac{2\left(\cos(\mathrm{K}H) - i\frac{\rho_1}{\rho_2}\sin(\mathrm{K}H)\right)}{\left(2\cos(\mathrm{K}H) - i\left(\frac{\rho_2}{\rho_1} + \frac{\rho_1}{\rho_2}\right)\sin(\mathrm{K}H)\right)} e^{i\mathrm{K}(h+H)} \right) e^{-i\mathrm{K}z} J_0(kr)\mathrm{K}\,kdk\,, \tag{8}$$

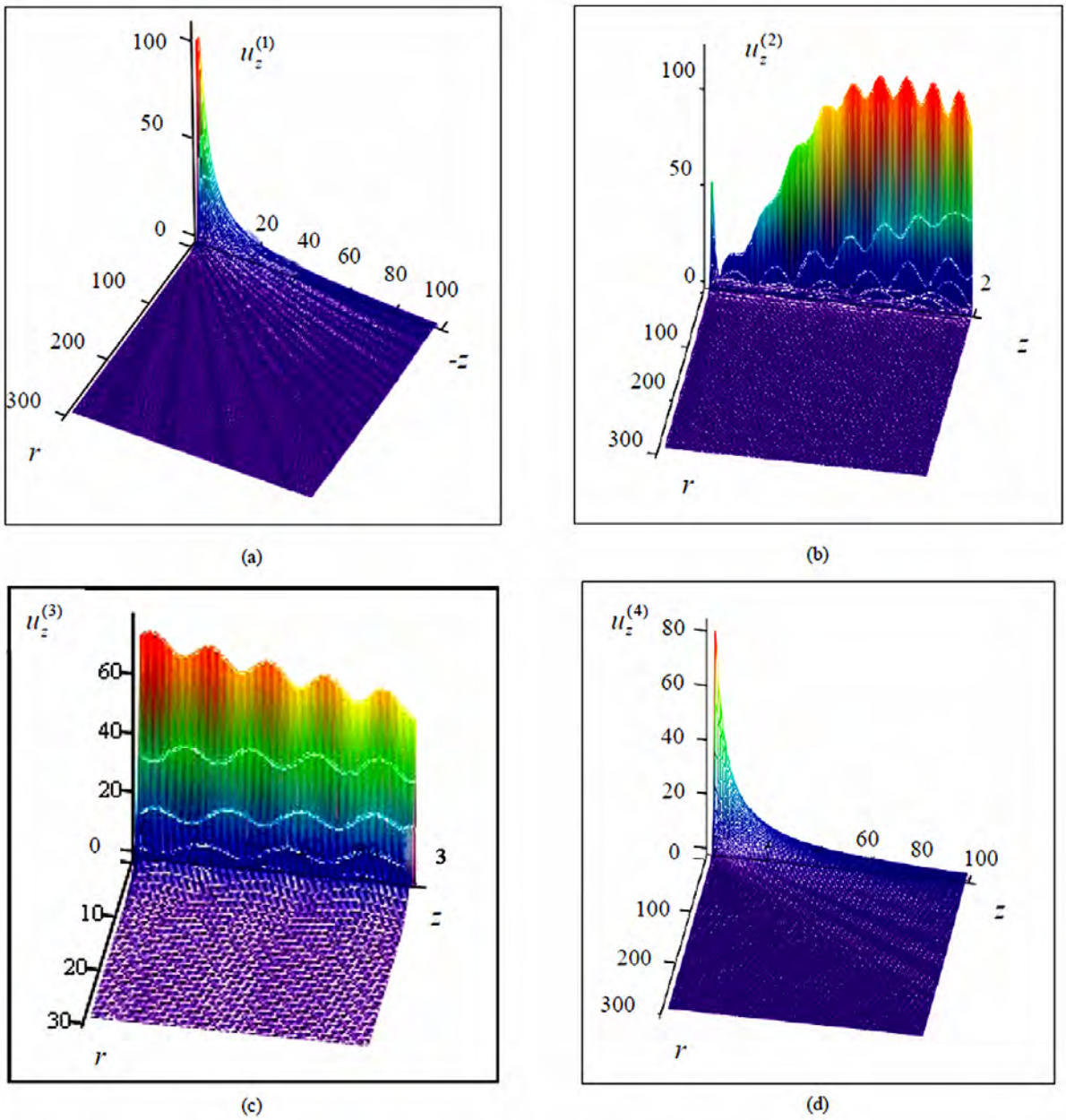

Figure 5. Fragments of the amplitude distribution pattern of the field $|u_z|$; relief over the coordinate plane $r-z$: (a) – Region 1; (b) – Region 2; (c) – Region 3, and (d) – Region 4. $c' = 1.1$, $\omega h/C = 9.1\pi$, $\omega H/c = 5\pi$

$$u_z^{(4)} = \frac{iF_0}{2\pi\rho_1\omega^2}\int_0^\infty \frac{e^{i\mathrm{K}(z-H)}}{2\cos(\mathrm{K}H) - i\left(\dfrac{\rho_2}{\rho_1}+\dfrac{\rho_1}{\rho_2}\right)\sin(\mathrm{K}H)} J_0(kr)\mathrm{K}\,kdk \ . \tag{9}$$

These formulae are employed to carry out numerical calculation and analysis of the near acoustic field structure for different density contrasts in the layer and in the Vicinity $\rho_2/\rho_1 > 1$, $\rho_2/\rho_1 < 1$, enabling one to determine the influence of variations in the ratio of the densities in inhomogeneity and in its vicinity. **Figures 6** and **7**

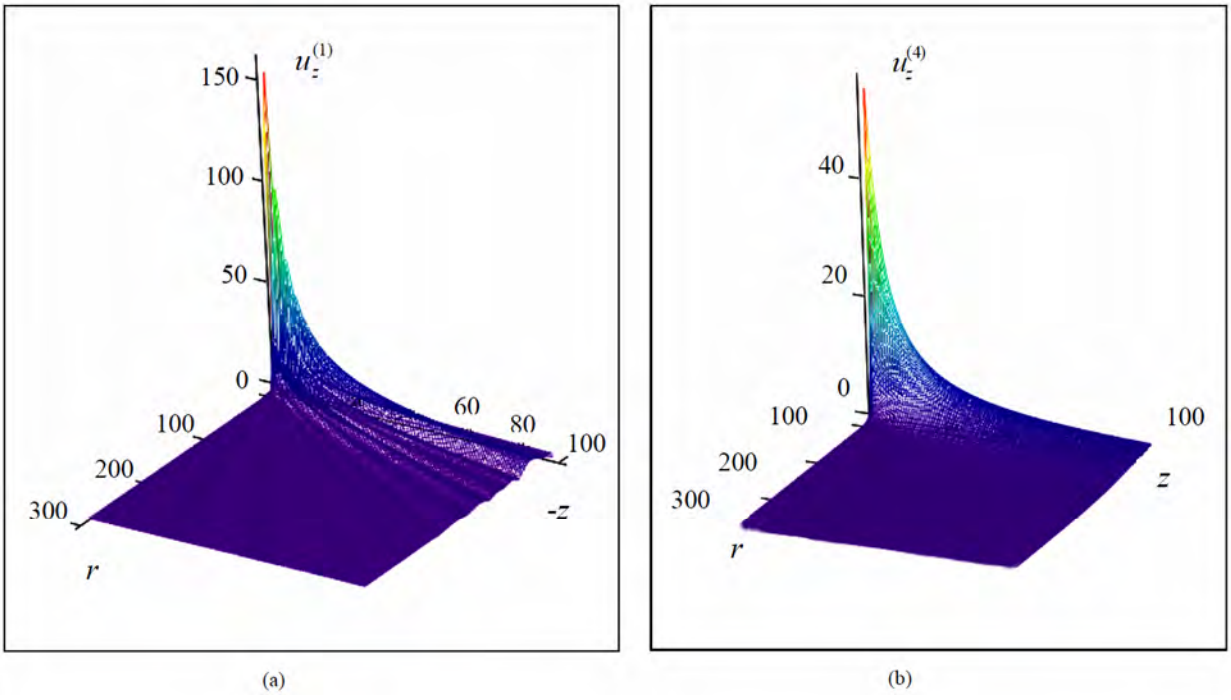

Figure 6. Fragments of the amplitude distribution pattern of the field $|u_z|$: $\omega h/C = 10\pi$, $\omega H/C = 5\pi$, $\rho_2/\rho_1 = 0.9$; (a) – Region 1; (b) – Region 4

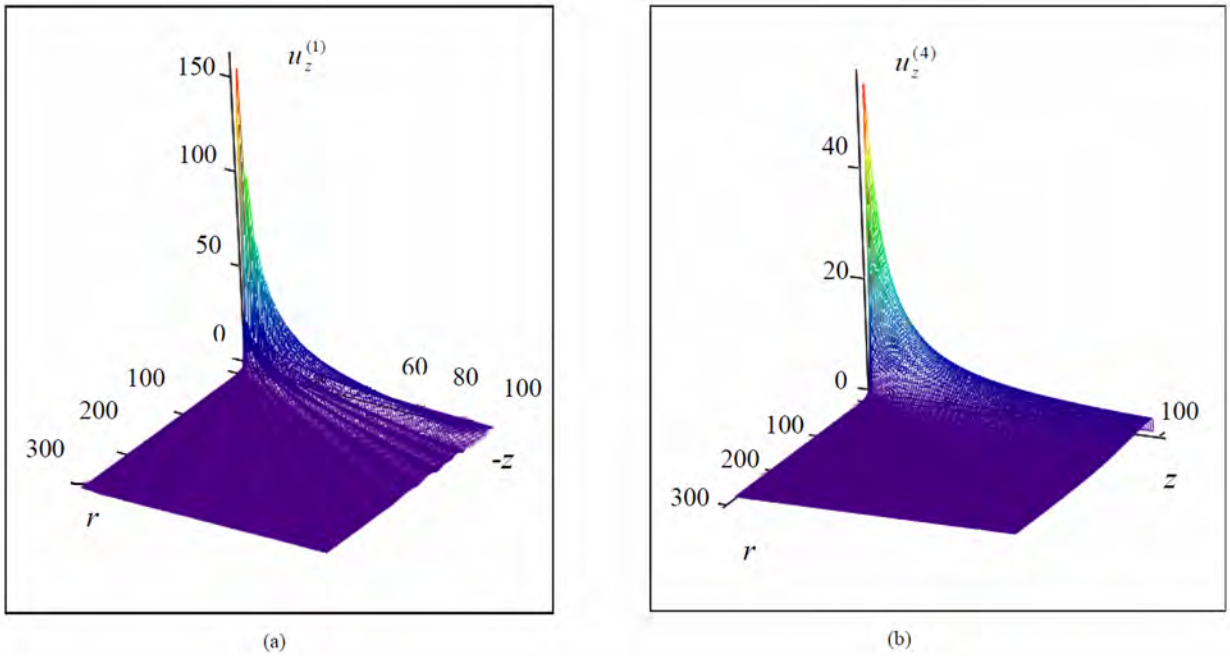

Figure 7. Fragments of the amplitude distribution pattern of the field $|u_z|$: $\omega h/C = 10\pi$, $\omega H/C = 5\pi$, $\rho_2/\rho_1 = 1.1$; (a) – Region 1; (b) – Region 4.

deal with fragments of relief above the plane r, z in regions 1 and 4, which are calculated by Formulae (8) and (9) using the same values of the density ratio as in the velocity ratio calculations, *i.e.*, $\rho_2/\rho_1 = 0.9$, $\rho_2/\rho_1 = 1.1$. These fragments are much similar to those considered above; the same picture is observed in interme-

diate regions 2 and 3, thus neither appropriate fragments are shown nor are calculation formulas for these regions. It is seen in **Figure 6(a)** that if the media differ in density ($\rho_2/\rho_1 = 0.9$), the distribution of the backscattered acoustic field is characterized (as in the previous case) by amplitude decrease and fan –shaped relief but of lower angular periodicity than that in **Figure 4(a)**. The level of the field transmitted through the layer (see **Figure 6(b)**) decreases at larger distances from the external boundary but angular periodicity of amplitude values is absent. For a higher density contrast, *i.e.*, for $\rho_2/\rho_1 = 1.1$ (see **Figures 7(a)** and **7(b)**), the amplitude distribution patterns in reflected waves and waves transmitted through the layer remain practically invariable, which indicates a weak influence of the density contrast variation on the near acoustic field configuration in the layer – vicinity structure, as distinct from the previously considered velocity jump.

Generally, when comparing differentiation of media in density and velocity inside and outside the layer, we come to the conclusion that the sound speed jump in homogeneity causes a more pronounced variation of the near field configuration; thus the search system sensitivity to variation of this parameter is higher than the sensitivity to density contrast variation. This is the main distinction of these cases, which should be taken into account in the search for inhomogeneities and can be considered as one of the diagnostic properties enabling one to differentiate "inhomogeneities in density" and "inhomogeneities in velocity".

Therefore, the obtained fragments of the near acoustic field of a dipole harmonic source operating close to a layer inclusion yield the entire field pattern in principally different cases of velocity and density contrasts inside and outside inhomogeneity. The revealed peculiarities provide qualitative information on their applicability as informative attributes in the search for inhomogeneity. The distance from the source to the nearest (face) boundary of the layer, the thickness of the layer, and hence the sound speed (density) in region 3, *i.e.*, in the zone occupied by probed inhomogeneity, is determined by the field configurations in regions 1, 2, and 4. Thus remote reading of the inhomogeneity parameters in the harmonic oscillation mode requires "reflection" and "transmittance" probing. More detailed numerical simulation of near fields will provide quantitative data on the relation of inhomogeneity contrast against the vicinity to the spatial structures of these fields in the parameters of density and sound speed. Finally, it can be noted that the illustrations confirm our statements only qualitatively; the problem of frequency choice optimization required for practical acoustic probing is not considered.

3. Transverse SH-Wave Field Generated in an Infinite Medium by an Extended Oscillating Power Source Close to a Layer Inclusion (Two-Dimensional Problem)

The considered vibration source $Z_0\vec{z}^0\delta(x)\delta(y)e^{-i\omega t}$ is the "force oscillating with the frequency ω" (the force vector is parallel to the unit vector $\vec{z}^0$ and has the amplitude Z_0; the factor $e^{-i\omega t}$ is omitted as previously) is uniformly distributed along the axis *z* due to the two-dimensional approximation used in the analysis (see **Figure 8**). The source is omnidirectional relatively to radiated *SH*-waves, *i.e.*, in the plane *x*, *y* oriented normally to the $\vec{z}^0$ direction. Thus besides comparing acoustic and vibroseismic cases in this analysis, it is possible to study the influence of the source directivity on the near field characteristics. As in the previous case, the layer occupies the spatial region $-\infty < x < \infty$, $h \le y \le h + H$, $-\infty < z < \infty$. The vicinity is characterized by the transverse wave velocity C_t and differs from the analogous value c_t inside the layer; both media have the same density ρ.

It is shown in References [4-6] that to describe the wave displacements u_z in the two-dimensional problem, it is sufficient to introduce one component of the vector potential ψ_x satisfying the homogeneous wave equation:

$$\Delta\psi_x^{(1,2,4)} - \frac{1}{C_t^2}\frac{\partial^2\psi_x^{(1,2,4)}}{\partial t^2} = 0,$$

$$\Delta\psi_x^{(3)} - \frac{1}{c_t^2}\frac{\partial^2\psi_x^{(3)}}{\partial t^2} = 0. \qquad (10)$$

By analogy with the previous case of a dipole source in a scalar medium, the entire space is divided into four especially distinguished regions (see **Figure 8**); in each region the value ψ_x is represented as the Fourier expansion, *i.e.*, by the following expressions:

$$\psi_x^{(1)} = \int_{-\infty}^{\infty} A(k)e^{-i\mathrm{K}_t y + ikx}dk, \quad y < 0,$$

$$\psi_x^{(2)} = \int_{-\infty}^{\infty}\left(B(k)e^{i\mathrm{K}_t y} + C(k)e^{-i\mathrm{K}_t y}\right)e^{ikx}dk, \quad 0 < y < h, \qquad (11)$$

$$\psi_x^{(3)} = \int_{-\infty}^{\infty}\left(a(k)e^{i\kappa_t y} + b(k)e^{-i\kappa_t y}\right)e^{ikx}dk,$$

$$h < y < h + H$$

$$\psi_x^{(4)} = \int_{-\infty}^{\infty} D(k) e^{i\mathrm{K}_t y + ikx} dk\,, \quad h + H < y < \infty$$

where $\mathrm{K}_t = \sqrt{\omega^2 / C_t^2 - k^2}$, $\kappa_t = \sqrt{\omega^2 / c_t^2 - k^2}$, C_t *and* c_t are the shear wave velocities in the vicinity and inside the layer and k is the integration variable.

The oscillation displacements u_z and significant stresses in the considered waves σ_{yz} are expressed through ψ_x using differential operations:

$$u_z^{(1..4)} = -\partial \psi_x^{(1..4)} / \partial y\,, \tag{12}$$

$$\sigma_{yz}^{(1,2,4)} = \rho C_t^2\, \partial u_z^{(1,2,4)} / \partial y\,, \sigma_{yz}^{(3)} = \rho c_t^2\, \partial u_z^{(3)} / \partial y\,, \tag{13}$$

where ρ is the density of the medium; the source operation is described by one of the conditions for $y = 0$ instead of appropriate expressions in the right-hand side of Equation (10). The boundary condition is:

$$\sigma_{yz}^{(2)}(y = 0) - \sigma_{yz}^{(1)}(y = 0) = Z_0 \delta(x) \tag{14}$$

The unknown coefficients $A(k)$, $B(k)$, $C(k)$, $a(k)$, $b(k)$, $D(k)$ are found by matching the indicated shift components and strains at the boundaries of the four distinguished regions. Omitting intermediate calculations, we write down the resultant expressions for the wave displacements:

$$u_z^{(1)} = \frac{-iZ_0}{4\pi\rho C_t^2} \int_{-\infty}^{\infty} \left(1 + \frac{2i\left(\frac{c_t^4 \kappa_t^2}{C_t^4 \mathrm{K}_t^2} - 1 \right) \sin(\kappa_t H)}{\left(\left(\frac{c_t^2 \kappa_t}{C_t^2 \mathrm{K}_t} + 1 \right)^2 e^{-i\kappa_t H} - \left(\frac{c_t^2 \kappa_t}{C_t^2 \mathrm{K}_t} - 1 \right)^2 e^{i\kappa_t H} \right)} e^{i2\mathrm{K}_t h} \right) \frac{e^{-i\mathrm{K}_t y + ikx}}{\mathrm{K}_t} dk\,,$$

$$u_z^{(2)} = \frac{-iZ_0}{4\pi\rho C_t^2} \int_{-\infty}^{\infty} \left(e^{i\mathrm{K}_t y} + \frac{2i\left(\frac{c_t^4 \kappa_t^2}{C_t^4 \mathrm{K}_t^2} - 1 \right) \sin(\kappa_t H) e^{-i\mathrm{K}_t (y - 2h)}}{\left(\left(\frac{c_t^2 \kappa_t}{C_t^2 \mathrm{K}_t} + 1 \right)^2 e^{-i\kappa_t H} - \left(\frac{c_t^2 \kappa_t}{C_t^2 \mathrm{K}_t} - 1 \right)^2 e^{i\kappa_t H} \right)} \right) \frac{e^{ikx}}{\mathrm{K}_t} dk\,, \tag{15}$$

$$u_z^{(3)} = \frac{-iZ_0}{2\pi\rho C_t^2} \int_{-\infty}^{\infty} \frac{\left(\left(\frac{c_t^2 \kappa_t}{C_t^2 \mathrm{K}_t} + 1 \right) e^{i\kappa_t (y - H - h)} + \left(\frac{c_t^2 \kappa_t}{C_t^2 \mathrm{K}_t} - 1 \right) e^{-i\kappa_t (y - H - h)} \right)}{\left(\left(\frac{c_t^2 \kappa_t}{C_t^2 \mathrm{K}_t} + 1 \right)^2 e^{-i\kappa_t H} - \left(\frac{c_t^2 \kappa_t}{C_t^2 \mathrm{K}_t} - 1 \right)^2 e^{i\kappa_t H} \right)} \frac{e^{i\mathrm{K}_t h + ikx}}{\mathrm{K}_t} dk\,,$$

$$u_z^{(4)} = \frac{-iZ_0 c_t^2}{\pi\rho C_t^4} \int_{-\infty}^{\infty} \frac{\kappa_t e^{i\mathrm{K}_t (y - H) + ikx}}{\mathrm{K}_t^2 \left(\left(\frac{c_t^2 \kappa_t}{C_t^2 \mathrm{K}_t} + 1 \right)^2 e^{-i\kappa_t H} - \left(\frac{c_t^2 \kappa_t}{C_t^2 \mathrm{K}_t} - 1 \right)^2 e^{i\kappa_t H} \right)} dk$$

It follows from (15) that similarly to the previous case with an acoustic dipole, the field $u_z^{(4)}$ does not depend on the parameter h, *i.e.*, the distance between the source and the nearest layer boundary, which is the consequence of the unlimited scale of inhomogeneity along the coordinate x and the absence of absorption in the medium. The obtained expressions are used in the numerical calculation enabling one (by means of computer graphics) to visualize the spatial distribution of wave amplitudes at the distances of up to several tens of wavelengths from the source for the layer thickness of the order of or smaller than the wavelength and to analyze the peculiarities of this spatial distribution. Specifically, these expressions are used to make calculations and obtain patterns of the wave displacement field (in the isometric projection) for the relative distance from the source and the layer thickness assigned in the dimensionless form: $\omega h / C_t = 9\pi$, $\omega H / c_t = 5\pi$. As previously, the calculations are carried out for two velocity jumps $c_t / C_t = 0.9$ and $c_t / C_t = 1.1$. As the integral expressions, each of the four fragments of the field pattern corresponds to its spatial region; the amplitude distribution is shown as a relief rising above the plane x, y.

Figures 9(a), (b), (c), and **(d)** should be considered in

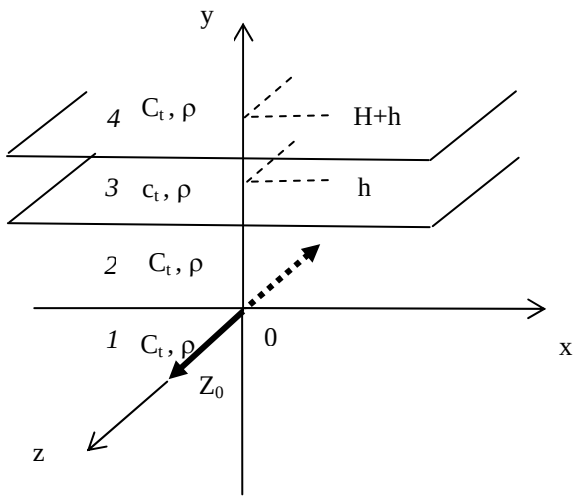

Figure 8. Mutual arrangement of the source and the layer scattering of shear *SH*-waves

the following sequence: **Figure 9(a)** – region 1, **Figure 9(b)** – region 2, etc., while for obtaining the entire field pattern in all the regions all the fragments should be joined. Since **Figure 9(a)** should be considered turned in the opposite direction along the transverse coordinate *y*, the corresponding axis in it is denoted -*y*. It follows from the given pattern that in region *1* at larger distances from the source, besides a decrease of the field $\left|u_z^{(1)}\right|$ we observe periodic sequences of maxima occupying fan-shaped angular sectors, which pass into directional lobes in the far field. Note that the scale of the longitudinal coordinate *x* is the same in all the figures, while the scale of the transverse coordinate *y* in **Figures 9(b)** and **9(c)** is two orders smaller than that in **Figures 9(a)** and **9(d)**, *i.e.*, the unit length in the transverse direction *y* in **Figures 9(b)** and **9(c)** is 100 times larger than that in **Figures 9(a)** and **9(d)**. Taking into account the scale difference it can be concluded that at larger distances from the source and approach to the layer boundary in the second region, the amplitude of the field $\left|u_z^{(2)}\right|$ decreases even more abruptly than that in **Figure 9(a)**. The amplitude of the field penetrating into the layer is maximum in the region opposite to the source, decreases abruptly when escaping along the coordinate x (symmetrically on both sides), and oscillates along the coordinate y. It is seen in **Figure 9(c)** that waveguide conditions for excitation and propagation of several first modes of *SH*-wave occur inside the layer. The field $\left|u_z^{(4)}\right|$ outside the layer (see **Figure 9(d)**) also decreases rapidly and the amplitude distribution in region *4* differs considerably from the analogous one in region *1*. A similar situation is considered in the first section for a dipole source in the scalar acoustic problem.

To gain a better understanding of wave reflections occurred in near-field probing in the near region of the source, it is expedient to consider antiwaveguide propagation for an inverse jump of *SH*-wave velocities inside the layer and in the vicinity, which equals, for example, $c_t/C_t = 1.1$.

Figures 10(a), **(b)**, **(c)**, and **(d)** exhibit analogous fragments of the spatial field distribution in the same format and in the same spatial regions as in the figure considered above. Comparison of the amplitude distributions with the analogous ones of the previous case (**Figure 9**) shows that the spatial dependence can be either the same or slightly different. The near field in the reflection region (**Figure 10(a)** – region 1) has practically the same structure as in the previous case. The configurations of the amplitude distributions in region 2 (**Figures 10(b)**) in those cases are also similar. The field configuration in the layer (**Figures 10(c)**), *i.e.*, in region *3*, differs by the absence of periodic structure indicating the excitation of *SH*-wave modes, in spite of the presence of a crest with undulatory amplitude modulation also typical of the previous case. In region *4* immediately outside the layer limits (see **Figures 10(d)**), an increased-amplitude angular sector forms being similar to that in the scalar acoustic problem.

The revealed peculiarities differentiating the structures of the near fields traveling in opposite directions from the layer in waveguide and antiwaveguide cases demonstrate the possibility of remote diagnostics of elasticity jump in the media occupying the internal and external regions of the layer and enable one to accept them as informative diagnostic attributes applicable, specifically, for solving problems of remote diagnostics and medium structure retrieval. Hence the previously formulated statement on the necessity of reflected and transmitted wave recording for diagnostics of inhomogeneity in its near-field probing, which is similar to reflection and transmittance location, is valid. Generally, similar results on peculiarities of wave reflection and transmittance through a layer several wavelengths thick are typical of the scalar acoustic problem and the problem with a source exciting *SH*-waves in an elastic medium.

4. Conclusions

Numerical simulation of near-field probing of inhomogeneity (layer inclusion) in acoustic and seismic media is carried out, which has confirmed its applicability with the use of near acoustic and elastic fields of harmonic sources and recording of waves reflected by in homogeneity and transmitted through it. The study is based on the analysis of the visual pattern of the spatial amplitude distribution in near and far wave fields calculated by the formulae derived in this paper. The simultaneously considered angular characteristics of the far

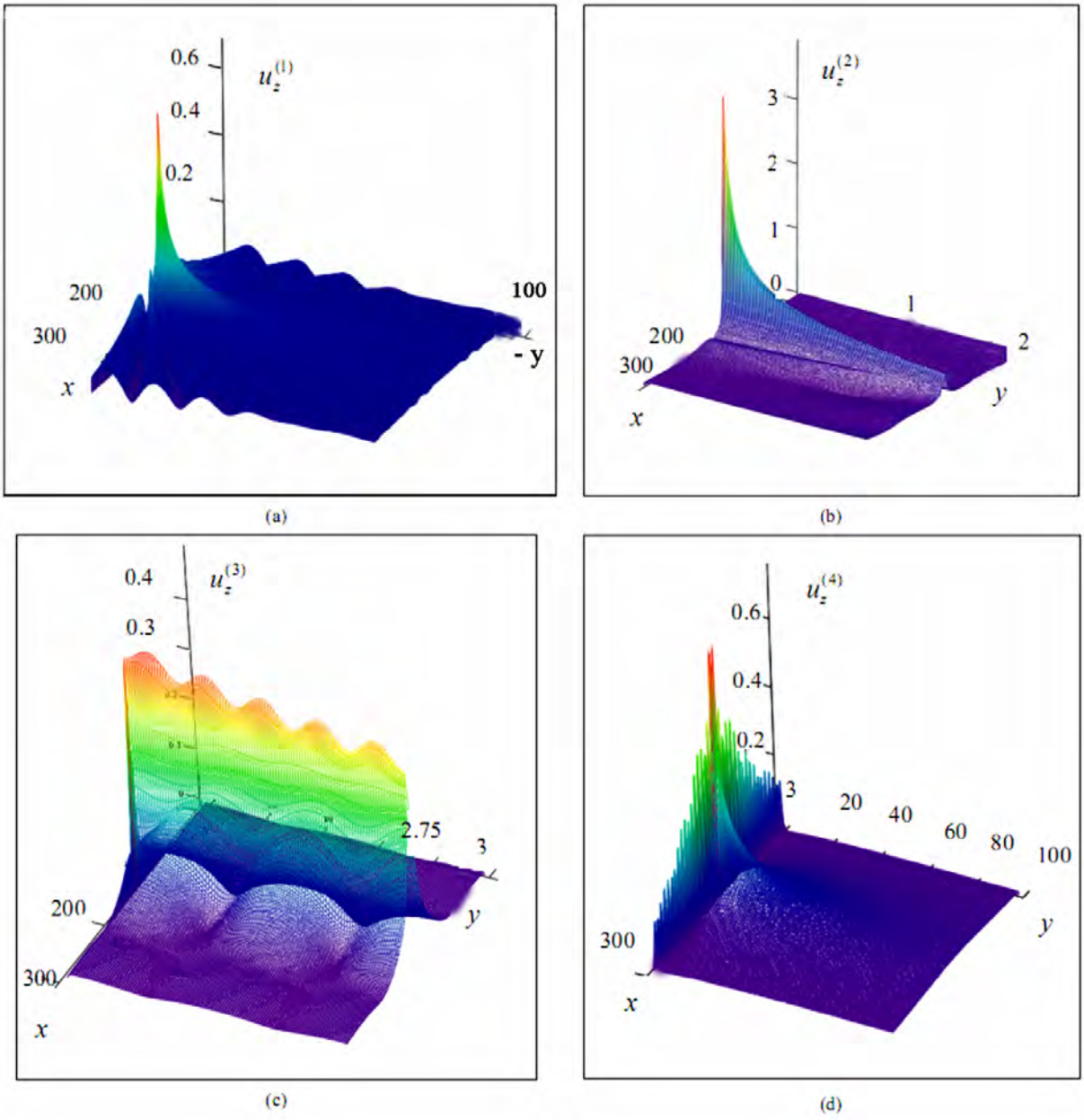

Figure 9. Fragments of the spatial distribution of wave amplitudes of an oscillating source for $c_t/C_t = 0.9$, $\omega h/C_t = 11.1\pi$, $\omega H/c_t = 5\pi$: (a) – Region 1; (b) – Region 2; (c) – Region 3; (d) – Region 4

acoustic field do not contradict the revealed peculiarities of the near field of elementary oscillation sources operating close to inhomogeneity. The employed values of inhomogeneity contrast characterize the relation of densities and sound speeds in the layer and ambient acoustic medium. To predict the distance from the source to the layer inclusion and to estimate its thickness, the qualitative character of the dependence $\omega H/c$, $\omega h/C$ ($\omega H/c_t$, $\omega h/C_t$) should be studied. Complete investigations require numerical simulation of a number of definite values of the mentioned parameters in addition to the given calculations. At the same time, the near field peculiarities found in this paper (even in a limited volume of simulation data) are useful for optimal arrangement of sources and recording receivers in design of experiments on seismic exploration of productive stratum in massif, characterized by an abrupt decrease of *SH*-wave velocity.

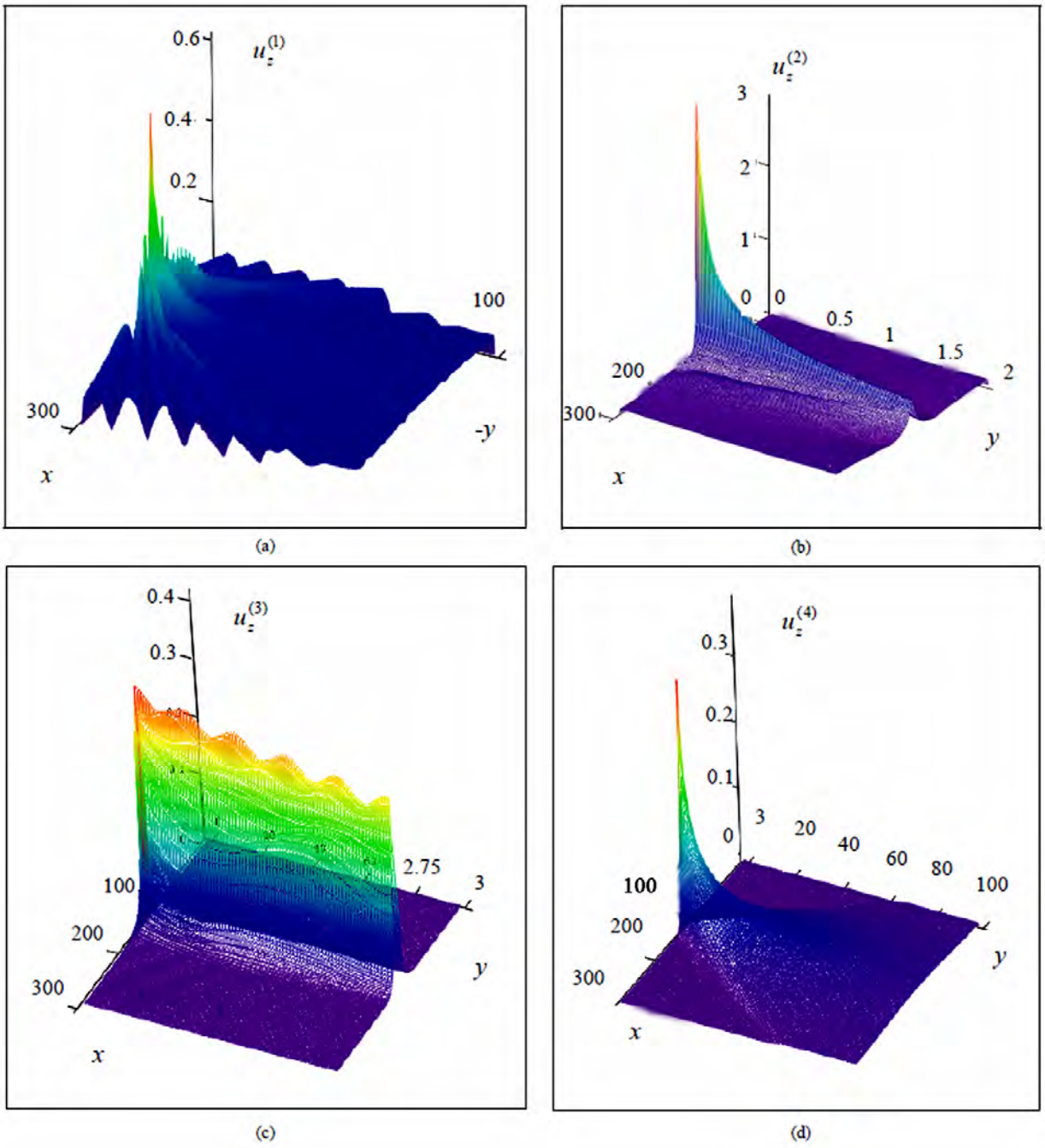

Figure 10. Fragments of the spatial distribution of the wave field for $c_t/C_t = 1.1$, $\omega h/C_t = 9.1\pi$, $\omega H/c_t = 5\pi$: (a) – Region 1; (b) – Region 2; (c) – Region 3; (d) – Region 4

The structures of the near fields of a vibration source, which are backscattered or transmitted through inhomogeneity, should be considered as a set of informative basic characteristics indirectly indicating the presence of a stratum with deposit. Shelf investigations of sea bottom sediments containing gas condensate layers can be similar to the search for hydrocarbon accumulation in geologic environment on land territories. In some cases, the search for inhomogeneities using harmonic oscillation sources can precede pulse location and determine only tentative information or boundary contours. In other cases, it is expedient to employ near-field probing using harmonic sources to increase reliability of pulse echo-sounding of geological structures or prediction accuracy

of their characteristics in remote diagnostics [9].

REFERENCES

[1] A. M. Derzhavin, O. V. Kudryavtsev and A. G. Semenov, "On Peculiarities of Numerical Simulation of a Vector Wave Field of a Low-Frequency Acoustic Source in the Ocean Medium," *Akusticheskii Zhurnal*, Vol. 46, No. 4, 2000, pp. 480-489.

[2] L. A. Bespalov, A. M. Derzhavin and O. V. Kudryavtsev, "On Simulation of a Seismoacoustic Field of a Low-Frequency Source for Variation in the Structure of Ocean Bottom Thickness," *Akusticheskii Zhurnal*, Vol. 45, No.1, 1999, pp. 25-37.

[3] L. M. Brekhovskikh, "Waves in Layered Media," Nauka, Moscow, 1973, p. 343.

[4] Y. M. Zaslavsky and V. Y. Zaslavsky, "Analysis of a Vibroacoustic Field in an Extended Layer and a Layer-Semispace Structure," *Izvestiya Vysshikh Uchebnykh Zavedenii*, *Radiofizika,* Vol. 7, No. 2, 2009, pp. 151-163.

[5] Y. M. Zaslavsky and V. Y. Zaslavsky, "Analysis of an Acoustic Field Excited by a Vibration Source in a Layer and its Vicinity," *Akusticheskii Zhurnal*, Vol. 55, No. 6, 2009, pp. 845-852.

[6] Y. M. Zaslavsky and V. Y. Zaslavsky, "Transverse Waves Excited by a Variable Power Source in a Layer and its Vicinity," *NNGU Vestnik*, *Radiofizika*, 2009, No. 5, pp. 61-68.

[7] Y. M. Zaslavsky, B. V. Kerzhakov and V. V. Kulinich, "Vertical Seismic Profiling on a Sea Shelf," *Akusticheskii Zhurnal*, Vol. 54, No. 3, 2008, pp. 483-490.

[8] Y. M. Zaslavsky, B. V. Kerzhakov and V. V. Kulinich, "Simulation of Wave Radiation and Phased Antenna Reception on the Ocean Shelf," *Akusticheskii Zhurnal*, Vol. 53, No. 2, 2007, pp. 264-273.

[9] J. L. Arroyo, P. Breton, H. Dijkerman, *et al*. "Superior Seismic Data from the Borehole," *Oilfield Review*, Vol. 15, No. 1, 2003, pp. 1-23.

J. Modern Physics, **2010, 1, 124-136**
doi:10.4236/jmp.2010.12018 Published Online June 2010 (http://www.SciRP.org/journal/jmp)

Exact Analytical and Numerical Solutions to the Time-Dependent Schrödinger Equation for a One-Dimensional Potential Exhibiting Non-Exponential Decay at All Times

Athanasios N. Petridis[1], Lawrence P. Staunton[1], Jon Vermedahl[1], Marshall Luban[2]

[1]Department of Physics and Astronomy, Drake University, Des Moines, USA;[2]Ames Laboratory and Department of Physics and Astronomy, Iowa State University, Ames, USA.
Email: athan.petridis@drake.edu

Received March 2nd, 2010; revised April 7th, 2010; accepted April 30th, 2010.

Abstract

The departure at large times from exponential decay in the case of resonance wavefunctions is mathematically demonstrated. Then, exact, analytical solutions to the time-dependent Schrödinger equation in one dimension are developed for a time-independent potential consisting of an infinite wall and a repulsive delta function. The exact solutions are obtained by means of a superposition of time-independent solutions spanning the given Hilbert space with appropriately chosen spectral functions for which the resulting integrals can be evaluated exactly. Square-integrability and the boundary conditions are satisfied. The simplest of the obtained solutions is presented and the probability for the particle to be found inside the potential well as a function of time is calculated. The system exhibits non-exponential decay for all times; the probability decreases at large times as t^{-3}*. Other exact solutions found exhibit power law behavior at large times. The results are generalized to all normalizable solutions to this problem. Additionally, numerical solutions are obtained using the staggered leap-frog algorithm for select potentials exhibiting the prevalence of non-exponential decay at short times.*

Keywords: *Non-Exponential, Decay, Exact, Solutions*

1. Introduction

The law of exponential decay is typically discussed in association with atomic transitions or resonances in scattering amplitudes. Even though the approximations made in order to arrive at exponential decay of excited states or resonances are well understood the mistaken impression that this law is universal and exact often prevails. This perception is reinforced by experiments often done in student laboratories geared towards studying the half-lives of radioactive nuclei or unstable particles and, very importantly, by numerous research publications and data tables in which exponential decay is tacitly assumed. The fact that these experiments measure counting rates during only finite time intervals and are focused on decays of quasi-stationary states is usually not discussed, let alone studied in detail.

The history of this particular problem is quite interesting. Early on Khalfin [1] used dispersion relations to show that even quasi-stationary states with spectral functions that have a lower bound in their energy spectrum must decay non-exponentially at large times. Winter [2] examined the infinite wall plus repulsive delta function potential and obtained a single implicit solution in the form of an integral for the special case in which the initial wavefunction is an eigenfunction of the infinite square well of the same width and as a result it is a near-resonance (quasi-stationary) state of the actual potential. His analytic approximation to the integral in the limit of low barrier transmittance (large strength of the delta function) proved that the survival probability exhibits exponential decay in the (intermediate) time interval-when the dominant quasi-stationary resonance prevails inside the well-while at very large times it decays following the power law t^{-3}. By means of numerical studies the same author found oscillations in the probability current at times before the power law sets

in if the initial state has a relatively wide energy spectrum.

The purpose of this article is to demonstrate explicitly the existence of systems that exhibit non-exponential decay at all times by developing exact, analytical, closed form solutions to the time-dependent Schrödinger equation for a one-dimensional potential and non-quasistationary initial states as well as to illustrate non-exponential decay using numerical solutions to specific problems for which analytical solutions are not obtainable. The clear advantage of the analytical approach without any approximations is that it yields an equation for the survival probability of the initial state that can be studied for any time interval and that is unequivocally non-exponential. The conclusions are easily generalized and the long-time behavior of the solutions is predicted and shown to follow an asymptotic power law. It is, thus, established that for a large class of systems, non-exponenential decay is the rule rather than the exception.

This paper also elucidates and generalizes previous research work. Recently there has been increasing interest in the time dependent Schrödinger equation and, in particular, in the decay of physical systems. The equivalence of exponential decay of a perturbed energy eigenstate with Fermi's golden rule when the final density of states is energy-independent and with the Breit-Wigner resonance curve has been long known and presented in several papers [3] and textbooks [4]. Dullemond [5] has verified this behavior for a simple but exactly solvable model and found, however, that if final-state energy-dependence is introduced into this model a non-exponential decay pattern will dominate at large times.

Oleinik and Arepjev [6] have shown that tunneling of electrons out of a finite potential well when a long-range electric field is suddenly switched on follows a t^{-3} probability decay law at large times. Specific systems that may exhibit non-exponential decay include systems with non-local interactions [7], certain closed many-body systems [8], quasi-particles in quantum dots [9], polarons [10], and non-extensive systems [11]. Petridis *et al.,* [12] have studied numerically a variety of systems in which the initial wave function is mostly or entirely set in a finite potential well and have observed rich behavior, including non-exponential decay into the continuum.

Non-exponential decay was experimentally observed for the first time by Wilkinson *et al.,* [13] in the tunneling of ultra-cold sodium atoms initially trapped in an accelerating periodic optical potential created by a standing wave of light. Kelkar, Nowakowski, and Khemchandani [14] have reported evidence for the non-exponential alpha decay of ^{8}Be. Rothe, Hintschich, and Monkman [15] have clearly measured non-exponential time-dependence in the luminescence decay of dissolved organic materials after pulsed laser excitation.

Time-dependent quantum mechanical problems are usually addressed using time-dependent perturbation theory, adiabatic or sudden approximations as well as several numerical techniques. Exact analytical solutions to certain problems are highly desirable, especially in cases when the approximate methods may be inadequate to describe all aspects of the solutions or when numerical treatments do not explicitly reveal their mathematical properties.

Burrows and Cohen [16] have developed exact solutions for a double-well quasi-harmonic potential model with a time-dependent dipole field. Cavalcanti, Giacconi, and Soldati [17] have solved the problem of decay from a point-like potential well in the presence of a uniform field and have indicated that, due to an infinitely large number of resonances, there may be deviations from the naively expected exponential time-dependence of the survival probability.

In this article a well established method for solving time-dependent quantum mechanics problems is used to develop exact, analytical, closed-form solutions to the infinite wall plus repulsive delta function potential. The large-time non-exponential decay for three solutions to this system is established and the asymptotic power law behavior is explicitly demonstrated to be t^{-3} for the first two and t^{-4} for the third. It is also proven that this result, (or a higher negative power of t), is valid for all square-integrable solutions to this system. Furthermore numerical solutions are developed for finite-range potentials and shown to exhibit a rich, non-exponential decay behavior, including oscillations.

2. The Exponential Decay Approximation

The time-dependent wavefunction, $\psi(x,t)$, can be expressed as a superposition of fixed energy states, $\Psi_E(x)$, each evolving in time as e^{-iEt},

$$\psi(x,t) = \int_{-\infty}^{\infty} \phi(E)\Psi_E(x)e^{-iEt}\,dE, \tag{1}$$

where $\Psi_E(x)$ are fixed-energy (stationary) solu- tions to the Schrödinger equation for the given Hamil- tonian and $\phi(E)$ is an energy distribution or "spectral function". It is important that this integral converge and the resulting wavefunction is square-integrable for the given boundary conditions (*i.e.*, it belongs to the related Hilbert space).

If the energy is non-negative and its distribution in the above integral has a dual-pole (resonance) structure in the complex plane, that is

$$\phi(E) = \frac{1}{(E-\varepsilon_0)(E-\varepsilon_0^*)} = \frac{1}{(E-E_0)^2+\Gamma^2}, \tag{2}$$

where $\varepsilon_0 = E_0 + i\Gamma$, and $0<\Gamma<<E_0$, then $\phi(E)$ is strongly peaked at E_0 and essentially only $\Psi_{E_0}(x)$ contributes, *i.e.*, to a good approximation

$$\psi(x,t) = \Psi_{E_0}(x)\int_0^\infty \frac{e^{-iEt}}{(E-E_0)^2+\Gamma^2}dE. \tag{3}$$

With the substitution $u = (E - E_0)/\Gamma$, the integral becomes

$$\psi(x,t) = \Psi_{E_0}(x)\frac{e^{-iE_0t}}{\Gamma}\int_{-E_0/\Gamma}^\infty \frac{e^{-i\Gamma tu}}{u^2+1}du. \tag{4}$$

Defining $\tau = \Gamma t > 0$ for forward evolution and $\mu = E_0/\Gamma > 0$ the above expression can be re-written as,

$$\psi(x,t) = \Psi_{E_0}(x)\frac{e^{-iE_0t}}{\Gamma}\left[C(\mu,\tau) - iS(\mu,\tau)\right], \tag{5}$$

where

$$C(\mu,\tau) = \int_{-\mu}^\infty \frac{\cos(u\tau)}{u^2+1}du,\ S(\mu,\tau) = \int_{-\mu}^\infty \frac{\sin(u\tau)}{u^2+1}du. \tag{6}$$

With $u' = -u$ the first integral is

$$\begin{aligned} C(\mu,\tau) &= \int_{-\infty}^\infty \frac{\cos(u\tau)}{u^2+1}du - \int_{-\infty}^{-\mu}\frac{\cos(u\tau)}{u^2+1}du \\ &= \pi e^{\tau} - \int_{\mu}^\infty \frac{\cos(u'\tau)}{(u')^2+1}du'. \end{aligned} \tag{7}$$

Similarly the second integral is

$$S(\mu,\tau) = \int_{-\infty}^\infty \frac{\sin(u\tau)}{u^2+1}du - \int_{-\infty}^{-\mu}\frac{\sin(u\tau)}{u^2+1}du = +\int_{\mu}^\infty \frac{\sin(u'\tau)}{(u')^2+1}du', \tag{8}$$

since the integrand in the first term is odd in u and vanishes as $|u|\to\infty$. The wavefunction, therefore, becomes (dropping the primes on u)

$$\psi(x,t) = \Psi_{E_0}(x)\frac{e^{-iE_0t}}{\Gamma}\left[\pi e^{\tau} - \int_{\mu}^\infty \frac{e^{iu\tau}}{u^2+1}du\right]. \tag{9}$$

At this stage the exponential-integral function

$$E_1(z) = \int_z^\infty \frac{e^{-y}}{y}dy \tag{10}$$

is useful. Clearly,

$$\frac{dE_1(z)}{dz} = -\frac{e^{-z}}{z}. \tag{11}$$

Upon defining the function

$$f(u,\tau) = -\frac{i}{2}\left[e^{\tau}E_1(\tau - iu\tau) - e^{-\tau}E_1(-\tau - iu\tau)\right], \tag{12}$$

its derivative is calculated to be

$$\begin{aligned} \frac{df}{du} &= -\frac{i}{2}\left[e^{\tau}\frac{dE_1(\tau-iu\tau)}{du} - e^{-\tau}\frac{dE_1(-\tau-iu\tau)}{du}\right] \\ &= \frac{\tau}{2}e^{iu\tau}\left[\frac{1}{\tau - iu\tau} - \frac{1}{\tau + iu\tau}\right] \\ &= \frac{e^{iu\tau}}{u^2+1}. \end{aligned} \tag{13}$$

Therefore,

$$\begin{aligned} \int_\mu^\infty \frac{e^{iu\tau}}{u^2+1}du &= f(u,\tau)|_\mu^\infty \\ &= -\frac{i}{2}\left[e^{\tau}E_1(\tau - i\mu\tau) - e^{-\tau}E_1(-\tau - i\mu\tau)\right]. \end{aligned} \tag{14}$$

Using the well-known expansion,

$$E_1(z) = \frac{e^{-z}}{z}\left(1 - \frac{1}{z} + \frac{2}{z^2} - ...\right), \tag{15}$$

and keeping only the two first terms for large $|\pm\tau - i\mu\tau|$, the wavefunction becomes

$$\begin{aligned} \psi(x,t) &\approx \Psi_{E_0}(x)\frac{e^{-iE_0t}}{\Gamma}\left[\pi e^{-\tau} - \frac{i}{\tau}\frac{e^{i\mu\tau}}{\mu^2+1}\right] \\ &= \Psi_{E_0}(x)\frac{e^{-iE_0t}}{\Gamma}\left[\pi e^{-\Gamma t} - \frac{i}{t}\frac{\Gamma e^{iE_0t}}{E_0^2+\Gamma^2}\right]. \end{aligned} \tag{16}$$

Thus, the probability density for times large relative to $(E_0^2+\Gamma^2)^{-1/2}$ is

$$\begin{aligned} |\psi(x,t)|^2 \approx |\Psi_{E_0}(x)|^2 &\left[\frac{\pi^2}{\Gamma^2}e^{-2\Gamma t} + \frac{1}{t^2}\left(\frac{1}{E_0^2+\Gamma^2}\right)^2\right. \\ &\left. + \frac{2\pi}{\Gamma}\frac{1}{t}\frac{e^{-\Gamma t}}{E_0^2+\Gamma^2}\sin(E_0t)\right] \end{aligned} \tag{17}$$

and it has a term decaying exponentially with constant 2Γ plus a t^{-2} term dominating at very large times as well as an "intermediate" decaying oscillatory term. In this example not only is the rise of exponential decay shown to emerge for a spectral function exhibiting a resonance (dual-pole) structure but the departure from this behavior at large times is clearly elucidated, having a power-law dependence. It is noteworthy that the non-exponential behavior is related to the cut-off in the energy interval. If the energy were to vary over the entire real axis then the residue theorem would yield exponential decay. The short time behavior is very complicated as Equation (9) indicates and it is also not exactly exponential.

3. Infinite Wall and Delta-function Potential

The method to be employed to address the problem of an infinite wall plus a delta-function potential is standard and consists of the following steps: a) The time-independent solutions to Schrödinger equation are found subject to the boundary conditions of the problem. These

are stationary solutions (energy eigenfunctions) that span the Hilbert space of the given Hamiltonian. b) Since any finite or infinite, discrete or continuous linear combination of the stationary solutions (basis functions), as long as it is square-integrable, is also a solution belonging to the given Hilbert space, exact analytical solutions can be developed by a superposition of the eigenfunctions with energy-dependent spectral functions multiplied by the standard oscillatory time-dependence of the stationary states. It is, obviously, necessary that the superposition integral over the energy converge. Spectral functions for which the resulting integrals are tractable are chosen here. The convergence as well as the square-integrability (normalizability) of the resulting wave functions are verified. c) The survival probability, *i.e.*, the probability for finding the particle inside the potential well is calculated and its properties are studied analytically.

The problem is defined by the one-dimensional repulsive potential,

$$V(x)=\begin{cases}\infty & -\infty < x \le 0\\ V_0\,\delta(x-L) & 0 \le x < \infty,\end{cases} \tag{18}$$

with $L>0$ and $V_0>0$. The steps outlined above are followed.

a) The solutions to the time-independent Schrödinger equation,

$$-\frac{1}{2}\frac{d^2\Psi_E(x)}{dx^2}+V(x)\Psi_E(x)=E\,\Psi_E(x), \tag{19}$$

(with particle mass $m=1$, $\hbar=1$, and $E\ge 0$ for this potential) are,

$$\Psi_E^{(0)}(x)=0,\ -\infty \le x \le 0\ (region\ "0"), \tag{20}$$

$$\Psi_E^{(I)}(x)=C_1\sin(px),\ 0\le x\le L\ (region\ "I"), \tag{21}$$

$$\Psi_E^{(II)}(x)=C_2\sin(px)+C_3\cos(px),\quad L\le x\le\infty\ (region\ "II"), \tag{22}$$

where $p=\sqrt{2E}$ and $C_{1,2,3}$ are constants in *x*. These functions obey the boundary conditions

$$\Psi_E^{(I)}(L)=\Psi_E^{(II)}(L), \tag{23}$$

$$\frac{d\Psi_E^{(I)}}{dx}(L)-\frac{d\Psi_E^{(II)}}{dx}(L)=2V_0\,\Psi_E^{(I)}(L), \tag{24}$$

while the boundary conditions at $x=0$ are automatically satisfied. The energy eigenfunctions, Ψ_E, are not required to vanish at infinity since time-dependent functions, $\psi(x,t)$, produced by Equation (1) for large *x* are acceptable solutions. Selecting C_1 as the overall normalization constant, the boundary conditions at $x=L$ yield

$$C_2=C_1\left[1+\left(\frac{2V_0}{p}\right)\sin(pL)\cos(pL)\right], \tag{25}$$

$$C_3=-C_1\left(\frac{2V_0}{p}\right)\sin^2(pL), \tag{26}$$

rendering C_2 and C_3 functions of the energy. The choice of C_2 or C_3 as the normalization constant would introduce an energy-dependence in C_1 and would effectively amount to different choices of spectral functions.

The linearly independent energy eigenfunctions obtained are orthogonal under the inner product

$$(\psi_1,\psi_2)=\int_0^L\psi_1^*(x)\psi_2(x)\,dx+\lim_{\varepsilon\to 0}\int_L^\infty e^{-\varepsilon(x-L)}\psi_1^*(x)\psi_2(x)\,dx, \tag{27}$$

with all wavefunctions in the defined Hilbert space identically vanishing for $x\le 0$. The orthogonality relation is

$$(\Psi_E,\Psi_{E'})=w(E)\,\delta(p-p'), \tag{28}$$

where $p=\sqrt{2E}$, $p'=\sqrt{2E'}$ and

$$w(E)=\frac{\pi}{2}\left[|C_2(E)|^2+|C_3(E)|^2\right]$$

$$=|C_1|^2\frac{\pi}{2p^2}\left[p^2+2V_0^2-2V_0^2\cos(2pL)+2pV_0\sin(2pL)\right]. \tag{29}$$

The Dirac δ-function representation used is

$$\delta(p-p')=\lim_{\varepsilon\to 0}\frac{1}{\pi}\frac{\varepsilon}{(p-p')^2+\varepsilon^2}. \tag{30}$$

b) The solution to the time-dependent Schrödinger equation,

$$i\frac{\partial\psi(x,t)}{\partial t}=-\frac{1}{2}\frac{\partial^2\psi(x,t)}{\partial x^2}+V(x)\psi(x,t), \tag{31}$$

can be written as the energy-convolution integral,

$$\psi(x,t)=\int_0^\infty\phi(E)\Psi_E(x)e^{-iEt}\,dE, \tag{32}$$

with $\phi(E)$ a spectral function such that this integral is convergent for all x and all t and the resulting wavefunction is square-integrable. Note that square-integrability of $\psi(x,t)$ also requires E to be real. The overall normalization constant is, then, calculated from

$$\int_0^\infty\psi^*(x,t)\psi(x,t)\,dx=1. \tag{33}$$

The first choice of spectral function to be considered is

$$\phi_1(E) = e^{-K^2 E}, \tag{34}$$

with K a positive constant. This offers the advantage that the integrals above can be evaluated in closed form and the resulting wave function is square-integrable even without the presence of the convergence factor that appears in Equation (27). The time-dependent solution is, then,

$$\psi^{(0)}(x,t) = 0, \tag{35}$$

$$\psi^{(I)}(x,t) = C_1 \sqrt{\frac{\pi}{2}}\, x e^{-\frac{x^2}{2(K^2+it)}} (K^2+it)^{-3/2}, \tag{36}$$

$$\psi^{(II)}(x,t) = C_1 \sqrt{\frac{\pi}{2}} e^{-\frac{2L^2-2Lx+x^2}{K^2+it}} (K^2+it)^{-3/2}$$

$$\left[e^{\frac{x^2}{2(K^2+it)}} (K^2+it)V_0 + e^{\frac{(-2L+x)^2}{2(K^2+it)}} (-K^2 V_0 - itV_0 + x) \right], \tag{37}$$

where

$$C_1 = \left[\frac{\pi^{3/2}}{8K^3} + \frac{e^{-\frac{L^2}{K^2}} L\pi^{3/2} V_0}{2K^3} + \frac{\pi^{3/2} V_0^2}{2K} - \frac{e^{-\frac{L^2}{K^2}} \pi^{3/2} V_0^2}{2K} \right]^{-1/2} \tag{38}$$

is the overall normalization factor obtained by means of Equation (33).

c) The probability density $\rho = \psi^*(x,t)\psi(x,t)$ can be calculated for the interior (region I) and the exterior (region II) of the potential well. It is presented in **Figure 1** at six times starting from $t = 0$, in increasing order. The initial wavefunction is not entirely localized inside the well. As time progresses the wavefunction spreads and tunnels through the potential barrier in both directions. The interference of the wave that propagates outwards through the barrier and the wave that is outside creates the observed ripples. Inside the well there are no ripples because the wavefunction is forced to be odd in x, having a node at $x = 0$. The centroid of the probability density in region II at $t = 0$ is always located at $2L$, regardless of the value of K.

The survival probability is, then, defined to be

$$P_{in}(t) = \int_0^L \psi^*(x,t)\psi(x,t)\, dx. \tag{39}$$

This yields the closed-form result

$$P_{in}(t) = C_1^2 \left[\frac{\pi^{3/2}}{8K^3} \mathrm{erf}\left(\frac{KL}{\sqrt{K^4+t^2}} \right) - \frac{2\pi KL}{8K^3\sqrt{K^4+t^2}} e^{-\frac{K^2 L^2}{K^4+t^2}} \right] \tag{40}$$

A plot of the survival probability versus time is given in **Figure 2**. $P_{in}(0)$ is controlled by K. It decreases as K increases, *i.e.*, as the momentum spectrum becomes sharper. For example, if $L = 3$, $P_{in}(0)$ is 0.9615 for $K = 0.1$, 0.5 for $K = 0.5$, and 0.1468 for $K = 1.2$. A physical interpretation of this effect is that at $t = 0$ some decays have already happened. On the other hand the decay becomes slower as K increases. The expansion of P_{in} in inverse powers of time includes only odd terms with alternating signs. At large times the leading term, that has a positive sign, is proportional to t^{-3}, a clearly non-exponential behavior.

4. Corrections to the Exponential Decay Law

The law governing the decay of physical systems is typically assumed to be a simple exponential time-dependence of the number $N(t)$ of the systems that have not decayed until time t, *i.e.*, $N(t) = N(0)\, exp(-\lambda t)$, where λ is the decay constant. As mentioned earlier this simple law is consistent with the Breit-Wigner curve and Fermi's golden rule if the final density of states is energy independent. It refers to the survival probability of a given initial energy resonance (quasi-stationary state). For the choice of spectral function given by Equation (34) the initial state is not a resonance state. If a very large number of systems is assumed to be initially described by $\psi(x,0)$ and a system is said to have decayed if the particle has exited the potential well, then the number of surviving systems is proportional to the probability P_{in}, *i.e.*,

$$\frac{N(t)}{N(0)} = \frac{P_{in}(t)}{P_{in}(0)}. \tag{41}$$

The differential decay law is

$$dN = -\lambda(t) N(t)\, dt, \tag{42}$$

where, λ is, in general, dependent on time. Substitution from Equation (41) gives

$$\lambda(t) = -\frac{1}{P_{in}} \frac{dP_{in}}{dt} = -\frac{d}{dt}[ln(P_{in}(t))]. \tag{43}$$

In the case studied, Equation (40) yields

$$\lambda(t) = \frac{4e^{-z^2} z^3 t}{(K^4+t^2)[-2ze^{-z^2} + \sqrt{\pi}\, erf(z)]}, \tag{44}$$

where $z = KL/\sqrt{K^4+t^2}$. This function is plotted versus time in **Figure 3**.

The decay parameter λ peaks in time. Its maximal value, λ_{max}, is smaller as K or L increases but does

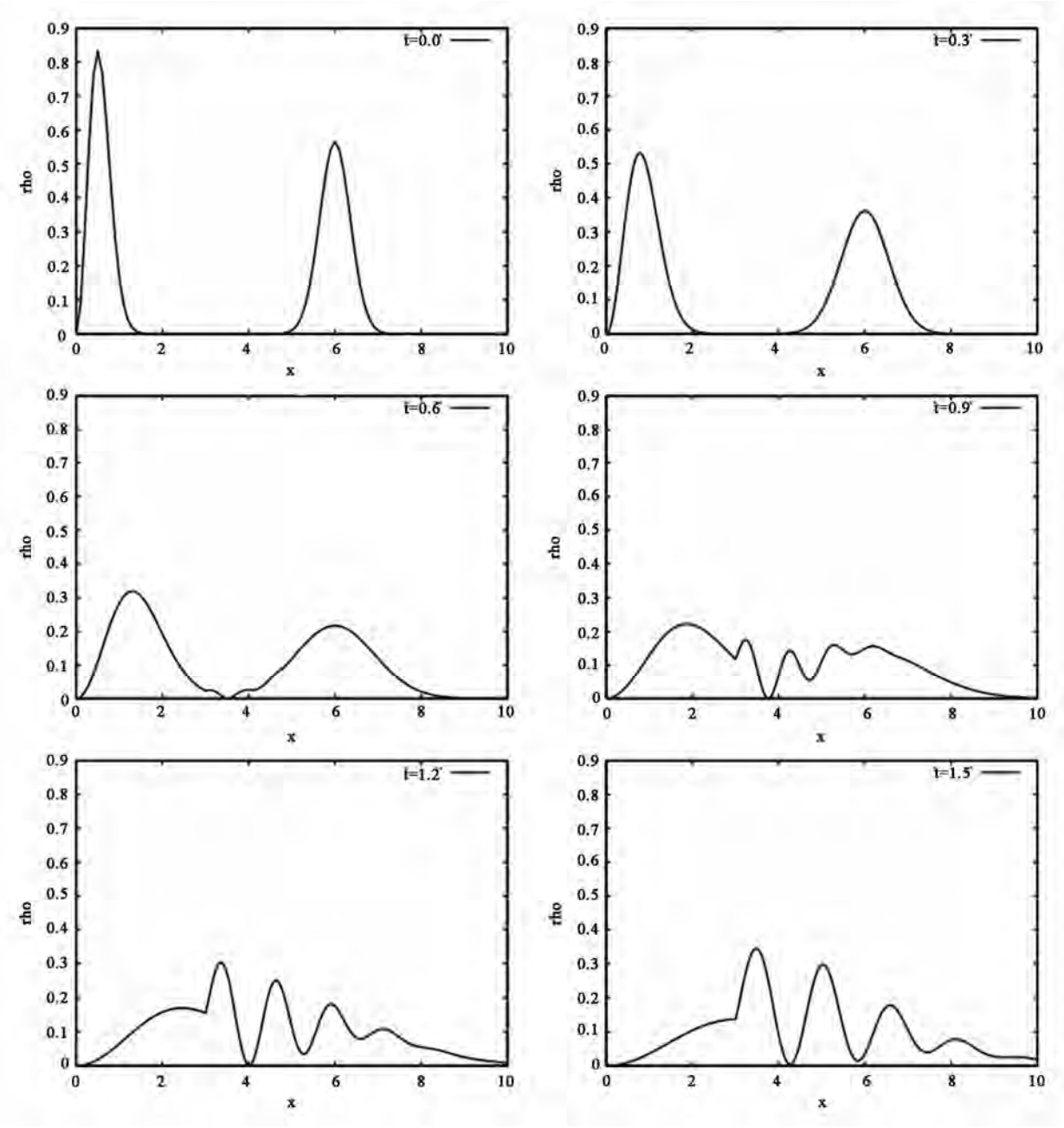

Figure 1. The probability density for a potential consisting of an infinite wall and a repulsive delta function and using the spectral function given by Equation (34) at six times (from the upper panel in the left colume to the lower panel in the right column, $t = 0.0, 0.3, 0.6, 0.9, 1.2, 1.5$). In this plot $L = 3$, $V_0 = 1$ and $K = 1/2$

not depend on V_0. The peak and the small time interval around it correspond to an almost exponential decay. This, however, cannot be directly associated with the dominant (lowest energy) resonance that this potential accommodates. Resonances in the energy can be identified as the maxima of the function [18]

$$g(E) = \frac{|C_1|^2}{|C_2|^2 + |C_3|^2} = \frac{2E}{2E + 2V_0^2[1-\cos(L\sqrt{8E})] + V_0\sqrt{8E}\sin(L\sqrt{8E})}, \quad (45)$$

plotted in **Figure 4** for $L = 3$ and $V_0 = 1$. It can be

seen that the resonances are not exactly of the Breit-Wigner shape, therefore they do not decay exactly exponentially. The dominant (lowest peak energy) resonance has a width at half maximum of ≈ 0.1 corresponding to a "life-time" of ≈ 10. In a resonant decay the width in energy is expected to be equal to the value of the decay constant. Clearly, the width here is very different from $\lambda_{max} \approx 1.3$ (**Figure 3**). The resonance peak energy and width depend only on the strength and the geometry of the potential, while λ_{max} also depends on the spectral function. The choice $\phi_1(E)$ used

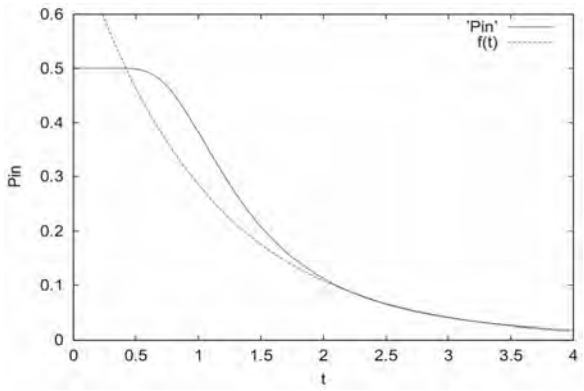

Figure 2. The survival probability for a potential consisting of an infinite wall and a repulsive delta function and using the spectral function given by Equation (34) versus time (solid line). In this plot $L = 3$, $V_0 = 1$ and $K = 1/2$. The dashed line represents the exponentially decaying function, $f(t) = a\exp(-bt)$, fitted to data points, calculated from the actual solution, in the range $t = 2$ to 4. The χ^2 per degree of freedom is of order 10^{-6}

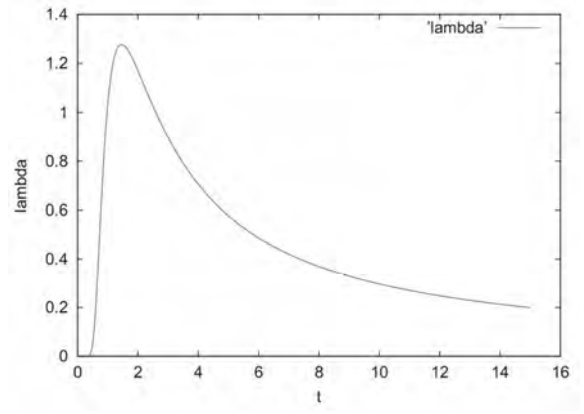

Figure 3. The decay parameter λ for a potential consisting of an infinite wall and a repulsive delta function and using a spectral function that is exponential in the energy versus time. In this plot $L = 3$ and $K = 1/2$. There is no dependence on V_0

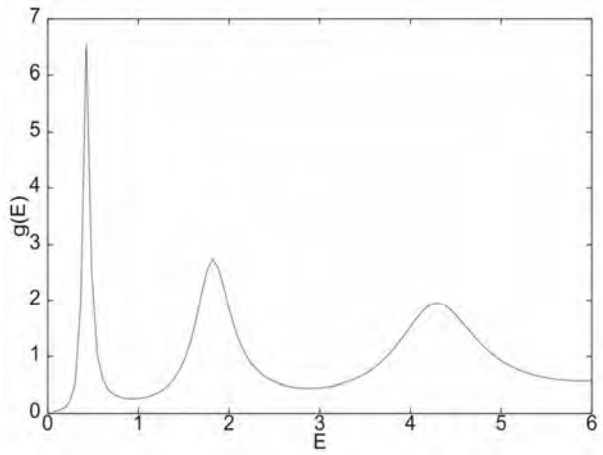

Figure 4. Energy resonances for the infinite wall plus repulsive delta function potential for $L = 3$ and $V_0 = 1$

here does not give this resonance a large weight (as opposed to Winter's choice which involves an initial state very close to the resonance for large V_0). The lower energy components of the wavefunction indeed dominate and tunnel through the barrier at a slow rate smearing the resonance effect. Therefore, the limited quasi-expo- nential behavior observed in this study is not of a resonance nature.

The expansion of λ in inverse powers of time includes only odd terms with alternating signs. At large times the leading term, that has a positive sign, is proportional to t^{-1}, affirming the non-exponential behavior. At very large times the change of λ with time is rather slow. A fit to P_{in} at large times with an exponential curve in a finite time interval (as it is done in experiments) gives a very small value of χ^2 per degree of freedom (of order 10^{-6}) so that the distinction between P_{in} at large times and a simple exponential decay function is numerically minute (**Figure 2**).

5. Generalization

Exact, closed-form, analytical solutions to the time-dependent Schrödinger equation for the potential consisting of an infinite wall and a repulsive delta function have been obtained by the authors of this article for other spectral function choices. For example, the choice

$$\varphi_2(E) = -\frac{i\left[1-\cos\left(\frac{L}{2}\sqrt{2E}\right)\right]}{2E\sqrt{\pi L}} \tag{46}$$

yields a square-integrable wavefunction. In the absence of the delta function at $x = L$ this would produce an effectively square density pulse at $t = 0$ located

between $x = 0$ and $x = L/2$. Due to the actual boundary conditions at $x = L$ this spectral function also produces a cusp centered at $x = 2L$. The survival probability is readily expressible in terms of Fresnel sine and cosine integrals [19]. Its asymptotic large time behavior is t^{-3}.

A question that naturally arises at this point is whether the asymptotic time behavior can be generalized to other possible solutions to this problem. This question was first addressed by Khalfin [1] specifically for the case of quasi-stationary initial states. Here a detailed answer is provided for non-resonance cases employing the general requirements of convergence and square-integrability. There is a one-to-one correspondence between spectral functions and square-integrable wavefunctions. This can be seen upon projecting the wavefunction at $t = 0$ on an energy eigenfunction and employing the orthogonality condition of Equation (28):

$$\phi(E) = \frac{1}{w(E)} \int_0^\infty \Psi_E^*(x)\psi(x,0)\, dx. \qquad (47)$$

Given an initial wavefunction the corresponding spectral function can, in principle, be constructed. Schrödinger's time-dependent equation then produces the wavefunction at any later (or earlier) time.

Convergence of the energy superposition integral in region (II) requires that the spectral function be finite at $E \to 0$. In addition, in order for $\psi(x,t)$ to be square-integrable, $\phi(E)$ must vanish at large energies. This requirement can be made precise by inserting Equation (32) into Equation (33) and applying Equation (28) to obtain

$$\int_0^\infty w(E)\,|\,\phi(E)\,|^2\, dE = 1. \qquad (48)$$

Inspection of the function $w(E)$, given in Equation (29), leads to the conclusion that $|\phi(E)|$ must vanish for $E \to \infty$ faster than $1/\sqrt{E}$ due to a constant term in $w(E)$.

Assuming that $\phi(E)$ satisfies the convergence conditions and has no resonance structure, its contribution to the energy superposition integral giving $\psi^{(I)}(x,t)$, in region (I), comes mostly from low energies. Again, this situation must be contrasted to the case studied by Winter [2]. Then at any x in region (I) the wavefunction can be approximated as

$$\psi^{(I)}(x,t) \approx C_1\varphi(0)\int_0^{E_{max}(t)} \sqrt{2E}\; x\, e^{-iEt}\, dE. \qquad (49)$$

The upper limit of the integration is chosen as follows: the factor $\exp(-iEt)$ oscillates more rapidly as a function of the energy as t increases. At very large times these oscillations eventually lead to a vanishing contribution to the integral. Therefore, the integral can be cut off at a point $E_{max}(t)$ whose first order term in the expansion in powers of $1/t$ is y_{max}/t, where y_{max} is constant in t. At low energies $\phi(E)$ is replaced by its (finite and non-zero) value at $E = 0$ and the function $\sin(x\sqrt{2E})$ is replaced by its argument at a given x. Then, the variable change $y = Et$ yields

$$\psi^{(I)} \approx C_1\phi(0)\; x\, t^{-3/2} \int_0^{y_{max}} \sqrt{2y}\; e^{-iy}\, dy. \qquad (50)$$

For small y_{max} the integral is approximately $\sqrt{2}[(2/3)\, y_{max}^{3/2} - i\,(2/5)\, y_{max}^{5/2}]$. The wavefunction in region (I) is to the first non-vanishing order

$$\psi^{(I)}(x,t) \approx C_1\phi(0)\, x M\, t^{-3/2}, \qquad (51)$$

where M is a constant and the survival probability (Equation (39)) decreases with time as t^{-3}. Therefore, in order for the wavefunction to be square-integrable, the spectral function must be finite at $E \to 0$ and decrease at large E faster than $1/\sqrt{E}$. Then, if $\phi(0) \neq 0$, necessarily, the survival probability asymptotically decreases as t^{-3}.

This argument can be extended to any finite value of x including region (II) since the coefficients C_2 and C_3 are at most of $O(1)$ for small E. Therefore, the integral of the probability density over any finite range of x is finite (even without the convergence factor present in Equation (27)) and it decreases asymptotically as t^{-3}.

The constant M in Equation (51) can be exactly evaluated if $\phi(E)$ decreases at large E faster than $1/E$. Then if $\phi(E)$ is analytic in the fourth quadrant of the complex E-plane the contour integral of $\varphi(E)\sin(x\sqrt{2E})\exp(-iEt)$ along a closed path, consisting of the positive real axis from R to 0, the negative imaginary axis from 0 to $-iR$ and a quarter-circle, Γ, of radius R, is zero (**Figure 5**). The integral along Γ is bounded by a constant times $1/R^k$ with $R = |E|$ and $k > 1$ and, consequently, vanishes in the limit $R \to \infty$. Then the integration over the real axis gives the same result as that over the imaginary axis. The variable change $E = -iy$ with y real, then, yields

$$\psi^{(I)}(x,t) = -iC_1\int_0^\infty \varphi(-iy)\sin\left(x\sqrt{-2iy}\right) e^{-yt}\, dy. \qquad (52)$$

For large times only small values of y contribute to the integral. The spectral function is substantially

different from zero only close to the origin and can be replaced by $\phi(0)$ and be pulled out of the integral while the sine function can be approximated by its argument in a finite range of x. The remaining integral is evaluated as a gamma function and gives

$$\psi^{(I)}(x,t) \approx C_1\phi(0)\, x\, e^{-i3\pi/4}\sqrt{\pi/2}\; t^{-3/2} \quad (53)$$

confirming the earlier result.

The survival probability, P_{in}, discussed thus far refers to the presence of the particle inside the potential well. As has been shown in the previous section the spectral function of Equation (34) produces non-zero probability density outside the well at $t=0$ for $K>0$. If the "interior" of the well is defined to extend to x much larger than $2L$ (without moving the delta function from $x=L$) then at $t=0$ the probability to find the particle "inside" can be arbitrarily close to unity. Specifically the "extended" survival probability $P_{in}(4L)$ can be defined by extending the integral of Equation (39) to $x=4L$. This integral has been evaluated analytically and is plotted in **Figure 6** as a function of time. As predicted and verified by an expansion of $P_{in}(4L)$ in inverse powers of time, its asymptotic time dependence is t^{-3}. An interesting feature of this plot is the presence of a step-wise behavior which can be attributed to interference between waves moving in opposite directions.

The spectral function

$$\varphi_3(E) = \begin{cases} E(V_0 - E) & \text{if } 0 \le E \le V_0 \\ 0 & \text{otherwise}, \end{cases} \quad (54)$$

has also been investigated. This yields an exact, closed form result which is square integrable [19]. In this case $\phi_3(0)=0$ so that the survival probability does not vary as t^{-3}. Rather, it varies as t^{-4}. A variation of the above analysis shows this to be the expected behavior. It should be clear that the lowest order non-vanishing term in an expansion of the spectral function about zero will control the behavior.

6. Numerical Examples

The discussion in the previous sections indicates that if the initial wavefunction is not near a resonance state of the given potential, exponential decay of the survival probability should not be expected. However, analytical, closed form solutions can only be obtained for a small number of potentials and initial states. A numerical approach is, then, needed to study arbitrary potentials and initial functions. To this end the time-dependent Schrödinger equation can be solved using the staggered leap-frog method on a grid of spatial points of lattice constant Δx and with an appropriate time-step Δt. The method consists of computing the wavefunction at time $t+2\Delta t$ starting with the function at time t and updating it with the Hamiltonian at $t+\Delta t$, as follows:

$$\psi(x,t+2\Delta t) = \psi(x,t) - i\,2\Delta t[\hat{H}(x)\psi(x,t+\Delta t)]. \quad (55)$$

This method being time-symmetric can be made very stable for a time step that is much smaller than the spacial lattice constant and, on a fine grid, it is also very accurate. The spatial derivative in the Hamiltonian, $\hat{H} = -1/2\, d^2/dx^2 + V(x)$, is computed using a spatially symmetric formula. The spatial grid is chosen to be much larger than the dimensions of the problem and on its edges reflecting boundary conditions are applied (*i.e.*,

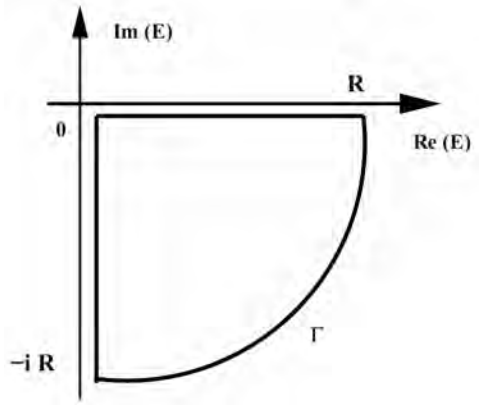

Figure 5. The complex plane contour used to calculate the integral over E.

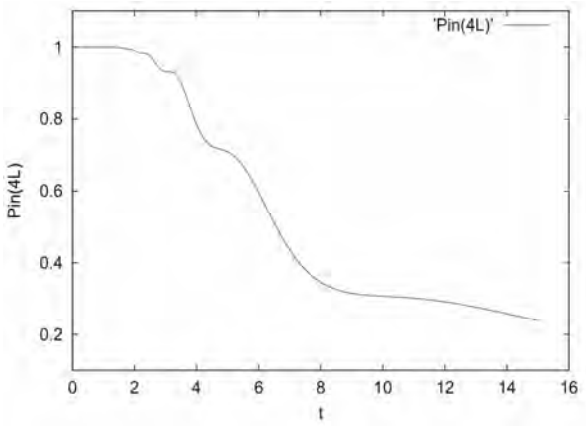

Figure 6. The "extended" survival probability for a potential consisting of an infinite wall and a repulsive delta function and using the spectral function given by Equation (34) versus time. In this plot $L=3$, $V_0=1$ and $K=1/2$. The step-wise behavior is due to interference of waves moving in opposite directions

the wavefunction is forced to be 0 there). This ensures that no probability density leaks out of the grid but requires that the reflected waves not interfere with the wavefunction in the region of interest. Therefore, when such interference starts (inevitably) occurring at appreciable levels the computation is stopped. The Schrödinger equation is self-dispersive and does not obey relativistic causality. As a result, very fast moving or even superluminal components of the wavefunction can occur and reflect on the grid boundaries. The stability of the numerical solution is checked by evaluating the norm of the wavefunction at regular intervals to ensure it is equal to 1. This is achieved with 10^{-9} precision. Several cases, such as free gaussian wavepackets (spreading with time) or a harmonic oscillator potential with an initial wavefunction that is a linear combination of eigenstates, have been solved to verify that the method accurately reproduces known analytical results.

The numerical technique is used to study the short-time behavior of a wavefunction that is initially set in a potential well of finite size and strength and then tunnels through its walls. Two simple potential functions are used to this end. The first one is a cut harmonic oscillator potential,

$$V(x) = \begin{cases} \frac{1}{2}\alpha(x-x_0)^2 & \text{if } |x-x_0| \le \frac{B}{2} \\ 0 & \text{otherwise,} \end{cases} \quad (56)$$

and the second is a cut linear potential,

$$V(x) = \begin{cases} k|x-x_0| & \text{if } |x-x_0| \le \frac{B}{2} \\ 0 & \text{otherwise .} \end{cases} \quad (57)$$

The initial wavefunction is chosen to be a gaussian with no initial central momentum. Results for the survival probability, P_{in}, defined as the integral of the density inside the potential well, for the case of the cut harmonic oscillator potential are shown in **Figure 7**. Here T_c indicates the classical period corresponding to the *infinite* harmonic oscillator potential with $m = 1$. There is a distinctive step-wise decay due to oscillations of the wavefunction. Each time the probability drops sharply a wavepacket is emitted on either side of the well. The derivative of P_{in} with respect to time is also shown to illustrate that it approaches 0 periodically. The qualitative features of the decay are not sensitive to the ratio of the standard deviation of the gaussian to the value of B. In the same manner results for the cut

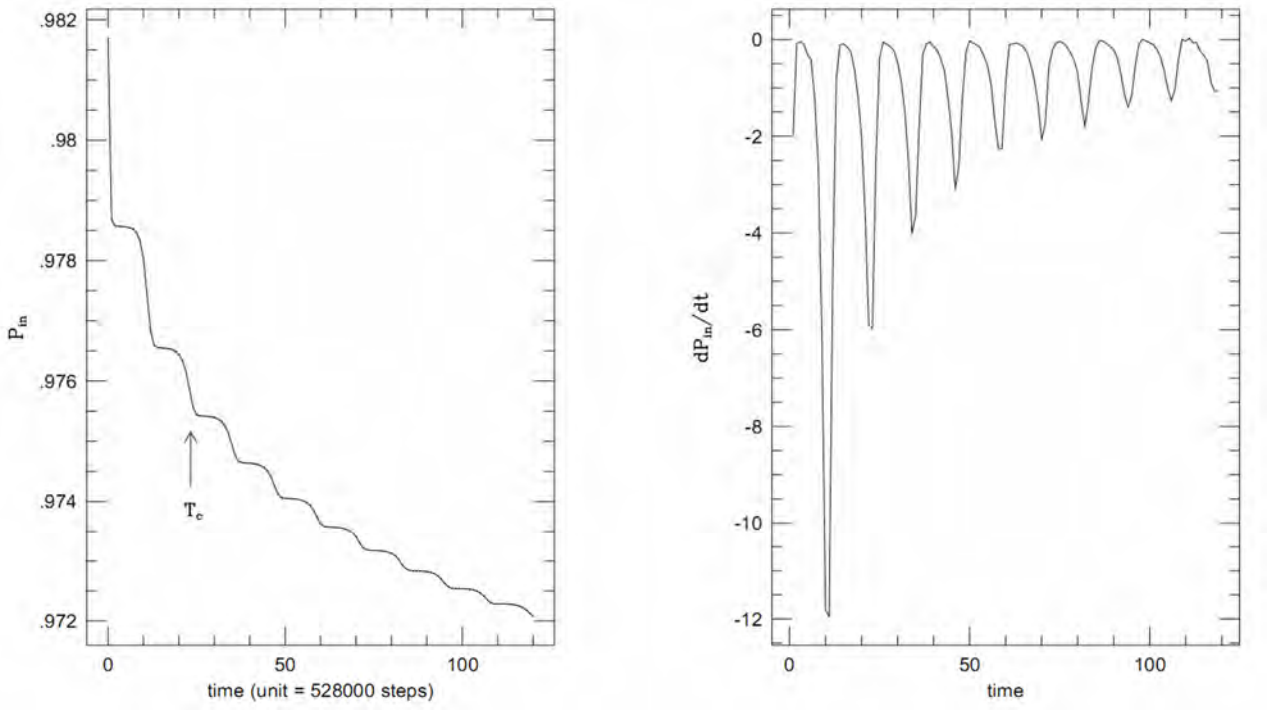

Figure 7. Results for a cut harmonic oscillator potential given by Equation (56) (α = 0.0001 and B = 200) with an initially gaussian wavepacket and 0 central momentum. Upper: the survival probability versus time exhibiting periodic flat regions; Lower: the derivative of the survival probability. The negative peaks occur when wavepackets emitted from the potential. T_c is the period for the infinite harmonic oscillator potential with spring constant, α. This behavior is similar to that seen with a cut linear potential

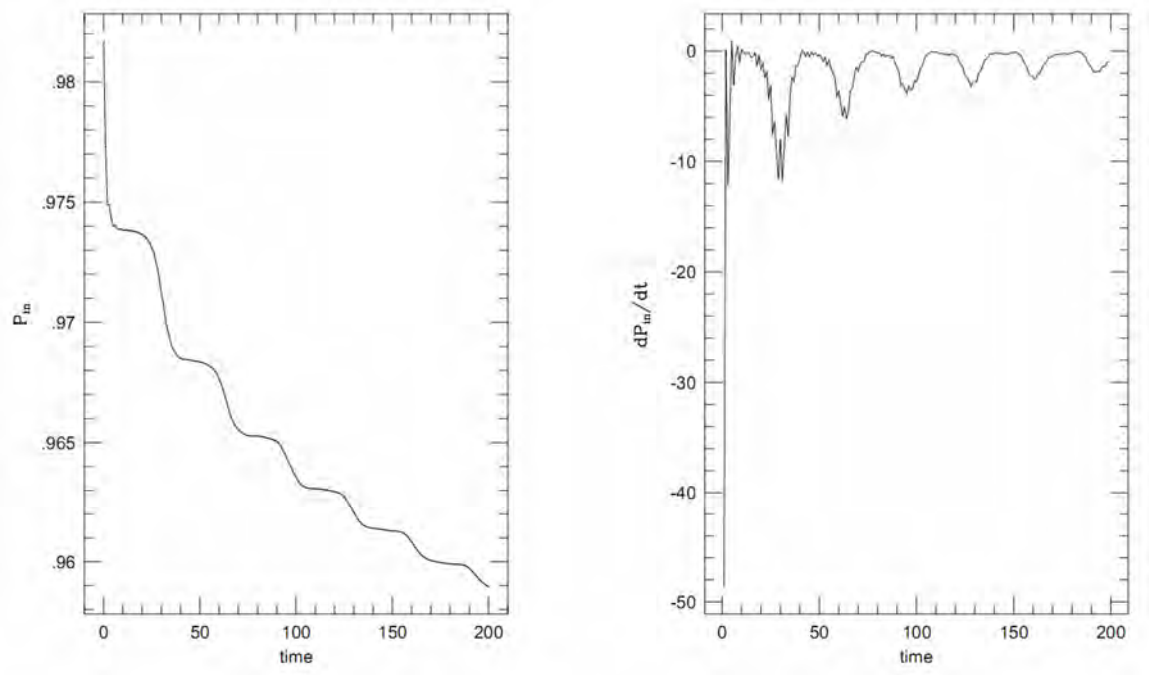

Figure 8. Results for a cut linear potential given by Equation (57) with an initially gaussian wavepacket having 0 central momentum. Upper: the survival probability versus time exhibiting periodic flat regions; Lower: the derivative of the survival probability. The negative peaks occur when wavepackets are emitted from the potential. This behavior is similar to that seen with a cut harmonic oscillator potential

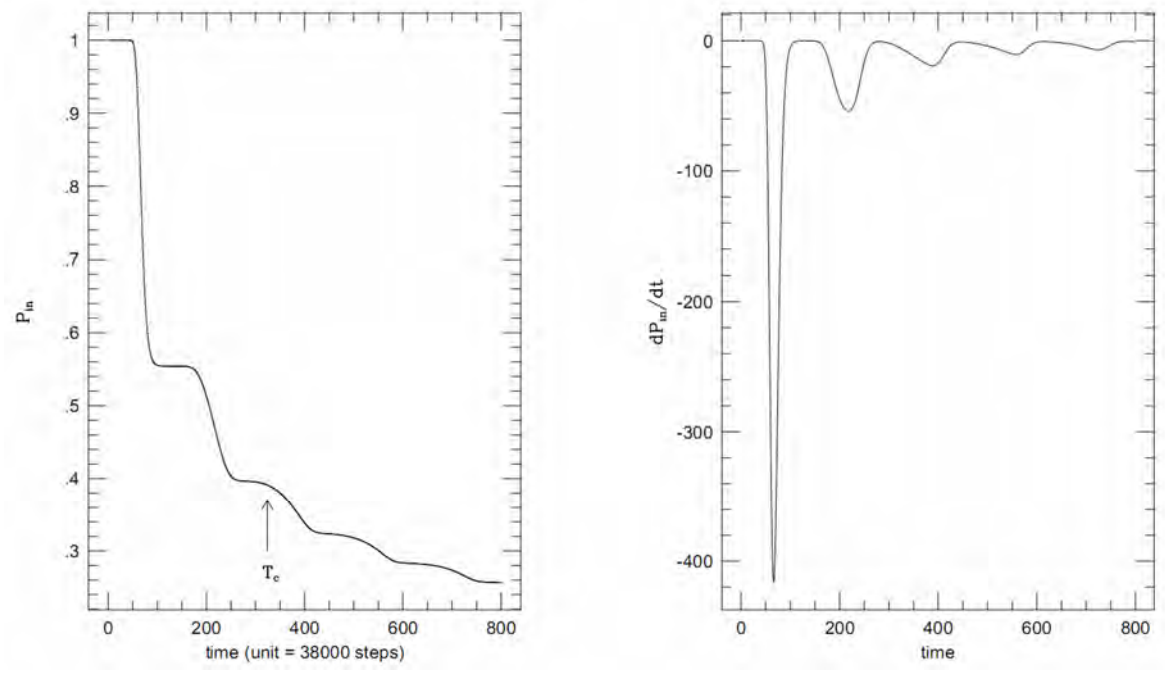

Figure 9. Results for a cut harmonic oscillator potential given by Equation (56) ($\alpha = 0.0001$ and B = 200) with an initially gaussian wavepacket that is the ground state of the infinite potential, having non-zero central momentum $p = 1.0$. Upper: the survival probability versus time exhibiting periodic flat regions; Lower: the derivative of the survival probability. The negative peaks occur when wavepackets emitted from the potential

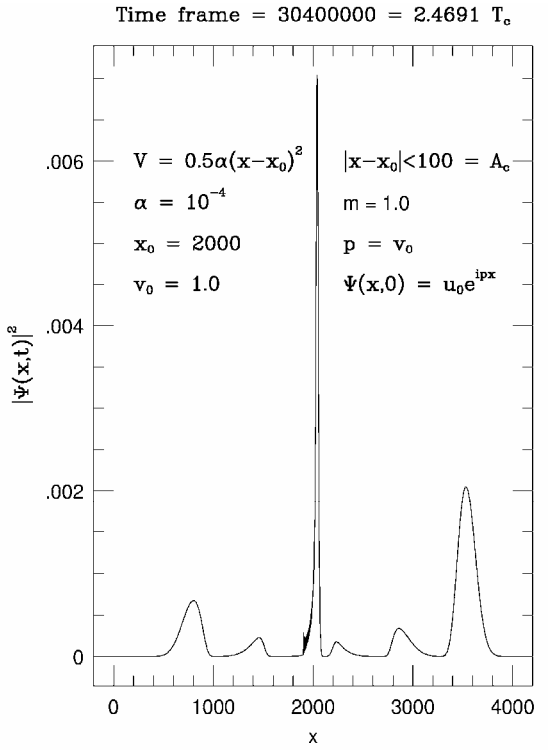

Figure 10. The probability density for a cut harmonic oscillator potential given by Equation (56) (α = 0.0001 and B = 200) with an initially gaussian wavepacket that is the ground state, u_0, of the infinite potential, having non-zero central momentum, $p = 1.0$, captured at about 2.5 classical periods of the infinite potential. The classical amplitude of oscillations is $A_c = 100$. All quantities are expressed in natural units. Wavepackets are periodically emitted from the non-zero potential region, propagate outwards and spread out. The first emitted packet is traveling to the right and at this time frame is centered at $x \approx 3500$. The second emitted packet is traveling to the left and at this moment is centered at $x \approx 900$. The interior wavefunction is hitting the left wall of the potential well at this moment

linear potential are shown in **Figure 8** with similar initial conditions. Again the decay is non-exponential with a step-wise behavior. To illustrate this result further an initial gaussian with non-zero central velocity, v_0, is set in a cut harmonic oscillator potential. This is accomplished by multiplying the initial gaussian by $\exp(ipx)$, where $p = mv_0$ is the central momentum. The results are shown in **Figure 9**. In this case P_{in} decays in larger steps. The emission of wavepackets is shown in **Figure 10**,where the probability density is plotted versus *x* at a particular time.

7. Conclusions

Exponential time-dependence has been shown to be only an approximation to any real decay process even in the case of commonly encountered resonance states. For resonances, at large times a t^{-2} dependence emerges preceded by some oscillations. The time-dependent Schrödinger equation for non-resonance initial states has been solved utilizing the eigenfunctions for a given Hamiltonian. It has been applied to the case of a potential consisting of an infinite wall and a repulsive delta function. Exact, analytical, normalized solutions have been obtained in closed form. In the case specifically exhibited, *i.e.*, the choice spectral function $\phi_1(E)$ (Equation (34)), the survival probability, which is exactly detailed in Equation (40), exhibits a non-exponential behavior at all times. At large times it decays as t^{-3}. To ensure square- integrability the spectral function must be finite at $E \to 0$ and decrease to 0 at large energies faster than $1/\sqrt{E}$. It was shown that this behavior pertains to all square-integrable wavefunctions that are solutions to this problem for which $\varphi(0) \neq 0$. Other spectral functions result in decays varying as t^{-n} with *n* greater than 3. With the appropriate choice of spectral functions which, due to linear independence need not be the same for waves propagating in different directions, the method could be applied to a variety of potentials. Numerical studies of finite potential wells show that non-exponential decay prevails at short times and can exhibit an interesting step-wise behavior. In conclusion quantum mechanics predicts non-exponential decay for all systems studied.

8. Acknowledgements

Ames Laboratory is operated for the U.S. Department of Energy by Iowa State University under Contract No. W-7405-Eng-82.

REFERENCES

[1] S. A. Khalfin, "Contribution to the Decay Theory of a Quasi-Stationary State," *Soviet Journal of Experimental and Theoretical Physics*, Vol. 6, 1958, pp. 1053-1063.

[2] R. Winter, "Evolution of a Quasi-Stationary State," *Physical Review*, Vol. 123, No. 4, 1961, pp. 1503-1507.

[3] V. Weisskopf and E. Wigner, "Berechnung der natürlichen Linienbreite auf Grund der Diracschen Lichttheorie," *Zeitschrift für Physik*, Vol. 63, No. 1-2, 1930, pp. 54-73.

[4] J. J. Sakurai, "Modern Quantum Mechanics," The Benjamin-Cummings Publishing Company, 1985.

[5] C. Dullemond, "Fermi's 'Golden Rule' and Non-Exponential Decay," arXiv:quant-ph/0202105, 2003.

[6] V. P. Oleinik and J. D. Arepjev, "On the Tunneling of Electrons out of the Potential Well in an Electric Field," *Journal of Physics A*, Vol. 17, No. 9, 1984, pp. 1817-1827.

[7] M. I. Shirokov, "Exponential Character of Decay Laws," *Soviet Journal of Nuclear Physics*, Vol. 21, 1975, pp. 347-353.

[8] V. V. Flambaum and F. M. Izrailev, Unconventional decay law for excited states in closed many-body systems. *Physical Review E*, Vol. 64, No. 2, 2001, pp. 026124-026130.

[9] P. G. Silvestrov, "Stretched Exponential Decay of a Quasiparticle in a Quantum Dot," *Physical Review B*, Vol. 64, No. 11, 2001, pp. 113309-113313.

[10] L. Accardi, S. V. Kozyrev and I. V. Volovich, "Non-Exponential Decay for Polaron Model," *Physics Letters A*, Vol. 260, No. 1-2, 1999, pp. 31-38.

[11] G. Wilk and Z. Wlodarczyk, "Nonexponential Decays and Nonextensivity," *Physics Letters A*, Vol. 290, No. 1-2, 2001, pp. 55-58.

[12] A. N. Petridis, L. P. Staunton, M. Luban and J. Vermedahl, Talk Given at the Fall Meeting of the Division of Nuclear Physics of the American Physical Society, Tucson, Arizona, Unpublished, 2003.

[13] S. R.Wilkinson, *et al*., "Experimental Evidence for Non-Exponential Decay in Quantum Tunnelling," *Nature*, Vol. 387, 1997, pp. 575-577.

[14] N. G. Kelkar, M. Nowakowski and K. P. Khemchandani, "Hidden Evidence of Nonexponential Nuclear Decay," *Physical Review C*, Vol. 70, No. 2, 2004, pp. 24601-24605.

[15] C. Rothe, S. I Hintschich and A. P. Monkman, "Violation of the Exponential-Decay Law at Long Times," *Physical Review Letters*, Vol. 96, No. 16, 2006, pp. 163601-163604.

[16] B. L. Burrows and M. Cohen, "Exact Time-Dependent Solutions for a Double-Well Model," *Journal of Physics A*, Vol. 36, No. 46, 2003, pp. 11643-11653.

[17] R. M. Cavalcanti, P. Giacconi and R. Soldati, "Decay in a Uniform Field: An Exactly Solvable Model," *Journal of Physics A*, Vol. 36, No. 48, 2003, pp. 12065-12080.

[18] A. Messiah, "Quantum Mechanics," Dover Publishers, Mineola, 1999.

[19] The expressions for this wavefunction and the probability density are very long and complicated. They are available from the authors upon request.

J. Modern Physics, **2010, 1, 137-142**
doi:10.4236/jmp.2010.12019 Published Online June 2010 (http://www.SciRP.org/journal/jmp)

Contradiction between Conservation Laws and Orthodox Quantum Mechanics

M. E. Burgos

Departamento de Física, Facultad de Ciencias, Universidad de Los Andes, Mérida, Venezuela
Email: mburgos25@gmail.com

Received February 28th, 2010; revised April 7th, 2010; accepted May 7th, 2010.

Abstract

In this paper, it showed that the orthodox version of quantum mechanics contradicts the idea that conservation laws are valid in individual processes of measurement.

Keywords*: *Conservation Laws, Orthodox Quantum Mechanics, Measuring Problem

1. Introduction

The Schrödinger evolution of a system leads, in some circumstances, to coherent superpositions of macroscopically distinct states. This is dramatically illustrated in Schrödinger's cat paradox, and constitutes the great puzzle of quantum measurements.

To explain this fact, several hypotheses have been proposed. The best known is the projection postulate, an ingredient of the so-called orthodox interpretation of quantum mechanics (due to von Neumann), which is at present almost the only version taught. The projection postulate establishes that when a measurement is performed, the system's state jumps to an eigenstate of the operator representing the dynamical variable measured, and the pointer of the measuring device is led to a definite position; *i.e.*, it breaks down the coherent superposition of macroscopically distinct states.

This postulate has been criticized on several grounds:
– it introduces a subjective element into the theory [1,2],
– it conflicts with the Schrödinger equation [2,3], and
– it implies a kind of action-at-a-distance [2,4].

The traditionally opposed approach faces the conceptual difficulties of the measurement problem by assuming that the state function $|\Phi_S\rangle$ is no more than a tool to calculate probabilities. Differing from the orthodox version, in this view $|\Phi_S\rangle$ is not an attribute of an individual system S but of an ensemble; hence a process state reduction is not required [1]. Nevertheless, many physicists think that $|\Phi_S\rangle$ refers to an individual system, so the ensemble interpretation of $|\Phi_S\rangle$ that allows rejection of the projection postulate is, paradoxically, the main reason that this approach is frequently discarded.

In order to find a solution to the measuring problem keeping as valid the individual interpretation of $|\Phi_S\rangle$, other theories close to, but different from, quantum mechanics have been proposed. In these theories, the Schrödinger equation is modified in a way that leads to spontaneous collapses. This is the case of those developed by Ghiradi, Rimini and Weber [5], Diosi [6], and Joos and Zeh [7]. Ballentine [8] has demonstrated that these theories violate energy conservation and are incompatible with the existence of stationary states.

Several authors [9-13] have studied the role of conservation laws in quantum measurements. It has been shown that the presence of an additive conserved quantity imposes restrictions on the measurement of dynamical variables incompatible with this quantity. The main object of the present paper is to point out an even deeper conflict between conservation laws and the orthodox version of quantum mechanics: if the individual interpretation of $|\Phi_S\rangle$ and the projection postulate are taken as valid, then conservation laws cannot be satisfied in measurement processes, except in cases where the initial state of S is an eigenstate of the operator representing the quantity to be measured.

2. Conservation Laws in Processes Involving an Individual System

In the framework of classical physics, in principle, the application and test of conservation laws does not present any difficulty. This is mainly due to the fact that physical quantities have definite values. So if the numerical value a of a physical quantity A does not change during the whole process, we can assert that A is conserved in this process.

The same is valid in the statistical version of quantum mechanics [1].

On the contrary, in the framework of orthodox quantum mechanics, in general, dynamical variables (or physical quantities) are not sharp. "A popular working rule of pragmatic quantum mechanics says that an observable has no value before a measurement." [14] But nobody has stated, to our knowledge, in which way a conservation law should be applied or tested in those cases where the dynamical variable *A* does not have a definite value. So if the orthodox interpretation is adopted, it is not evident in which way it could be decided whether *A* is conserved or not. This means that in this version of quantum mechanics, *a priori* it does not make any sense to say that a dynamical variable which is not sharp, is conserved, even if the process follows the Schrödinger equation.

This radical conclusion can be avoided in the following way: If the operator A_S represents the dynamical variable A_S referred to the individual system S and H_S is its Hamiltonian, in processes that are ruled by the Schrödinger equation, the conditions

$$\partial A_S/\partial t = 0 \tag{1}$$

and

$$[A_S, H_S] = 0 \tag{2}$$

ensure that

$$\langle A_S\rangle = \langle \Phi_S|A_S|\Phi_S\rangle \tag{3}$$

remains a constant in time for every state $|\Phi_S\rangle$ of S.

Messiah *postulates* that the mean value of the dynamical variable A_S is $\langle A_S\rangle$ [15]. Taking into account this postulate we shall claim that if A_S is conserved, then $\langle A_S\rangle$ cannot change with time for every state $|\Phi_S\rangle$ of S. Hence, in those processes that are governed by the Schrödinger equation, the statement "A_S is conserved" can be given a meaning, whether A_S is sharp or not.

On one hand, let us stress that *a necessary condition for the dynamical variable A_S to be conserved is that $\langle A_S\rangle$ be a constant* (observe, nevertheless, that this does not imply that A_S takes on the value $\langle A_S\rangle$). On the other hand, it should be emphasised that in the framework of the version of quantum mechanics that we are analysing, both $|\Phi_S\rangle$ and A_S refer to the individual system S. As a consequence, *the quantity* $\langle A_S\rangle$ given by (3) *cannot concern something different from this individual system.* This quantity is called expectation value by some authors and mean value by other authors. Since some people do not conceive that a mean value can be related to an individual system, let us quote some orthodox authors saying that $\langle A_S\rangle$ refers to an individual system.

a) According to von Neumann, the main architect of orthodox quantum mechanics, "everything which can be said about the state of *the system* must be derived from its wave function Φ. What pronouncements can now be made regarding *a system* which is in the state Φ?... For the expectation value of R in the state Φ, we have (RΦ, Φ) [= $\langle\Phi|R|\Phi\rangle$] (emphases added)." [16]

b) In Messiah's words, "the mean value of the dynamical variable *A* when *the system* is in the dynamical state defined by the [normalised] function Ψ is $\langle A\rangle = \langle\Psi, A\Psi\rangle$ (emphasis added)." [15]

c) Merzbacher calls expectation value the quantity $\langle X\rangle = \langle\Phi|X|\Phi\rangle$. This author points out that "in quantum mechanics the term 'expectation value' is preferred when it is desirable to emphasise... the fact that the behaviour *of a single particle* is involved rather than that of an ensemble of particles (emphasis added)." [17]

d) Cohen-Tannoudji *et al.* use expressions like "the mean value $\langle X\rangle(t)$ of the position of *the particle* at time t..." and "the mean value of the energy of *the particle* in the state $|\Psi(t)\rangle$... (emphases added)." [18]

The precedent list of authors considering that the expectation (or mean) value refers to an individual system is not exhaustive. But it suffices, we think, to show that in general authors adopting the individual interpretation of $|\Phi_S\rangle$ assert that $\langle A_S\rangle = \langle\Phi_S|A_S|\Phi_S\rangle$ refers also to the individual system S. In the following we are going to use the term *mean value* for individual systems, and the term *average* when some set or ensemble is involved.

3. Conservation Laws in Processes of Measurement (Case of a Discrete Spectrum)

Now we shall address the problem of the validity of conservation laws when a measurement of A_S is performed. In this section we shall deal with the discrete case and, in the next one, with the continuous case. Let a_k (k = 1, 2,…) be an eigenvalue of A_S, g its degree of degeneracy and $|a_k^i\rangle$ (i = 1. 2,… g) an eigenvector corresponding to the eigenvalue a_k. We shall assume that $|m_0\rangle$ represents the initial state of a measuring device M of A_S, and $|\psi_k^i\rangle$ the orthonormal states of S+M when the measurement process is over. In the ideal measurement scheme, the transition

$$|a_k^i\rangle\,|m_0\rangle \rightarrow |\psi_k^i\rangle \tag{4}$$

has a probability of one. This scheme is supposed to be valid in cases where the measured dynamical variable is compatible with every conserved quantity referred to S+M [9-13].

Let A be the operator representing a dynamical variable *A* referred to S+M, and H be its Hamiltonian. We can then write

$$H = H_S + H_M + H_{int} \tag{5}$$

where H_M refers to M, and H_{int} is due to the interaction between S and M. We assume that the conditions

$$\partial A/\partial t = 0 \tag{6}$$

and

$$[A, H] = 0 \tag{7}$$

are fulfilled.

To ensure that measurements of A_S can be performed according to the ideal scheme, we suppose that A_S commutes with every operator representing another conserved quantity referred to S+M; and, since the transition (4) has a probability of one, it can be assumed that it is a result of the Schrödinger evolution.

If at t_0 (when the interaction between S and M starts) it is possible to write

$$A = A_S + A_M \tag{8}$$

(where A_M refers to M), we have

$$\langle A\rangle_k^i(t_0) = \langle a_k^i|A_S|a_k^i\rangle + \langle m_0|A_M|m_0\rangle = a_k + \langle m_0|A_M|m_0\rangle \tag{9}$$

And, since at t_f (when the interaction between S and M is over)

$$\langle A\rangle_k^i(t_f) = \langle \psi_k^i|A|\psi_k^i\rangle \tag{10}$$

the validity of (6) and (7) implies that $\langle A\rangle_k^i(t_f) = \langle A\rangle_k^i(t_0)$, and hence

$$\langle \psi_k^i|A|\psi_k^i\rangle = a_k + \langle m_0|A_M|m_0\rangle \tag{11}$$

for every i. As $\langle \psi_k^i|A|\psi_k^i\rangle$ does not depend on i, it can be written

$$\langle A\rangle_k(t_f) = \langle A\rangle_k^i(t_f) = a_k + \langle m_0|A_M|m_0\rangle \tag{12}$$

This relation must necessarily be fulfilled in the ideal measurement scheme. As a consequence, it can be said that in those cases where the initial state of S is an eigenstate of the operator A_S representing the dynamical variable A_S to be measured, the corresponding conservation law is valid. This result can also be seen as a natural consequence of the hypothesis that the process described by (4) is governed by the Schrödinger equation.

Now, if the initial state of S is

$$|\Phi_s(t_0)\rangle = \sum_{r,i} c_r^i |a_r^i\rangle \tag{13}$$

(where at least two coefficients c_r^i and $c_{r'}^{i'}$ with $r \neq r'$ are non-null) and the Schrödinger equation rules the measurement process, then the Hamiltonian H, referred to S+M, induces the evolution

$$\sum_{r,i} c_r^i |a_r^i\rangle |m_0\rangle \rightarrow \sum_{r,i} c_r^i \psi_r^i\rangle \tag{14}$$

Making

$$\langle A\rangle(t_0) = (\langle \Phi_S(t_0)| \langle m_0|) A (|\Phi_S(t_0)\rangle |m_0\rangle) \tag{15}$$

and

$$\langle A\rangle(t_f) = (\sum_{r,i} c_r^{i*} \langle \psi_r^i|) A (\sum_{r',i'} c_r^{i'} |\psi_{r'}^{i'}\rangle) \tag{16}$$

the validity of (6) and (7) allow us to ensure that $\langle A\rangle(t_0) = \langle A\rangle(t_f)$. Nevertheless, the linear superposition on the r.h. of (14), mentioned in Section 1, constitutes the great puzzle of quantum measurements.

On the contrary, the projection postulate states that in measurement processes coherent superpositions break down. According to this postulate, the evolution of S+M is not given by (14) and the transition

$$\sum_{r,i} c_r^i |a_r^i\rangle |m_0\rangle \rightarrow \sum_i c_k^i |\psi_k^i\rangle \tag{17}$$

has probability $\sum_i |c_k^i|^2$ to happen. In this last case,

$$\langle A\rangle(t_0) = \sum_i |c_k^i|^2 a_r + \langle m_0|A_M|m_0\rangle \tag{18}$$

and, as stated in (12),

$$\langle A\rangle_k(t_f) = a_k + \langle m_0|A_M|m_0\rangle \tag{19}$$

As a consequence, it results

$$\langle A\rangle(t_0) \neq \langle A\rangle_k(t_f) \tag{20}$$

for every k, even though conditions (6) and (7) are fulfilled.

It is worth noticing that inequalities (20) are obtained under the assumptions that the individual interpretation of the state vector and the projection postulate are valid. In this case the condition that $\langle A\rangle$ be a constant, a necessary condition for *A* to be conserved, is not satisfied. We are thus forced to conclude that if the initial state of S is not an eigenvector of A_S, the dynamical variable *A* is not conserved in processes of measurement of A_S. In other articles we have given examples of processes of measurement of the type analyzed in this section [19-22].

A similar conclusion resulting from a different analysis has been obtained by Pearle [23]. He says that "it should first be noted that quantum theory itself, with the reduction postulate indiscriminately applied, does not necessarily satisfy the conservation laws..." In his view, "this is a serious problem for quantum theory with a reduction postulate."

We have said that $\langle A\rangle(t_0) = \sum_{r,i} |c_r^i|^2 a_r + \langle m_0|A_M|m_0\rangle$. Now we are going to calculate the *average* of $\langle A\rangle_k(t_f)$ when the process of measurement of A_S is repeated N times. Let f_k be the frequency corresponding to the possible results a_k (k = 1, 2,…) and to the mean value $\langle A\rangle_k(t_f)$. If the process is repeated N times, the resulting average is

$$\bar{A} = \sum_k f_k \langle A\rangle_k(t_f) \tag{21}$$

and, taking into account (19),

$$\bar{A} = \sum_k f_k a_k + \langle m_0|A_M|m_0\rangle. \tag{22}$$

Now, if N is big enough, we can assert that $f_k \approx \sum_i |c_k^i|^2$. As a consequence, we obtain

$$\bar{A} \approx \sum_{k,\,i} \left|c_k^i\right|^2 a_k + \langle m_0 | A_M | m_0 \rangle \quad (23)$$

$$\langle A \rangle (t_0) = \sum_{k,\,i} \left|c_k^i\right|^2 a_k + \langle m_0 | A_M | m_0 \rangle \quad (24)$$

and

$$\bar{A} \approx \langle A \rangle (t_0) \quad (25)$$

So we can say that conservation laws still have a statistical sense.

4. Conservation Laws in Processes of Measurement (Case of a Continuous Spectrum)

Let α be an eigenvalue included in the continuous part of the spectrum of A_S; we shall assume that α can take any value in the interval (0, ∞). If the ket $|\alpha\rangle$ is

$$|\alpha\rangle = \int_{\alpha-\delta/2}^{\alpha+\delta/2} \mathrm{dac}\,(a)\,|a\rangle \quad (26)$$

where δ is a small interval in the α semi-axis (if Δα is the error in the measurement of α, the condition $\delta < \Delta\alpha$ should be fulfilled), we shall say that $|\alpha\rangle$ is a "quasi-eigenstate" of A_S corresponding to the eigenvalue α. We shall call $|m_0\rangle$ the ket that represents the initial state of a measuring device M of A_S, and $|\psi(\alpha)\rangle$ the orthonormal states of S+M when the process of measurement is over. If the initial state of S is $|\alpha\rangle$, according to the ideal measurement scheme, the transition

$$|\alpha\rangle\,|m_0\rangle \rightarrow |\psi(\alpha)\rangle \quad (27)$$

has a probability of one.

Let A be the operator representing a dynamical variable *A* referred to S+M, and H be its Hamiltonian. We can then write

$$H = H_S + H_M + H_{int} \quad (28)$$

where H_M refers to M, and H_{int} is due to the interaction between S and M. As previously, we assume that the conditions (6) and (7) are fulfilled.

If at t_0 (when the interaction between S and M starts) it is possible to write

$$A = A_S + A_M \quad (29)$$

(where A_M refers to M), we have

$$\langle A \rangle_\alpha (t_0) = \langle \alpha | A_S | \alpha \rangle + \langle m_0 | A_M | m_0 \rangle \quad (30)$$

And since at t_f (when the interaction between S and M is over)

$$\langle A \rangle_\alpha (t_f) = \langle \psi(\alpha) | A | \psi(\alpha) \rangle \quad (31)$$

the validity of (6) and (7) implies that $\langle A \rangle_\alpha (t_f) = \langle A \rangle_\alpha (t_0)$, and hence

$$\langle A \rangle_\alpha (t_f) = \langle \alpha | A_S | \alpha \rangle + \langle m_0 | A_M | m_0 \rangle \quad (32)$$

This relation must necessarily be fulfilled in the ideal measurement scheme. As a consequence, it can be said that in cases where the initial state of S is a "quasi-eigenstate" of A_S, the corresponding conservation law is valid.

Now, if the initial state of S is

$$\left|\Phi_s(t_0)\right\rangle = \int_0^\infty \mathrm{dac}\,(a)\,|a\rangle \quad (33)$$

where $c(a) \neq 0$ outside the interval $(\alpha-\delta/2, \alpha+\delta/2)$, and the Schrödinger equation rules the measurement process, then the Hamiltonian H induces the evolution

$$\begin{aligned} \int_0^\infty \mathrm{dac}\,(a)\,|a\rangle\,|m_0\rangle &\rightarrow \int_0^\infty \mathrm{dac}\,(a)\,|\psi(a)\rangle \\ &= \int_0^{\alpha-\delta/2} \mathrm{dac}\,(a)\,|\psi(a)\rangle + \int_{\alpha-\delta/2}^{\alpha+\delta/2} \mathrm{dac}\,(a)\,|\psi(a)\rangle \\ &+ \int_{\alpha+\delta/2}^{\infty} \mathrm{dac}\,(a)\,|\psi(a)\rangle \end{aligned} \quad (34)$$

As a consequence, making

$$\langle A \rangle (t_0) = (\langle \Phi_S(t_0)| \langle m_0|)\, A\, (|\Phi_S(t_0)\rangle\, |m_0\rangle) \quad (35)$$

and

$$\langle A \rangle (t_f) = \left[\int_0^\infty \mathrm{dac}^*\,(a) \langle \psi(a)| \right] + \int_0^\infty \mathrm{da'}\; c\,(a')\,|\psi(a')\rangle \quad (36)$$

the validity of (6) and (7) allow us to ensure that $\langle A \rangle (t_0) = \langle A \rangle (t_f)$. But, as it happened in the case of the discrete spectrum, we obtain a linear superposition in the r.h. of (34), previously mentioned, and that constitutes the great puzzle of quantum measurements.

On the contrary, the projection postulate states that in measurement processes coherent superpositions break down. According to this postulate, the evolution of S+M is not given by (34), and the transition

$$\int_0^\infty \mathrm{dac}\,(a)\,|a\rangle\,|m_0\rangle \rightarrow \int_{\alpha-\delta/2}^{\alpha+\delta/2} \mathrm{dac}\,(a)\,|\psi(a)\rangle \int_0^\infty \quad (37)$$

has a probability close to $|c(\alpha)|^2\,\delta$ to happen. So, since

$$\langle A \rangle (t_0) = \int_0^\infty \mathrm{da}\;|c(a)|^2\; a + \langle m_0 | A_M | m_0 \rangle \quad (38)$$

and

$$\begin{aligned} \langle A \rangle_\alpha (t_f) &= \int_{\alpha-\delta/2}^{\alpha+\delta/2} \mathrm{da}\;|c(a)|^2\, a + \langle m_0 | A_M | m_0 \rangle \\ &= \alpha + \langle m_0 | A_M | m_0 \rangle \end{aligned} \quad (39)$$

it results

$$\langle A \rangle (t_0) \neq \langle A \rangle_\alpha (t_f) \quad (40)$$

for every α, even though conditions (6) and (7) are fulfilled.

It is worth noticing that inequalities (20) and (40) are obtained under the assumptions that the individual interpretation of the state vector and the projection postulate are valid. In this case the condition that $\langle A \rangle$ be a constant, a necessary condition for *A* to be conserved, is not satisfied. We are thus forced to conclude that if the initial state of S is not an eigenvector of A_S (in the discrete case) or a "quasi-eigenvector" of A_S (in the continuous case), the dynamical variable *A* is not conserved in measurement processes of A_S. The proof that also in this last case conservation laws still have a

statistical sense is straightforward.

5. Concluding Remarks

We have seen that during Schrödinger evolutions, the validity of (6) and (7) ensures that the expectation value $\langle A \rangle$ referred to the individual system S and its measurement device M remains constant in time. But if the rule governing the process is replaced with a law different from Schrödinger equation, the validity of conservation laws cannot be guaranteed *a priori* [19-24]. Ballentine points out that some theories that modify the Schrödinger equation in order to include spontaneous state reductions lead to the non-conservation of the energy [8]. Our study shows that projections induced by measurements, as they are considered in the framework of orthodox quantum mechanics, conflict with the conservation laws.

However, the results of these two analyses have a difference worth noticing. In the theories Ballentine refers to, energy is continuously gained, although its magnitude is too small to be detected [8]. In collapses occurring in the framework of orthodox quantum mechanics, the change $\langle A \rangle(t_f) - \langle A \rangle(t_0)$ is not necessarily small but, when the process of measurement of A_S is repeated many times, the *average* of $\langle A \rangle(t_f)$ is close to $\langle A \rangle(t_0)$. This is why we claim that in measurement processes, conservation laws still have a statistical sense.

In an approach to quantum mechanics previously formulated we have included, as an essential ingredient, a postulate that ensures the statistical sense of conservation laws in every process involving projections [25,26]. In this approach no reference to the subject or to measurement devices is made. We there assume that in nature two kinds of spontaneous processes occur: those ruled by the Schrödinger equation, which is a deterministic equation, and those ruled by the rules of probability, where projections happen.

Let us conclude by pointing out that, in our view, there is nothing sacred about conservation laws. Like every other scientific law, they could be false. The same is true of the orthodox interpretation of quantum mechanics. The intent of our contribution is to show that there is a contradiction between these two ideas, both of which are adopted, perhaps, by the majority of physicists.

6. Acknowledgements

We thank Professor G. Díaz de Delgado for her help with stylistic matters. This work was supported by the CDCHT-ULA.

REFERENCES

[1] L. E. Ballentine, "The statistical interpretation of quantum mechanics," *Reviews of Modern Physics*, Vol. 42, 1970, p. 358.

[2] M. Bunge, "Treatise on Basic Philosophy," Vol. 7, Reidel, Dordrecht, 1985, pp. 191-205.

[3] P. Busch and A. Shimony, "Unsolubility of the Quantum Measurement Problem for Unsharp Unobservables," *Physical Review D*, Vol. 9, 1974, p. 2321.

[4] M. Jammer, "The Philosophy of Quantum Mechanics," John Wiley & Sons, New York, 1974.

[5] G. C. Ghirardi, A. Rimini and T. Weber, "The Puzzling Entanglement of Schrödinger Wave Function," *Foundations of Physis C*, Vol. 18, No. 1, 1987, pp. 1-27.

[6] L. Diosi, "Models for Universal Reduction of Macroscopic Quantum Fluctuations," *Physical Review A*, Vol. 40, No. 3, 1989, pp. 1165-1174.

[7] E. Joos and H. D. Zeh, "The Emergence of Classical Properties through Interaction with the Enviroment," *Zeitschrift für Physik B*, Vol. 59, 1985, p. 223.

[8] L. E. Ballentine, "Failure of Some Theories of State Reduction," *Physical Review A*, Vol. 43, No. 1, 1991, pp. 9-12.

[9] E. P. Wigner, "Die Messung Quantenmechanischer Operatoren," *Zeitschrift für Physik*, Vol. 131, 1952, pp. 101-108.

[10] H. Araki and M. M. Yanase, "Measurement of Quantum Mechanical Operators," *Physical Review*, Vol. 120, No. 2, 1960, pp. 622-626.

[11] H. Stein and A. Shimony, "Limitation on Quantum Measurements," in: B. d'Espagnat, Ed., *Foundations of Quantum Mechanics*, Academic, New York, 1971.

[12] G. C. Ghirardi, F. Miglietta, A. Rimini and T. Weber, "Limitation on Quantum Measurements," *Physical Review D*, Vol. 24, No. 2, 1981, pp. 353-358.

[13] M. Ozawa, "Does a Conservation Law Limit Position Measurements?" *Physical Review Letters*, Vol. 67, No. 15, 1991, pp. 1956-1159.

[14] H. Primas, "Realism and Quantum Mechanics," *Proceedings of* 9th *International Congress of Logic, Methodology and Philosophy of Science*, Vol. 134, 1991, pp. 609-631.

[15] A. Messiah, "Quantum Mechanics," North-Holland Pub.lishing Company, Amsterdam, 1974.

[16] J. von Neumann, "Mathematical Foundations of Quantum Mechanics," Princeton University Press, Princeton, New Jersey, 1955.

[17] E. Merzbacher, "Quantum Mechanics," John Wiley and Sons, New York, 1977.

[18] C. Cohen-Tannoudji, B. Diu and F. Laloë, "Quantum Mechanics," John Wiley and Sons, New York, 1977.

[19] M. E. Burgos, "Conservation Laws and Deterministic Evolutions," *Physics Essays*, Vol. 7, No. 1, 1994, pp. 69-71.

[20] M. E. Burgos, "Does Conservation of Energy Apply in Processes Ruled by Quantum Mechanical Laws?" *Speculations in Science and Technology*, Vol. 20, 1997, pp. 183-187.

[21] M. E. Burgos, F. G. Criscuolo and T. L. Etter, "Conservation Laws, Machines of The First Type and Superluminal Communication," *Speculations in Science and Technology*, Vol. 21, No. 4, 1999, pp. 227-233.

[22] F. G. Criscuolo and M. E. Burgos, "Conservation Laws in Spontaneous and Mesurement-Like Individual Processes," *Physics Essays*, Vol. 13, No. 1, 2000, pp. 80-84.

[23] P. Pearle, "Suppose the State Vector is Real: The Description and Consequences of Dynamical Reduction," *Annals of the New York Academy of Sciences*, Vol. 480 1986, pp. 539-551.

[24] A. Afriat and F. Selleri, "The Foundations of Quantum Mechanics-Historical Analysis and Open Questions," in: C. Garola and A. Rossi, Eds., Kluwer Academic Publishers, Dordrecht, 1995.

[25] M. E. Burgos, "Which Natural Processes Have the Special Status of Measurements?" *Foundations of Physisc*, Vol. 28, No. 8, 1998, pp. 1323-1346.

[26] M. E. Burgos, "Transitions to the Continuum: Three Different Approaches," *Foundations of Physisc*, Vol. 38, No. 10, 2008, pp. 883-907.

J. Modern Physics, **2010, 1, 143-146**
doi:10.4236/jmp.2010.12020 Published Online June 2010 (http://www.SciRP.org/journal/jmp)

Scientific Research

On Collapse of Uniform Density Sphere with Pressure

Mahesh Chandra Durgapal[1], Pratibha Fuloria[2]

[1]Retired Professor of Physics, Kumaun University, Naintal, India; [2]Department of Physics, SSJ Campus, Kumaun University, Almora, India.
Email: garciluiz@gmail.com

Received March 1st, 2010; revised April 18th, 2010; accepted May 10th, 2010.

ABSTRACT

Adiabatic collapse solutions of uniform density sphere have been discussed by so many authors. An analysis of these solutions has been done by considering the baryonic conservation law and the no heat transfer condition. We have examined whether the pressure can remain finite or not during the collapse.

Keywords*: *Genral Relativity, Astrophysics, Collapse

1. Introduction

Radial adiabatic motion of perfect fluid spheres of uniform density, $E = E(t)$, but non-uniform pressure were discussed by Bonnor and Faulkes [1], Thompson and Whitrow [2,3] and Bondi [4] under various assumed relationships between central pressure and density. These authors discussed the problem of collapse and bounce under two assumptions: first, that the motion is isotropic or shear-free; and second, that the density is uniform. But Mishra and Shrivastava [5] showed that the condition of uniform density and regularity at the centre necessarily lead to the isotropic motion.

The theme of this paper is rather different from that of the other authors. We have examined whether the pressure can remain finite or not. We have considered the no-heat transfers (NHT) conditions (explained in the text) and baryon conservation law during the collapse. It is shown that if the fluid is isentropic or (and) the surface temperature remains constant during the collapse the pressure can not remain finite (it vanishes). On the other hand if the fluid is neither isentropic nor the surface temperature remains constant during the collapse, then the results obtained by earlier authors (Bondi, 1969) are found to be inconsistent with the baryonic conservation and NHT condition.

2. The Metric and Uniform Density Sphere

Vanishing shear implies that one can simultaneously introduce isotropic and co-moving coordinates

$$ds^2 = y^2dt^2 - R^2(dr^2 + r^2d\Omega) \tag{1}$$

$$y = y(r,t), R = R(r,t), d\Omega^2 = d\vartheta^2 + \sin^2\vartheta d\varphi^2$$

It is assumed that the fluid's viscosity vanishes, and the adiabatic flow condition makes T_{10} component of energy momentum tensor vanish in the co-moving coordinates. The energy momentum tensor can thus be written as

$$T_{\alpha\beta} = (P+E)U_\alpha U_\beta - Pg_{\alpha\beta} \tag{2}$$

where E and P are energy density and pressure, respectively and the four-velocity,

$$U_\alpha \equiv (y,0,0,0) \tag{3}$$

The hydrodynamic equations,

$T^{\alpha\beta}_{;\beta} = 0$ and $U_\alpha T^{\alpha\beta}_{;\beta} = 0$, and the equation of baryon conservation, $(nU^\alpha)_{;\alpha} = 0$ (where n = number density) give us (Misner and Sharp) [6], (Demianski) [7]

$$(y'/y) = -P'/(P+E) \tag{4}$$

and

$$U^\alpha s_{,\alpha} = 0 \quad \text{or} \quad s^\circ = 0 \quad \text{and} \quad s' \neq 0 \tag{5}$$

$(') \equiv$ partial differentiation w.r.t. $r; r; (\circ) \equiv$ partial differentiation w. r. t. t.

3. The Boundary Condition and Thermodynamic Relation

For the exterior solution some authors have chosen Schwarzschild vacuum solution while others have chosen Vaidya's radiative solutions in the exterior. In the later case the heat flow is given by Kramer [8]

$$q = -(K / yR^2)(Ty)'$$

Here, K is thermal conductivity. But in the cases where the exterior solution is chosen as Schwarzschild solution we get NHT conditions ($q = 0$) given by either

$$(Ty)' = 0, \quad \text{that is,} \quad Ty = T_b y_b \quad \text{where} \quad T_b = T(r = r_b) \tag{6}$$

$$\text{Or} \quad T = 0 \quad (\text{for cold stars}) \tag{7}$$

$$\text{Or} \quad K = 0 \tag{8}$$

The basic law of thermodynamic change is

$$Tds = dU + Pd(1/n) \tag{9}$$

$$nTds = dE - hdn \quad \text{and} \quad (\partial E / \partial s)_n = nT \tag{10}$$

where, $U \equiv$ specific internal energy, $s \equiv$ specific entropy and $h = (P + E)/n \equiv$ specific enthalpy. The units of n are chosen so that, $P \to 0, E \to n,$ and $h \to 1$.

Writing Bondi's results (1969) in the present notations, one gets

$$nR^3 = B(r) \tag{11}$$

$$R = \alpha / (1 - \beta r^2) \quad \text{and} \quad nR^3 = B(r) \tag{12}$$

$$y = FR^\circ / R \tag{13}$$

$$R^\circ / R = (\alpha^\circ / \alpha) + \beta^\circ r^2 / (1 - \beta r^2) \tag{14}$$

$$y_b / y = (P + E)/E = -\frac{E^\circ}{3E}\frac{R}{R^\circ} \tag{15}$$

And

$$P / E = \frac{\beta^\circ (r_b^2 - r^2)}{(1 - \beta r_b^2)[\alpha^\circ + r^2(\alpha\beta^\circ - \beta\alpha^\circ)]} \tag{16}$$

$\alpha = \alpha(t), \beta = \beta(t), F = F(t), y_b = y(r = r_b), r_b \equiv r$ at the boundary.

Since $E=E(t)$ or $E' = 0$, we write [using Equation (10)]

$$(n'/n^2) = -Ts'/(P + E) \tag{17}$$

$$= -(Ty / Ey_b)s' \text{[using Equation (15)]} \tag{18}$$

4. Collapse of Uniform Density Sphere

The collapse of uniform density sphere is discussed under various physical conditions. [We have assumed that $A(t) \equiv$ any arbitrary function of t and $B(r) \equiv$ any arbitrary function of r]

4(a) using NHT condition (6a):
Using Equation (6) in (18) one gets,

$$n'/n^2 = -(T_b / E)s' \quad \text{or}$$

$$(E/n) = 1 + T_b(s - s_b) \tag{19}$$

$$s_b = s(r = r_b).$$

It is obvious from Equation (19) that the entropy of an adiabatic uniform density sphere is minimum at the boundary.

4(a) (i): Isentropic case: Let the entropy be constant throughout the sphere, that is, s = constant = s_b. Equation (19) gives

$$E = n \tag{20}$$

[Using Equation (11)]

$$ER^3 = B(r) \quad R = A(t) \times B(r) \tag{21}$$

$$R^\circ / R = A(t)$$

[From Equation (13)]

$$y = A(t) \quad \text{or} \quad y' = 0 \tag{22}$$

[From Equation (4)]

$$P' = 0, \quad \text{or} \quad P = P(t) \tag{23}$$

Since, $P(r = r_b) = 0 = P(t)$, the pressure vanishes within the sphere. Hence, an isentropic uniform sphere undergoes a collapse with vanishing pressure only.

4(a) (ii) Non-isentropic case with constant surface temperatures: We assume that the surface temperature remains constant during the collapse. This is very likely because there is no energy loss to the surrounding from the surface of the sphere. With T_b = constant during the collapse one gets

$$n = E/[1 + T_b(s - s_b)] = A(t) \times B(r) \tag{24}$$

[From Equation (11)]

$$R = A(r) \times B(r) \tag{25}$$

Arguments similar to those in 4(i) show that the pressure vanishes inside the sphere.

Hence, an adiabatic uniform density sphere with constant surface temperature collapses with vanishing pressure.

4(a) (iii) General case: Neither the fluid is isentropic nor the temperature of the surface remains constant. In this case

$$E = n[1 + T_b(s - s_b)]$$

On differentiating with respect to time we obtain

$$\frac{E^{\circ}}{E}=\frac{n^{\circ}}{n}+\frac{T_b^{\circ}(s-s_b)}{1+T_b(s-s_b)} \tag{26}$$

For an adiabatic motion the total mass energy is a constant of motion, that is,

$$M=(4\pi/3)ER_b^3=\text{constant} \quad \text{or} \quad E^{\circ}/E=-3R_b^{\circ}/R \tag{27}$$

Using Equations (11), (14), (26) and (27) we get

$$\begin{aligned}\frac{T_b{}^0(s-s_b)}{1+T_b(s-s_b)}&=\frac{3\beta^{\circ}r^2}{1-\beta r^2}-\frac{3\beta^{\circ}r_b^2}{1-\beta r_b^2}\\&=\frac{3\beta^{\circ}(r^2-r_b^2)}{(1-\beta r^2)(1-\beta r_b^2)}\\&=\frac{3\beta^{\circ}(r^2-r_b^2)}{1-\beta(r^2+r_b^2)+\beta^2r^2r_b^2}\end{aligned} \tag{28}$$

No choice of functions $s=s(r)$, $\beta=\beta(t)$ and $T_b = T_b(t)$ can satisfy this equation. The solutions obtained by various authors for collapsing/expanding uniform density [with Schwarzschild exterior solutions] are inconsistent with the conservation law and NHT.

4(a) (iv) Explanation of inconsistency: Equation (10) shows that $(\partial E/\partial s)_n = nT$, but from Equation (19) we see that $(\partial E/\partial s)_n = nT_b$. Therefore, $nT = nT_b$ or $T = T_b$. Since, $Ty = T_b y_b$ [from Equation (6)] we get $y = y_b = A(t)$.

Hence, $y'=0$ or [from Equation(4)] $P'=0 \quad \therefore P = P(r=r_b)=0$

The pressure vanishes throughout the sphere.

4(b) using NHT condition (7):

When $T = 0$ Equation (14) gives $n'=0$ or $n=n(t)$ or, $R = A(t)\times B(r)$ [from Equation (9)]. As shown in 4(a) (i) the pressure vanishes inside the sphere.

4(c) using NHT condition (8):

When thermal conductivity $K = 0$, it seems that all the relations of Bondi's paper are consistent. However, let us analyse this condition in some details. From Equation (10) we can see that

$$n^{\circ}/n=E^{\circ}/(P+E) \quad \text{and} \quad n'/n=E'/(P+E)-(T/h)s' \tag{29}$$

$$\text{And for } E=E(t),\ (T/h)s'=-n'/n \tag{30}$$

When $K = 0$, no heat enters or leaves any layer within the structure during the collapse that is we can consider temperature of each layer to be independent of time or $T = T(r)$.

Eliminating n from the twin Equations (29) we obtain (Nariai) [9]

$$\left(\frac{T}{h}\right)^{\circ}s'=\frac{E^{\circ}P'-P^{\circ}E'}{P+E}\neq 0=\frac{E^{\circ}P'}{P+E}\ \text{for } E=E(T) \tag{31}$$

or

$$nT^{\circ}=(T/h)P^{\circ}+E^{\circ}(P'/s') \tag{32}$$

It can be seen from Equation (16), that the right hand side of Equation (32) can not be made zero in any case.

Now, we consider a hypothetical case that during the collapse, though $K = 0$, somehow the temperature of each layer changes with time making $T = T(r, t)$, but at the surface the temperature will not change with time, that is, $T_b^{\circ}=0$. It can be seen that

$$ET_b^{\circ}=[E^{\circ}(P'/s')+P^{\circ}T]_{r=r_b} \tag{33}$$

The right hand side of equation can not be made zero.

5. Conclusions

After studying adiabatic collapse of a uniform density sphere using baryon conservation law and NHT condition it is concluded that, a uniform density sphere [with Schwarzschild geometry in the exterior] always collapses adiabatically with vanishing pressure. Collapse with pressure will involve violation of either the baryonic conservation law or the no-heat flow condition. Or we can say that when the exterior geometry is defined by Schwarzschild vacuum solution then the solution given by Oppenheimer and Snyder [10] is the only valid solution for the collapse of a uniform density sphere.

REFERENCES

[1] W. B. Bonnor and M. C. Faulkes, "Exact Solutions for Oscillating Spheres in General Relativity," *Monthly Notices of the Royal Astronomical Society*, Vol. 137, 1967, pp. 239-251.

[2] I. H. Thompson and G. J. Whitrow, "Time-Dependent Internal Solutions for Spherically Symmetrical Bodies in General Relativity-I. Adiabatic collapse," *Monthly Notices of the Royal Astronomical Society*, Vol. 136, 1967, pp. 207-217.

[3] I. H. Thompson and G. J. Whitrow, "Time-dependent internal solutions for spherically symmetrical bodies in general relativity-II. Adiabatic radial motions of uniformly dense spheres," *Monthly Notices of the Royal Astronomical Society*, Vol. 139, 1968, pp. 499-513.

[4] H. Bondi, "Gravitational Bounce in General Relativity," *Monthly Notices of the Royal Astronomical Society*, Vol. 142, 1969, pp. 333-353.

[5] R. M. Misra and D. C. Srivastava, "Relativity-Bounce of Fluid Spheres," *Nature Physical Science*, Vol. 238, 1972, p. 116.

[6] C. W. Misner and D. H. Sharp,"Relativistic Equations for Adiabatic, Spherically Symmetric Gravitational Collapse," *Physical Review B*, Vol. 136, No. 2B, 1964, pp.

B571-576.

[7] M. Demianski, "Relativistic Astrophysics," Pergamon Press, New York, 1985.

[8] D. Kramer, "Spherically Symmetric Radiating Solution with Heat Flow in General Relativity," *Journal of Mathematical Physics*, Vol. 33, No. 4, 1992, pp. 1458-1462.

[9] H. Nariai, "A Simple Model for Gravitational Collapse with Pressure Gradient," *Progress of Theoretical physics*, Vol. 38, No. 1, 1967, pp. 92-106.

[10] J. R. Oppenheimer and H. Snyder, "On Continued Gravitational Contraction," *Physical Review*, Vol. 56, No. 5, 1939, pp. 455-459.

J. Modern Physics, **2010, 1, 147-149**
doi:10.4236/jmp.2010.12021 Published Online June 2010 (http://www.SciRP.org/journal/jmp)

Empirical Relations about the Number of Dimensions in Theoretical Physics with the Concept of Common and Unshared Dimensions

Tomofumi Miyashita

Miyashita Clinic Mitsuya-Kita, Osaka, Japan
Email: tom_miya@plala.or.jp

Received April 21st, 2010; revised May 16th, accepted May 21st, 2010.

Abstract

How many dimensions are there in the universe? *Currently, there is confusion about the number of dimensions in the universe. Empirical relations about the number of dimensions in theoretical physics with the concept of common space-time* 4 *dimensions and unshared dimensions are described in this report.*

Keywords*: *Kaluza-Klein, Superstring, Super gravity, Nambu String, Unshared Dimensions

1. Introduction

Einstein discovered space-time 4 dimensions. In order to complete the theory of everything (TOE), the numbers of dimensions have been increased. Currently, there is confusion about the number of dimensions in the universe. There is a simple question, "How many dimensions are there in the universe?"

The concept of "unshared dimensions" is very suitable solution. Unshared dimensions belong to each particle and the numbers of unshared dimensions are different between the different kinds of particles.

This paper presents empirical relations about the number of dimensions in theoretical physics with the concept of common space-time 4 dimensions and unshared dimensions.

2. Empirical Relations about the Number of Dimensions in Theoretical Physics

2.1 The Concept of Unshared Dimension

There are two kinds of dimensions. One is common space-time 4 dimensions and the other is unshared dimensions which belong to each particle. The common space-time 4 dimensions are entirely same dimensions which Einstein discovered.

Unshared dimensions are something internal dimensions in each particle. The concept of unshared dimensions is discovered empirically. So, the mathematical explanation of "unshared dimensions" is the next stage argument. It is important that even the space has one unshared dimension. So, the definition of the space is different from the common space-time 4 dimensions.

2.2 Empirical Relations about the Number of Dimensions in Theoretical Physics

The number of unshared dimensions can be expressed empirically as:

$$\text{Unshared dimension} = 4 \times (4 - N + 1)/N \quad (1)$$

N is the number related with the symmetry. Calculated unshared dimensions are shown in **Table 1**. Empirical relations about the number of dimensions in theoretical physics are shown in **Table 2**.

When N = 3, then unshared dimensions are 8/3. In this case, explaining for quarks is difficult. 8 and 1/3 is related with a quark, because the number of gluon is 8 and a quark must exist with three particles.

Simple evidences supported unshared dimensions can be shown in the next section.

3. The Evidence of Unshared Dimensions

3.1 Empirical Relations between the Masses of Leptons

If leptons have 6 unshared dimensions, the mass of leptons are expected like this.

$$M = k \times \int x^6 dx = \frac{k}{7} x^7 \quad (2)$$

Here, M, k and x are the mass of lepton, constant coefficient and the value of unshared dimensions.

$$y = \left(\frac{M}{m} \right)^{\frac{1}{7}} \quad (3)$$

Here, m and y are the mass of electron and the seventh power root of ratio with electron. The calculation results are shown in **Table 3**.The square of correlation coefficient between the generation and the seventh power root of mass ratio is 0.9996 shown in **Figure 1**. It is impossible that this result is only coincidence. The expected mass of the forth lepton and the fifth lepton are 14.3 GeV and 70.5 GeV respectively. The peak of 14.3 eV was reported [1] and there remains the possibility of the forth lepton.

The expected leptons which have larger generation number should be very unstable, since they cannot be discovered still yet. But there are many experimental reports about the reactions around the expected energy. The reports published in the internet are much more than those around the unexpected energy.

3.2 The Mass of Weak Boson

Weak boson is related with electrons and neutrino. Then, the number of unshared dimension is 26 (= 10 + 20 – 4). The 27th power root of ratio between Weak boson and electron are shown in **Table 4**. The result is near the generation number 2. If the generation number is 3, the mass of Weak boson is 4×10^6 TeV and it is impossible to observe.

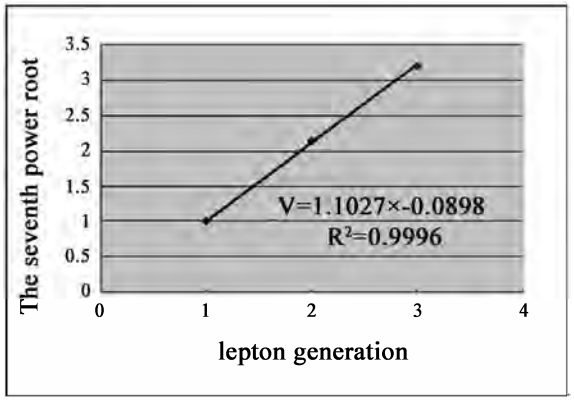

Figure 1. Empirical Relation about the mass of lepton

Table 1. Calculated unshared dimensions

N	4	3	2	1	(0)
particle	The space	quark	lepton	neutrino	consciousness
Unshared dimension	1	8/3	6	16	infinite

Table 2. Empirical relations about the number of dimensions in theoretical physics

Theory	common	The space	quark	lepton	neutrino	total
Kaluza-Klein	4	1	-	-	-	5
Superstring (~1980s)	4	-	-	6	-	10
Super gravity	4	1	-	6	-	11
Nambu string	4	-	-	6	16	26
Superstring (~2000s)	4	1	-	6	16	27

Table 3. The seventh power root

	Generation	mass (MeV)	Mass ratio	The seventh power root of mass ratio
electron	1	0.51099906	1	1
Muon	2	105.6	206.6540005	2.141653053
Tauon	3	1776.99	3477.481935	3.20549411
4th	4	14371.76031	28124.82729	4.321
5th	5	70548.8140	138060.5555	5.424
6th	6	257713	504331	6.526
7th	7	768658	1504226	7.629
8th	8	1977637	3870138	8.732

Table 4. The 27th power root

	Generation	mass (MeV)	Mass ratio	The 27th power root of mass ratio
electron	1	0.51099906	1	1
W-boson	2	80398	157334.9274	2.021601712
Z-boson	2	91187.6	178449.6433	2.036632582

4. Summary

The concept of common space-time 4 dimensions and unshared dimensions are discovered empirically. Simple evidences supported unshared dimensions can be shown from the mass of particles. It is very useful concept to answer for the question, "How many dimensions are there in the universe?"

REFERENCES

[1] C. Friberg, E. Norrbin, T. Sjöstrand, "QCD Aspects of Leptoquark Production at HERA," *Physics Letter B*, Vol. 403, No. 3-4, June 1997, pp. 329-334.

Call for Papers

Journal of Modern Physics

ISSN Print: 2153-1196 ISSN Online: 2153-120X

http://www.scirp.org/journal/jmp/

Journal of Modern Physics(JMP) is an international journal dedicated to the latest advancement of modern physics. The goal of this journal is to provide a platform for scientists and academicians all over the world to promote, share, and discuss various new issues and developments in different areas of modern physics.

Editor-in-Chief

Prof. Victor Yashnikov Russian Academy of Sciences, Russia

Executive-Editor-in-Chief

Dr. Marko Markov Erie Community College, USA

Editorial Board

Subject Coverage

Journal of Modern Physics publishes original papers including but not limited to the following fields:

Theoretical High Energy Physics
Biophysics and Medical Physics
Earth and Planetary Sciences
Instrumentation and Measurement
Plasma Physics
Materials Sciences and Technology
Nuclear Science and Engineering
Computational Physics
Interdisciplinary Physics
Other Topics in Physics

We are also interested in: 1) Short Reports—2-5 page papers where an author can either present an idea with theoretical background but has not yet completed the research needed for a complete paper or preliminary data; 2) Book Reviews—Comments and critiques.

Notes for Intending Authors

Submitted papers should not have been previously published nor be currently under consideration for publication elsewhere. Paper submission will be handled electronically through the website. All papers are refereed through a peer review process. For more details about the submissions, please access the website.

Website and E-Mail

http://www.scirp.org/journal/jmp **E-mail: jmp@scirp.org**

J. Modern Physics, 2010, 1, 93-149
Published Online June 2010 in SciRes (http://www.SciRP.org/journal/jmp).

TABLE OF CONTENTS

Volume 1 Number 2 **June 2010**

